University of Miyazaki

Ph.D. Thesis

Development of Solar to Gas Conversion System Using High Efficiency Photovoltaic and Catalyst

（高効率太陽電池と触媒を用いた太陽光由来ガス変換システムの開発）

September 2022

Department of Materials and Informatics

Interdisciplinary Graduate School of Agriculture and Engineering

University of Miyazaki

Soe Htet Wai

University of Miyazaki

Ph.D. Thesis

Development of Solar to Gas Conversion System Using High Efficiency Photovoltaic and Catalyst

（高効率太陽電池と触媒を用いた太陽光由来ガス変換システムの開発）

September 2022

Interdisciplinary Graduate School of Agriculture and Engineering

Department of Materials and Informatics

University of Miyazaki

Soe Htet Wai

Contents

Abstract

The first chapter: Introduction.

In this chapter, we describe a brief history of renewable energy and the concept of solar to gas conversion to realize a zero-carbon society. This chapter explains the basic techniques of the electrolysis process and methanation reaction. This chapter also provides the objectives and outlines of this thesis.

The second chapter: Evaluation of a Sabatier reaction utilizing hydrogen produced by concentrator photovoltaic modules under outdoor conditions.

This chapter explains the concept of outdoor solar to gas conversion system experimental procedures, the results of the methanation system, and the estimation method of solar to methane conversion efficiency performed at the University of Miyazaki, Japan. Solar-derived outdoor methanation system was operated using highly efficient InGaP/InGaAs/Ge triple-junction concentrator photovoltaic (CPV) modules and Ni-based ZrO_2 catalyst. The methanation reaction was conducted on the solar-derived hydrogen and pure CO_2 supplied via a tank. DC/DC converters and polymer electrolyte membrane (PEM) cells were utilized to generate hydrogen from solar energy. They were connected in parallel with three CPV modules.

In this study, we investigated the performance of methanation reaction on a sunny day and an overcast day. CO_2 to CH_4 conversion efficiency was analyzed by varying operating temperatures and stoichiometric ratios. Then, optimum parameters (setting temperature of the reactors) that provided a high CO_2 to CH_4 conversion were determined. The amount of methane generation was calculated on the amount of hydrogen provided to the methanation system. The conversion efficiency of solar to methane was estimated on the stored energy of generated methane, the input sunlight energy, and the energy required by the reactors.

Since the reactors required initial energy to activate the reaction, external electricity was supplied to the reactors. Accordingly, the energy consumption of the reactors was studied under two operating conditions. Moreover, the methanation reaction is a heat release process. Therefore, we measured the temperature of the reactors and analyzed it on the operating set temperature during the reaction process. Results in this study provided that the temperature of the first reactor increased over the set temperature (260 °C) while the second reactor was constant at 260 °C. Whereas the first reactor consumed initial energy and maintained the reaction by its released heat. On the other hand, the second reactor required more than the first reactor throughout the operation period. As a result of solar to methane conversion efficiency, the highest outdoor value (13.8%) was achieved.

The third chapter: Performance analysis of a Sabatier reaction on direct hydrogen inlet rates based on power-to-gas conversion system.

This chapter discusses a more detailed study of the methanation energy consumption on the amount of hydrogen generation rate (GR_{H2}) since generated hydrogen was directly provided to the methanation reactors. The amount of consumed energy in two different operating conditions has been introduced in chapter 2. We used solar-derived hydrogen in the study of chapter 2, and its outdoor hydrogen production rate was intermittent in the sunlight. Therefore, we regulated DC supply for the electrolysis process to steady the production rate.

The concentration of methane was analyzed at various hydrogen generation rates and measured at 30 min intervals on each GR_{H2} at the operating temperature of 260 °C. Based on the results, the highest methane concentrations were observed at 0.337 and 0.449 NL/min of GR_{H2}. After that, we analyzed the system on these GR_{H2} by varying the operating temperature and each operation was performed for 4 h. The results showed that the highest CH_4 concentration was identified at 220 °C and 0.449 NL/min of GR_{H2}.

We measured the inner temperature of the reactors and the energy consumption of it. The results showed that the temperature of the reactors was steady at operating temperature owing to stable GR_{H2}. The energy consumed was low at a high GR_{H2}, whereas a low GR_{H2} consumed more energy to maintain the reaction. The results in this chapter 3 provided that a stable flow rate with a moderate amount of hydrogen contributed to a steady temperature of the reactors and low energy consumption.

The fourth chapter: Forecasting solar-to-hydrogen and solar-to-methane energy conversion efficiency using Si and IMM PV-modules: a case-study in Japan.

In this chapter, we proposed a simulation study to approximate the potential solar-to-hydrogen (StH) and solar-to-methane (StM) conversion efficiencies of 837 locations in Japan (which were reported by the New Energy and Industrial Technology Development Organization, NEDO). Various prediction methods for the output energy of PV systems have been established. Miyazaki spectrum to energy (MS2E) method provided an improved estimation of solar spectrum on various climate conditions. Based on this method and meteorological test data for the photovoltaic systems (METPV-11) database, we predicted the output energy of PV, DC/DC converters, EC cells, and the conversion efficiencies of solar to hydrogen and solar to methane, respectively.

In this study, we proposed the conversion system for two types of flat PV: Silicon (Si) PV and inverted metamorphic (IMM) PV and forecasted the annual output energy of these modules. Since the DC/DC converters and EC cells were utilized in our system, we approached their conversion efficiencies based on the outdoor results. Similarly, the energy consumed by the reactors was also approximated on outdoor performance. After that, we estimated the conversion efficiencies of DC/DC converter, EC cells, the methanation energy consumption,

amount of hydrogen and methane production in the simulation. Subsequently, we forecasted the annual StH and StM conversion efficiencies of these two PV systems.

In this chapter, we described the simulation concept and the nationwide forecasted results in detail. In addition, the types of PV that can provide efficient solar to gas conversion in Japan are discussed in this chapter. Predicted results showed that IMM modules provided higher and double conversion of StH and StM than Si modules. On the other hand, the results provided that a high conversion was achieved in the northern parts of Japan, and the solar cell's conversion efficiency is one of the important factors in StG conversion system.

The fifth chapter: Summary and conclusion.

This chapter wraps up the results of this thesis and provides a conclusion about the methanation system based on our study. It wraps up the concept and wraps up each chapter. It also discusses some suggestions to improve the system in the future.

In this thesis, we approached outdoor solar to gas conversion systems using highly efficient CPV modules and catalysts. The first step we needed to conduct was to investigate a high CO_2 to CH_4 conversion under various experimental procedures. After many experiments, we were able to demonstrate the highest outdoor value of solar to gas conversion efficiency under a sunny day operation. We described the estimation methods for solar to methane conversion efficiency. In this study, we figured out the amount of methanation energy consumption on a sunny day and an overcast operations.

The next step is to improve the system, especially to better understand the methanation energy consumption and maintain the reactor's temperature at the operating set temperature by investigating the influence of inlet hydrogen rate on the energy consumption. We conducted this study by using a DC supply while regulating the hydrogen generation rate provided to the methanation reactors. The results proved that reactors' temperature was uniform under a steady

hydrogen generation, and total power consumption decreased at a moderate and constant hydrogen rate. We consider these previous improvements and suggest potential solutions to further improve the solar-to-gas conversion system.

Acknowledgement

This work was done, at the Nishioka laboratory, department of materials and informatics, Interdisciplinary Graduate School of Agriculture and Engineering, University of Miyazaki, under the supervision of Professor Kensuke Nishioka. Part of this work was supported by JSPS KAKENHI Grant Number 18K05015 and by a grant for Scientific Research on Priority Areas from the University of Miyazaki.

The author would like to express her respectful gratitude to her supervisor, Professor Dr. Kensuke Nishioka for providing an invaluable chance to advance her study at the University of Miyazaki, Japan, and for accepting her as a member of the Nishioka laboratory. The author would like to express her sincere thanks to Professor Nishioka for his kindness, detailed guidance, generous support, supervision, numerous suggestions, and enormous encouragement to accomplish this research throughout the author's doctoral degree. The author would like to express her deepest gratitude to Professor Nishioka for providing tremendous favors and inspiring mental support to publish the International journals, join the International conferences, and proceed with the author's study during the time of her doctoral degree.

The author would like to express her deep gratitude to Associate Professor, Dr. Yasuyuki Ota for his kind guidance, support, and enthusiasm during her research and advising ideas during her study for the doctoral degree. The author would like to express her sincere thanks to him for all the enormous technical advice for the content of this work and impressive ideas and detailed reviews to enrich the scientific level of the author and in the publication of the author's work.

The author would like to express special thanks to Dr. Kenji Araki for the great chance to study MATHCAD simulation software under his guidance and enlightened her knowledge with

his great expertise and impressive proficiency in the field of that software. The author would like to acknowledge him for providing suggestions regarding the author's work.

The author would like to acknowledge Dr. Naokazu Kumagai and Dr. Hiroyuki Shinomiya from Hitachi Zosen Corporation for providing the catalyst and literature on the methanation process using catalysts regarding the author's work.

The author would like to express her gratitude to the examiners for providing valuable suggestions, reviews, and ideas to accomplish this thesis book.

The author would like to express her special thanks to Professor Dr. Thi Thi Zin from the University of Miyazaki for providing mental support and motivation during her study in Japan.

The author would like to truly appreciate her supportive and collaborative lab mates and tutors who give support, friendliness, and kindness and create unforgettable memories while her stay in Miyazaki. The author would like to express sincere thanks to her juniors and Eto San for their efforts to communicate and overcome the language barrier and for their warmest endless help to the author for comfortable student life in Miyazaki.

The author would like to express her deepest emotions to her parents and sisters, who always offer strong moral support mentally and physically, care and kindness, and unconditional love throughout her way to proceed with her doctoral degree. The author would like to express her unconditional gratitude to her parents for believing in her abilities during the author's study abroad and always being behind her every time.

List of figures

List of tables

Chapter 1

Introduction

1.1 2050 Carbon neutral network

Greenhouse gas emissions are a critical matter in today's energy production. A growing carbon dioxide emissions and energy demand have been a significant impact on the world climate. Energy usage and supply, especially in electricity, heat, and transport attributed to the greatest proportion of global greenhouse gas emissions as shown in Fig. 1.1 [1–3]. Accordingly, the Paris Agreement set urgent frameworks to maintain the global temperature at 1.5 ℃ or less than 2 ℃ [4]. Following the Paris Agreement at the Paris conference in 2015, 197 signatory parties intended to build a long-term decarbonized pathway to mitigate carbon emissions by 2050. Each signed nation establishes new energy roadmaps and submits its progress every year.

Presently, global electricity and heat generation relies on fossil fuels which are notable energy sources to drive increasing pollution and global temperature. According to the statics, a large amount of CO_2 was emitted by fossil fuel combustion, as shown in Fig. 1.2. In 2017, their emissions for energy production were about 32 Gt [5], and the highest amount was 33 Gt in 2018 [6]. In the 2021 global energy review, the international energy agency (IEA) reported that the global CO_2 emission related to energy and industrial sectors significantly increased in 2021 after a reduction in 2020 during the Covid Pandemic [7]. IEA projected that the global emissions are the potential to increase by approximately 57 Gt in 2050 if the emission continues.

Coal, oil, and gas are the main drivers of increasing fossil fuel combustion, which are induced by worldwide population growth, rapid urbanization, and industrialization. They contributed approximately 80% of global primary energy [1]. Over the past decades, their consumption has significantly increased, as shown in Fig. 1.3. In comparison, coal generates more CO_2 and air pollution than oil and gas. Nowadays, coal consumption is decreasing in

some countries with the awareness of climate change and adopting new technologies. However, oil and gas consumption are still increasing.

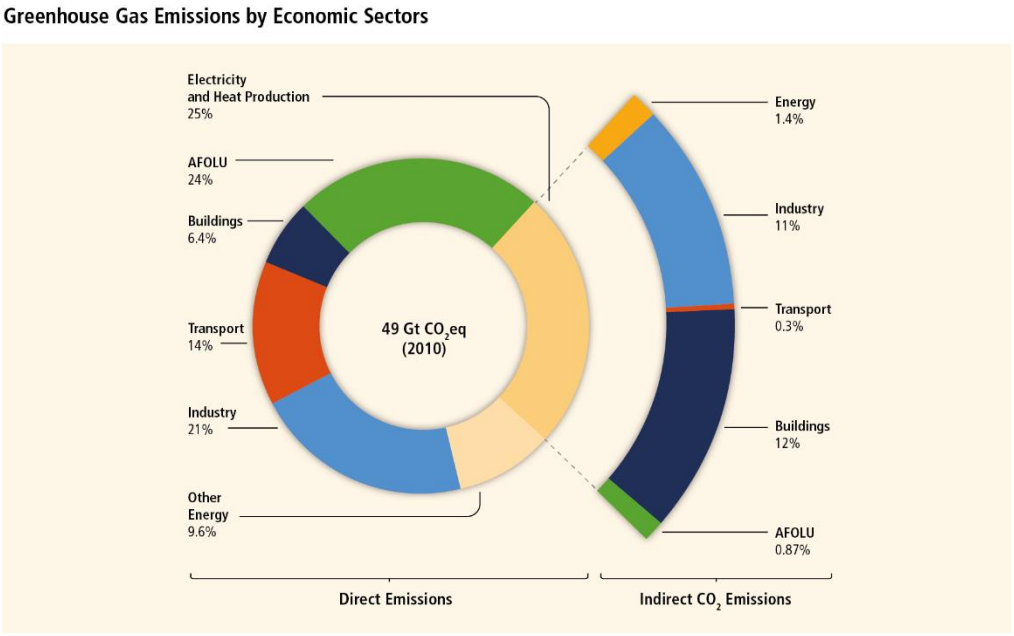

Fig. 1.1 Global GHG emissions per sector. Data provided by ref. 3.

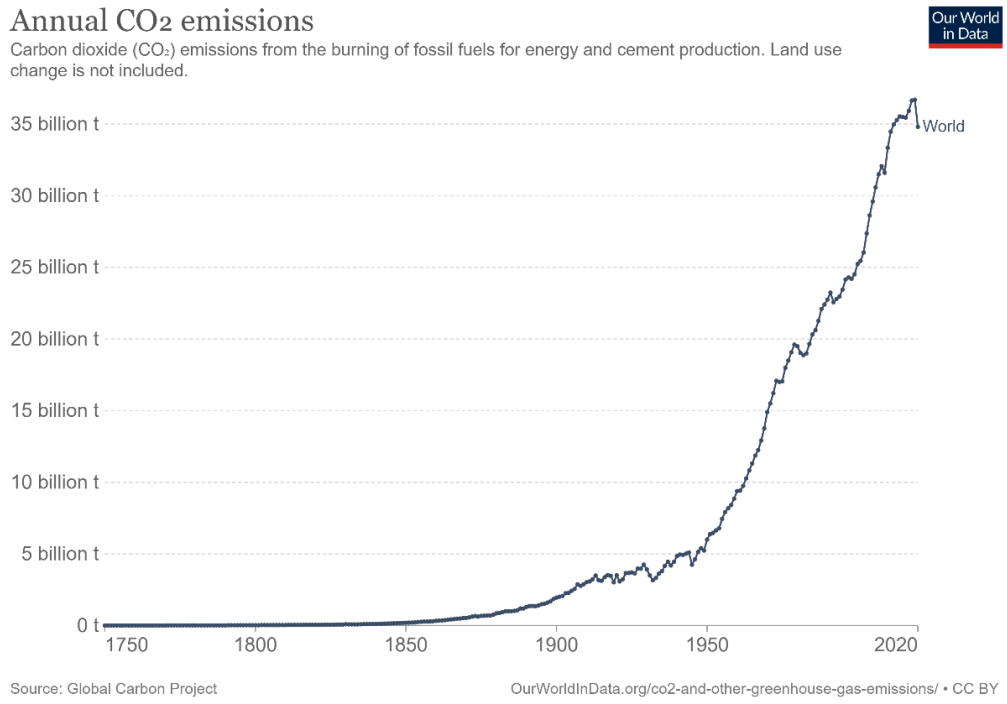

Fig. 1.2 Trend in energy-related global CO_2 emissions from fossil fuel combustion by energy and cement production, 1750-2020. According to the data reported in ref.1.

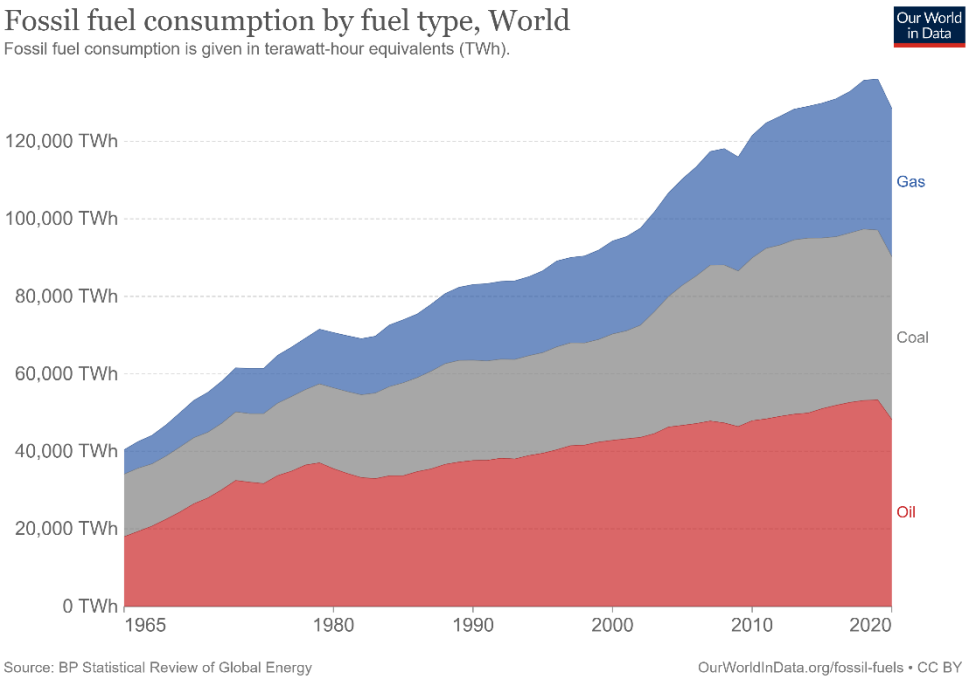

Fig. 1.3 Worldwide fossil fuel consumption by types, 1965-2020. According to the data reported in ref 1.

As a consequence, a new significant energy policy is needed to adopt in all sectors; alternatively, sustainable energy production is required to meet the growing energy demand. Currently, the signatory countries are accelerating roadmaps to develop and deploy 2050 low-carbon technologies. They include realizing sustainable resources by 2030 and 2050 while mitigating carbon usage and emission. In this regard, the electricity supply will provide a decarbonized network through renewable energy and fuel-based generation with carbon capture, storage, and utilization technologies.

1.2 Renewable energy

In the current global energy production, renewable sources are sustainable to bring out a zero-carbon society, especially solar and wind resources. Since 1990, fossil fuels provide about 70% of global electricity generation [1]. Considering all energy perspectives, the most

promising method is to encourage the renewable sector to mitigate CO_2 and other fuels. In the last few decades, renewable technologies have been developed. In the energy roadmap for the 2050 CO_2 reduction scenario, renewable energy will play a vital role in providing long-term electricity production to substitute for fuels [7]. Renewable energy will share almost 50% of global electricity generation in the future energy outlook [2].

Solar (including photovoltaic and concentrator photovoltaic) and wind technologies have been developed over the past years. They shared two-thirds of renewable growth [7]. According to the 2021 BP statistical report, the expansion of global renewable generation is rapidly increasing year by year [8]. The highest growth is in the wind solar power generation, as shown in Fig. 1.4 [7, 8]. Electricity generation by photovoltaic (PV) technology is clean and sustainable since solar radiation is directly converted to electrical energy by solar cells. Nowadays, highly efficient solar cells are commercially available in the world. Besides, several researchers are investigating advanced solar cells and techniques.

Since electricity and energy demand is expected to significant grow with the world's population, renewable capacity is required to cover it. However, voltage mismatching in solar and wind production leads to energy losses when directly integrating into the network. The possible solution to balance the growing demand due to the increasing global population and energy yield from renewable sources is to store the intermittent renewable energy.

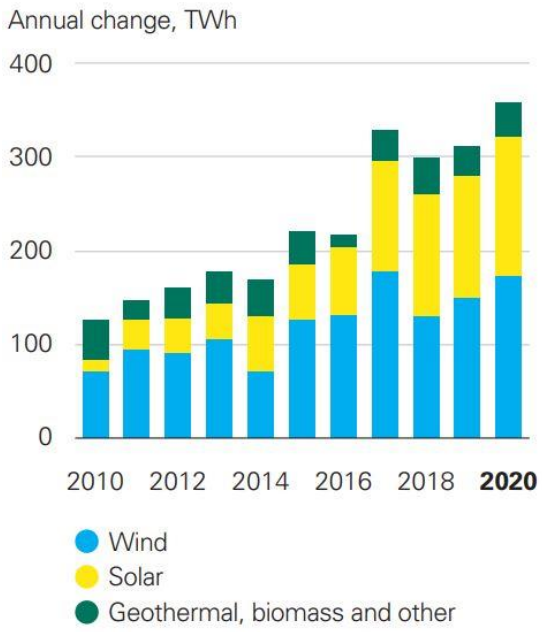

Fig. 1.4 Worldwide annual renewable power generation from 2010-2020. Data copied from ref. 8.

1.3 Power-to-Gas (PtG) pathway

With growing advanced techniques, a major challenge in integrating solar and wind energy production into the energy mix is storage methods to compensate for their intermittent nature. Their electricity production varies with the seasonal condition and cannot be effectively stored for the long term. A stable electricity generation is required to balance supply and demand and penetrate renewable energy into the conventional electrical grid. The renewable pathway will be an environmentally friendly to cover increasing demand if the generated power is effectively stored and discharged. Numerous studies have been analyzed to provide efficient storage technology in solar and wind production, such as flywheels, batteries, super-capacitors, and the energy vectors [9–25].

A flywheel storage system stores electricity as mechanical energy, such as kinetic energy [10]. Then, this kinetic energy is reconverted into electricity via generators, resulting in a high initial cost and requirement of other facilities for such a back-and-forth conversion.

Supercapacitors buffer direct electric field between conducting electrodes [14]. Although these components provide long cycle life of up to 8-10 years [9, 12], their energy density is relatively low, and capital cost is high. While battery storage systems are mature technologies. Various types of batteries are commercially available, and some are in the experimental stage. It stores electrochemical energy in which multiple cells are connected in series or parallel, depending on the desired system [10, 16]. There are conducting electrodes and electrolytes in each cell.

However, these methods provided a short-term whereas energy vectors such as electrolytic hydrogen and synthetic methane could realize a flexible, long-term pathway. Integrating intermittent renewable energy into synthetic natural gas (SNG) is an alternative approach to meet the growing demand and achieve sustainable development goals (SDGs). There will be losses in renewable energy production when generation exceeds the demand. If renewable-based surplus electricity is provided to generate synthetic natural gas, it will act as a flexible energy carrier to the conventional gas grid [10, 11, 15, 26]. Besides, it offers an adaptable storage medium to address the intermittency of solar and wind generation.

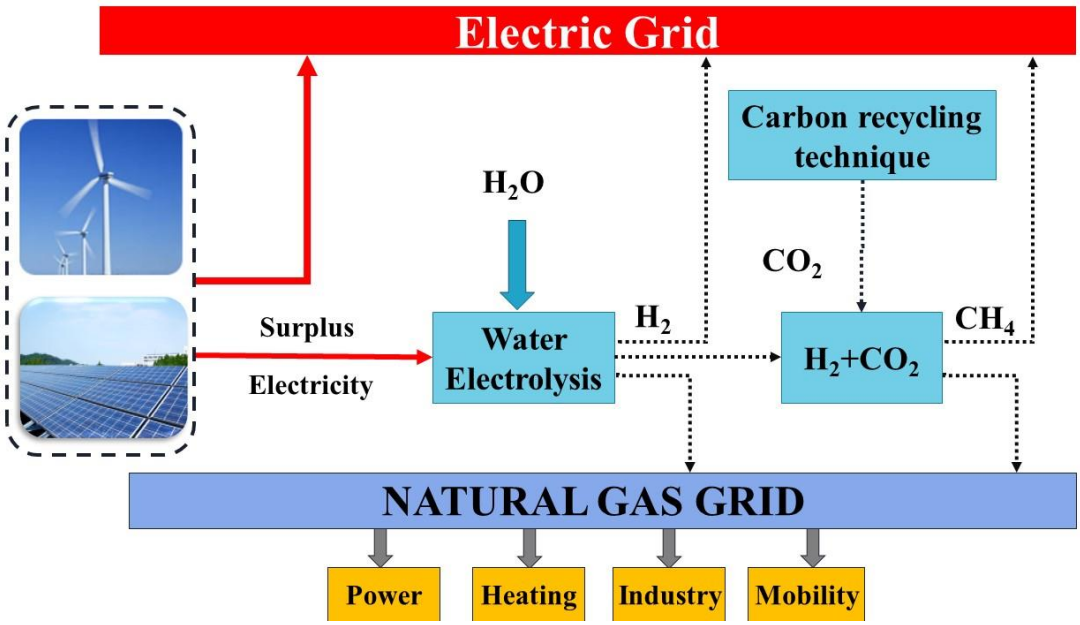

Fig. 1.5 An overview of the power-to-gas concept.

Fig. 1.5 illustrates a concept of a power to gas conversion system. Renewable-based (mainly from solar or wind) energy is transformed into synthetic gases (hydrogen and methane) possessing high energy density that can substitute fossil fuels. In this approach, the electricity generated by the renewables is applied as an input to the electrolysis and Sabatier process. This technology is known as power-to-gas (PtG) as well as power-to-x conversion, depending on the final product. A carbon-free roadmap can be expected from the PtG conversion since the produced synthetic gases can be directly distributed into the natural gas grid [27, 28]. PtG approach offers to store and provide energy in terms of gas through the gas network whereby the gas is sustainable and versatile to apply for several purposes. The PtG method is attractive since the chemical energy can be stored and shipped for long periods.

1.4 Japan's energy policy

As a signatory party to the Paris Agreement, the Japanese Government proposed long-term plans to reduce GHG emissions to 26% compared to 2013 levels and 40% in the residential sector by 2030 [29–31]. In this 2030 outline, nuclear energy will provide 20–22% of the nation's electricity, as shown in Fig. 1.6. On the other hand, renewable will cover 22–24%, and fossil fuels account for 56% [32–35]. In Japan, 90% of country-wide CO_2 emission is related to the energy sector [36]. So, the Government of Japan aimed to achieve carbon neutrality, especially in energy and industrial infrastructure, followed by transport sectors.

The Fukushima disaster in 2011 has deepened to accelerate the development of renewable networks in Japan. Japan's energy supply is currently dependent on fossil fuels imported from abroad, and the import price is relatively high [30, 36, 37]. In addition, as a global, Japan is the fifth-largest CO_2 emission country [30, 38]. Following the newest policy upgraded in 2020, the Government of Japan is making efforts to realize a 2050 carbon-neutral network through PtG conversion, hydrogen production, carbon capture, storage, and utilization. In this context, the renewable sector occupies 50–60% of nationwide electricity generation, and nuclear and fossil

fuel-fired power equipped with carbon recycling techniques supply 30–40%, as shown in Fig. 1.7. Whereas hydrogen and ammonia, combustion will share the rest of 10% [30].

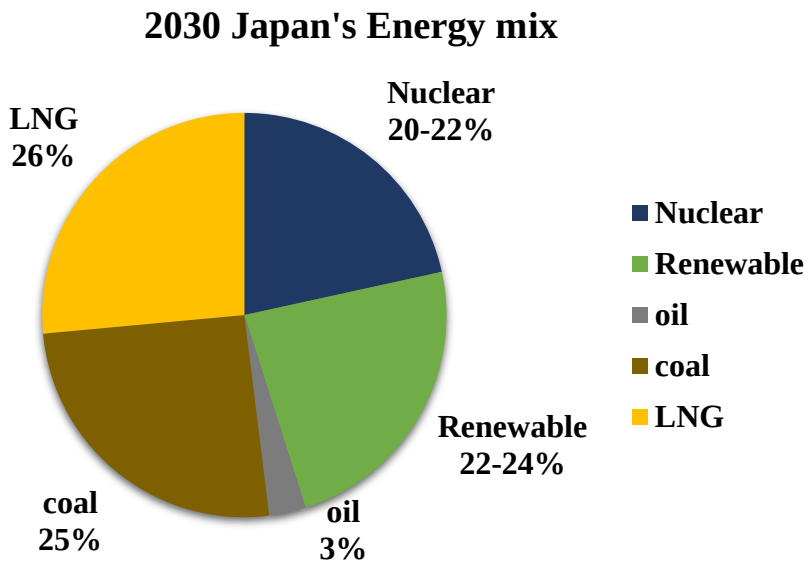

Fig. 1.6 Projected energy mix of Japan in 2030. Data source: METI.

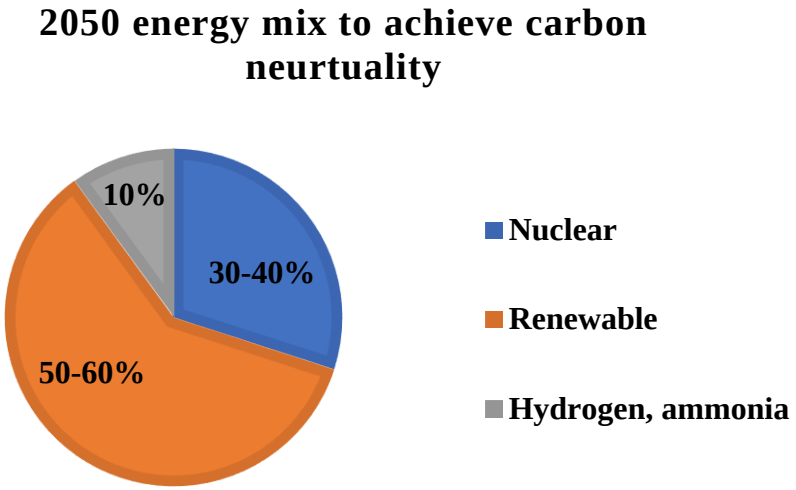

Fig. 1.7 2050 energy mix of Japan to achieve carbon neutrality in 2050. Data source: METI.

However, nuclear power is required to improve and conform to safety regulations on both existing and new plants, although it is well-established decarbonized technology. Besides, there are no commercially operating plants for fossil fuel power with carbon capture and recycling. It has led to an increase in the share of renewables. It is an economically friendly perspective way to expand renewable energy in Japan. Currently, the Japanese Government is encouraging innovative technologies such as next-generation solar cells with cost reduction. Renewable energy is expected as a long-term primary source in the power sector [37]. Surplus renewable electricity is aimed to deploy in synthetic gas production by 2050 to balance the supply and demand.

Hydrogen will be an alternative key to apply in the transport sector or as a sustainable fuel since its combustion does not emit any greenhouse gas effects. Recently, the Japanese Government is accelerating hydrogen production technologies (such as from renewable sources and industrial processes) and its use in fuel cell vehicles. Carbon-free green hydrogen production is expected to realize in 2050 [37]. Electric vehicles operated by hydrogen gas have been introduced to the market. However, hydrogen power generation is in the developing stage [39]. Hydrogen can contribute decarbonized network if the renewable-based hydrogen is available and utilized as a fuel in the transport sector. For a while, carbon recycling technologies are being advanced and proposed to emerge with cost reduction in 2030 [29, 40, 41].

Subsequently, Japan's PtG concept is gaining attention as an additional roadmap to a carbon-neutral network. Renewable solar and wind energy production is being accelerated in Japan. As shown in Fig. 1.8, a whole process would be a clean and sustainable approach and simultaneously reduce the dependency on foreign imported fuels if the surplus electricity is provided to generate hydrogen and methane.

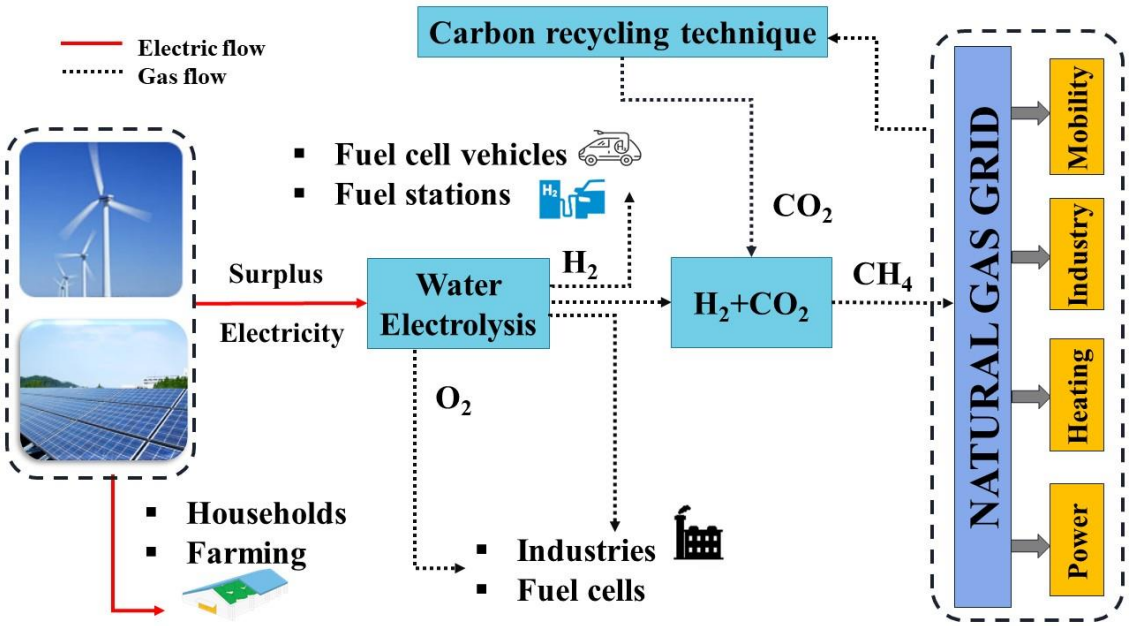

Fig. 1.8 A power to the gas concept as a roadmap of carbon-neutral society in Japan.

1.5 Hydrogen

According to the energy technology perspectives 2020, the electricity demand is expected to increase with the increasing population. With a rapid increase in fuel cell vehicle sales and developments, hydrogen demand will grow in future energy scenarios. In today's industrial hydrogen production, its primary supply is a non-renewable fossil fuel that results in significant greenhouse gas emissions. Most of its production is from natural gas and coal, while a small fraction is from the electrolysis process. This production from fossil sources could be effective in the short term if carbon recycling technology is adopted in hydrogen production industries. However, the whole process would increase the capital cost unless a cost-effective carbon recycling method was not developed. On the contrary, sustainable, and eco-friendly hydrogen can be obtained through simple electrolysis with renewable surplus energy. Since water decomposition only releases hydrogen with by-product oxygen, it has attracted various attention to researchers providing carbon-free fuel.

Besides, renewable-based hydrogen is promising and attaining three times higher specific energy density per mass than gasoline and kerosene. It has taken advantage of fossil fuel substitutes and flexible energy carriers in industries, transportation, and power-to-gas conversion. It can be employed in several ways and converted back to electricity. Besides, the generated hydrogen can further be utilized in synthesizing other fuels and methane; as a result, the whole process minimizes the carbon footprint. Beyond 2030, hydrogen will be a primary fuel for Japan's future energy as an environmentally and economically footprint. Fuel-cell electric vehicles powered by hydrogen have been launched and commercially available both in Japan and globally. In addition, several hydrogen fuelling stations are in operation and promoting [42–44]. By 2050, the share of hydrogen is expected to increase in Japan and contribute to 13% of the nation's energy supply [39, 43]. Currently, technical developments in hydrogen research are being accelerated in Japan.

1.5.1 Types of water electrolysis

Nowadays, various methods and studies on hydrogen production from renewable sources have been established. The simple technique to generate large-scale hydrogen is water electrolysis since water is one of the most abundant natural sources in the world. Depending on the electrolytes used for the electrolysis, the type of the electrolyzer and their operations are different. Commercially available methods are alkaline electrolysis (AEL) and proton exchange membrane (PEM) electrolysis. In that former type, the primary solution to perform electrolysis is an aqueous solution, and OH^- ions are the major carrier to generate hydrogen. The latter is also known as the polymer electrolyte membrane method. In the PEM type, deionized or ultrapure water is utilized, and H^+ ions are moved through the membrane to produce hydrogen. While high-temperature solid oxide method is promising and currently in the development phase. Accordingly, the concepts of two mature technologies (AEL and PEM) are provided in this section.

1.5.1.1 AEL electrolysis method

Alkaline technology is well-established and cost-effective one among the electrolysis method. As shown in Fig. 1.9, the AEL electrolyzer consists of a permeable membrane, two electrodes, and an electrolyte (KOH or NaOH solution). Aqueous electrolytes are provided, and the membrane separates the two electrodes are immersed in the aqueous solution. During the electrolysis process, hydroxide (OH^-) ions are moved through the electrolyte, as shown in equations (1) and (2). It normally operates within a temperature of 70–140 °C and pressure of 1–200 bars [45]. It provides 60–70% efficiency [46].

$$\text{Anode reaction: } 2OH^- \rightarrow 1/2O_2 + H_2O\ (l) + 2e^- \quad (1)$$

$$\text{Cathode reaction: } 2H_2O\ (l) + 2e^- \rightarrow H_2\ (g) + 2OH^- \quad (2)$$

AEL electrolysis is suitable for large-scale production. Although it is economically well-developed, it remains drawbacks in system operation, such as hydrogen gas permeation, low operating current densities, and corrosion due to electrolytes.

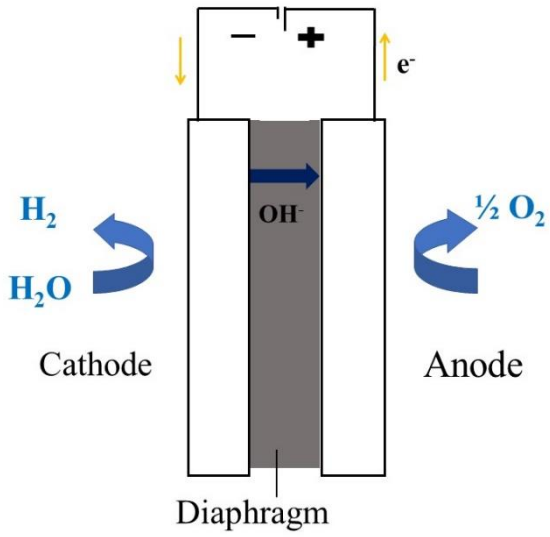

Fig. 1.9 Overview configuration of AEL electrolysis.

1.5.1.2 PEM electrolysis

Whereas the PEM method provides flexible advantages over AEL, which include providing high current density, compact design, and high energy conversion efficiency [47–58]. A PEM electrolyzer is composed of a thin-film membrane electrode. Nafion membrane performs as a separator in which noble anode and cathode catalysts are attached at both ends of the membrane, as shown in Fig. 1.10. Only pure water is provided to the system, which splits into a proton (H^+) and oxygen at the anode. Then, H^+ ions are passed through the electrode membranes. As provided in equations (3) and (4), hydrogen gas is generated at the cathode. PEM electrolyzers are efficient about 65–85% [46].

$$\text{Anode reaction: } H_2O\ (l) \rightarrow 2H^+ + 2e^- + 1/2O_2\ (g) \quad (3)$$

$$\text{Cathode reaction: } 2H^+ + 2e^- \rightarrow H_2\ (g) \quad (4)$$

The system provides highly pure (99.99%) hydrogen. It is suitable for small-scale production, while up to now, there are challenging obstacles like high-cost novel catalysts and degradation aspects on PEM cells. Various researchers are conducted to develop the system's performance and reduce its high capital costs on low-cost metal catalysts.

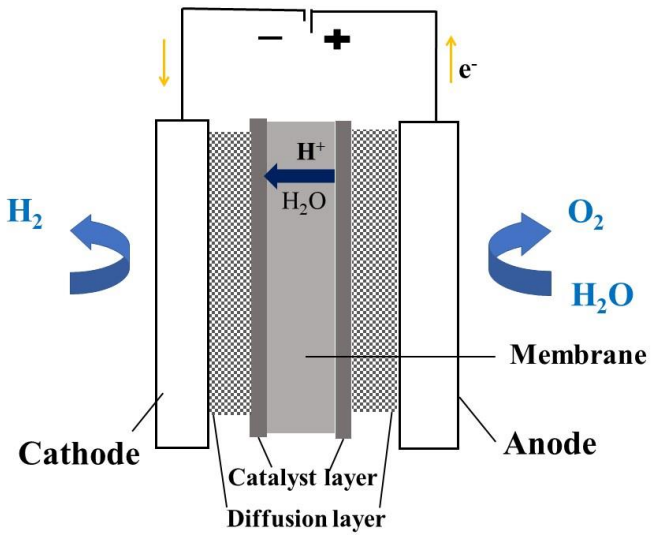

Fig. 1.10 Overview configuration of PEM electrolysis.

1.6 Methane

In addition to hydrogen, renewable energy can bring out synthetic methane with a further step of carbon dioxide hydrogenation. There were numerous efforts to develop ways to capture CO_2 and reuse it as a feedstock to lessen the CO_2 emission. As an alternative pathway, CO_2 can be transformed into various carbon-based compounds such as methanol, hydrocarbon fuels or methane, esters, ethers, and etc [59]. Although hydrogen provides attractive advantages, its technologies still have challenging issues to improve in storing gas, transportation, and combustion. Combining technologies, renewable surplus electricity, and CO_2 is the key promoter for renewable production and recycling CO_2. CO_2 can be captured through biomass gasification [60] and fermentation [61]. Several studies have been conducting to integrate the captured CO_2 and H_2 to obtain fuels such as methanol or ethanol [62, 63]. But the technique requires further analysis to develop commercially in infrastructures.

Hydrogen-based methane production is a flexible and prospective route to employing renewable energy as an effective alternative to diminishing carbon footprint and fossil fuel. Natural gas, mainly composed of methane, is a well-known core fuel in the global energy system. If methane is produced from non-fossil sources and used as a fuel, its combustion offers fewer pollutants and greenhouse gas emissions, providing better environmental benefits. Additionally, it contains a higher energy density than H_2 and other fossil fuels. Methane can be generated via CO_2 hydrogenation through catalyst-packed reactors under renewable energy. Herein, hydrogen driven from renewable energy through water splitting and CO_2 in a pure state or carbon recycling are used as reactants in methanation reactions.

Recently, there has been increasing interest in solar-driven carbon-based fuels such as methane. The storage gas is versatile to reconvert to electricity, apply to heating and cooling, and to use as a fuel in the transportation sector. The system is more flexible to connect to the conventional gas grid. The infrastructures for methane transportation and combustion

technologies have been established. Besides, generated CO_2 can be recycled after methane combustion. Alternatively, it can consecutively utilize as a feedstock in the Sabatier reaction through carbon recycling techniques. The integration of two technologies: renewable-based hydrogen and Sabatier reaction, does not emit CO_2 into the atmosphere and can repeatedly apply CO_2 into the system. In this way, the resulting methane is a sustainable and promising candidate for carbon neutrality if the carbon capture and utilization technology are realized.

1.6.1 Biological methanation

The methanation process can be performed chemically or biologically, in which the latter is applied in biogas production. This technique has been known for the past few decades; however, there are still requirements to develop technically. In this process, a biocatalyst, microorganism, is provided to proceed with the conversion. The biological methanation process operates at low temperatures (30-60 °C), whereas the reaction is slow, has limitations in massive hydrogen transfer, and is less flexible [27, 64]. Since the reaction proceeds in the aqueous solution with the support of a microorganism, the challenging issue is the poor solubility of hydrogen fed to the reaction. It results in a low reaction rate and conversion, and needs multiple consecutive reactors compared to an adiabatic fixed-bed type [27]. Accordingly, several concepts of reactors are being established to reduce these limitations [27, 65].

1.6.2 Sabatier reaction

In this section, the operating parameters related to catalytic methanation are discussed. Hydrogenation of CO_2 on hydrogen obtained by the renewable-based electrolysis is known as the Sabatier reaction [27, 28, 64, 65], as below:

$$CO_2 + 4H_2 \rightleftharpoons CH_4 + 2H_2O \quad \Delta H^\circ_{298} = -164.9 \text{ kJ/mol} \qquad (1)$$

Depending on the operating parameters such as temperature and catalysts, undesired kinetic barriers like CO formation (which is known as reverse water gas shift reaction) and catalyst

sintering can initiate. Providing low temperatures is required due to this reason since these barriers are mostly preferred at a high-temperature operation [27, 64, 66–73]. The methanation reaction is an exothermic process, and it releases extreme heat during the process. In addition, thermodynamic equilibrium limits this reaction. The conversion to methane can be enhanced at low operating temperatures. Typically, the operating parameters are between 200 and 500 °C [27, 64].

Since the thermodynamic equilibrium of the methanation favors low temperatures, it requires a high catalyst to enhance methane yield within low temperatures. The preferable noble catalysts in the Sabatier reaction are Group VIII metals such as Ru, Rh, Ni, Co, Pd, Pt, Ir, and Fe [74]. Herein, Ni-based catalysts are widely used in CO_2 methanation due to their low cost and high CO_2 to methane selectivity [68, 69, 75–81]. In addition, another material is required to support the activity of Group VIII catalysts. State of the literature review, Ni supported Al_2O_3, TiO_2, SiO_2, CeO_2, MgO, ZrO_2, and zeolite catalysts have been commonly examined to promote the conversion efficiency of CO_2 to methane [69, 70, 76, 77, 82–84]. Besides, various research efforts have been endeavored to enhance the catalytic activity using different synthesis action processes [65, 72, 73, 85–90].

Besides temperature and catalysts, the types of reactors coupled with them are also crucial factors in the Sabatier reaction. The process releases extreme heat during the reaction. Accordingly, it requires selecting the appropriate reactors that can relatively cope with the heat to avoid damage to the catalysts. In some cases, the released heat is effectively provided to the system. There are various reports about the types of reactors that can adapt to methanation [86, 91–98]. The most commercialized designs are fluidized-bed reactors and adiabatic fixed bed reactors. Fixed-bed adiabatic reactors packed with catalyst pellets are commonly used in the methanation process [27]. These rectors have been utilized in industrial operations. However, controlling temperature and heat dissipation in that type can be challenging because a hot spot

can favor heat management [99, 100]. Fixed-bed reactors require multiple reactors (at least two) in series connection since heat exchange are typically provided within or between the rectors to cool the reactant gases before passing to the next reactor. By doing so, the reaction temperature of the next reactors becomes reduced and attains a high conversion. However, this may cause undesired energy losses. Among the other types of reactors, fixed-bed adiabatic reactors are a simple design, have low investment costs, and well-established method [64].

1.6.2.1 Effects of parameters

As mentioned above, the reactor temperature and the supported catalysts are the primary cores of the methanation system. Additionally, the performance of reactors is essential to withstand the released heat and adapt to the quick temperature change during the reaction without affecting the catalysts. Catalysts can be degraded by the operating parameters, especially the temperature. Catalyst sintering or cracking is typically proceeded by this temperature variation and significantly minimizes their activity. It is a process where the catalyst suffers a loss in the active area due to physical change when it is subjected to a high temperature. Furthermore, coke or carbon formation is one of the common undesired barriers since hydrocarbons are decomposed at high temperatures approximately above 500 °C resulting in coke. When the coke deposits, it will deactivate the catalyst [27, 101].

Accordingly, it is required to emphasize the operating temperature concerning applied catalysts. Alternatively, selecting efficient catalysts that exhibit comparatively high activity in low-temperature operations is crucial. Nowadays, the concepts of reactors have already been developed with their optimum characteristics. Several studies have been conducted on the performance activity of various catalysts while maintaining a high methane selectivity. Moreover, numerous research groups have focused on selecting the appropriate temperature that can provide the highest conversion while the type of catalyst is fixed.

1.7 Objectives of the research

This study aims to analyze the solar to gas conversion concerning the operation parameters under actual field operation and to provide the potential conversion efficiency in Japan based on the outdoor test performed at the Nishioka Laboratory, the University of Miyazaki.

Problem statement

1. Unlike hydrogen production, the methanation system is complex because the reaction is thermodynamically limited by temperature. Therefore, we analyzed the system operation to provide a high methane conversion with an optimum operating condition.
2. After many experiments, we found that the methanation energy consumption is related to the rector's temperature and hydrogen flow rate. The conversion efficiency can be improved by decreasing the reactor's energy consumption. The energy consumption decreased by providing a stable and moderate hydrogen flow rate. Hydrogen production fluctuates on the electricity provided by solar energy. In this study, it was consecutively applied to the methanation. Therefore, it is crucial to identify the minimum hydrogen flow rate required for the rection. The higher the flow rate, the faster the reaction with a high temperature.

   To investigate this, we controlled hydrogen flow and analyzed the energy consumption while maintaining the maximum conversion efficiency and minimizing the temperature.
3. To realize the solar to gas conversion in Japan, it is essential to estimate the potential conversion efficiency of the intended places before implementation. Additionally, conversion efficiency is a crucial factor in estimating the overall capital cost of the system. Therefore, we approached the potential conversion efficiency at 837 places in Japan based on the optimum outdoor results.

1.8 Outlines of thesis

This thesis is organized and divided as follows:

Chapter 1

This chapter aims to introduce the basic knowledge and general introduction to proceed with the following chapters. It includes the concept of the system, objectives of the research, and outlines of this thesis.

Chapter 2

This chapter provides an approach to the solar-to-gas conversion system installed at the University of Miyazaki, Japan. The concept of outdoor solar to hydrogen and solar to methane systems is described in detail. Additionally, the components of actual solar to gas conversion, such as concentrator photovoltaics, the DC/DC converters, the electrochemical cells, and the methanation system, are provided. The experimental procedures and attempts to perform the methanation system are fully described. The methanation system was investigated on sunny days and cloudy days. The operation parameters and methane concentration were analyzed. It also describes the estimation methods for solar to methane conversion efficiency. The concept of methanation energy consumption is outlined in this section.

Chapter 3

Chapter 3 focuses on a detailed analysis to better understand the power consumption of the methanation system on the hydrogen generation. The factors increasing its consumption are reviewed to improve the system with less energy consumption. Although the heat released during the reaction maintains the reaction and reduces power consumption, extreme heat can result in catalyst degradation. Therefore, it is crucial to decrease the heat without increasing the power consumption while improving the methane concentration.

The reaction rate is mainly dependent on the flow rate of the feed gases, and it is the main factor of the reaction heat. Furthermore, hydrogen from the solar-based electrolysis is provided

to the methanation system. Therefore, in this section, the influence of hydrogen flow rate on the energy consumed by the Sabatier reaction is highlighted. In addition, methane concentration is analyzed at various hydrogen generation rates. Improving or maintaining the methane concentration while minimizing the operation temperature and power consumption is also important.

Chapter 4

In this section, an approach to estimate the potential solar-to-hydrogen and solar-to-methane conversion efficiencies at 837 places in Japan is expressed in detail. It is important to identify the efficient system providing a high conversion on the intended locations prior to realizing the outdoor implementation. Based on the outdoor results, nationwide annual solar-to-gas conversion efficiency from the flat-PV modules was proposed and approximated. The simulation concept to approach the conversion efficiencies of each part is fully described. The nationwide forecasted results are provided in graphs. In addition, the types of PV that can provide efficient solar to gas conversion in Japan are discussed in this chapter.

Chapter 5

This chapter summarizes and concludes the present study. It wraps up the concept and wraps up each chapter. It also discusses the potential to improve the system in the future.

References

[1] Ritchie H, Roser M, Rosado P. CO_2 and greenhouse gas emissions. Our World in Data. Available online: https://ourworldindata.org/co2-and-other-greenhouse-gas-emissions. [Accessed on 22 February 2022].

[2] IEA (Jul 2009). Energy technology perspectives 2010: scenarios and strategies to 2050. Available online: https://doi.org/10.1787/energy_tech-2010-en [Accessed on 22 February 2022].

[3] IPCC. Climate change 2014: mitigation of climate change. Contribution of working group III to the Fifth assessment report of the Intergovernmental panel on the climate change. Cambridge Univ Press. 2014. Cambridge, United Kingdom and New York, NY, USA. Available online: https://www.ipcc.ch/site/assets/uploads/2018/02/ipcc_wg3_ar5_full.pdf [Accessed on 22 February 2022].

[4] UNFCC. Adoption of the Paris Agreement. Report No. FCCC/CP/2015/L.9/Rev.1. 2015. Available online: http://unfccc.int/resource/docs/2015/cop21/eng/l09r01.pdf [Accessed on 22 February 2022].

[5] Birol F. CO_2 emissions from fuel combustion highlight 2019 edition. International energy agency.

[6] IEA (Mar 2019). Global energy and CO_2 status report: the latest trends in energy and emissions in 2018. Available online: https://iea.blob.core.windows.net/assets/23f9eb39-7493-4722-aced-61433cbffe10/Global_Energy_and_CO2_Status_Report_2018.pdf [Accessed on 22 February 2022].

[7] IEA. Global energy review 2021: assessing the effects of economic recoveries on global energy demand CO_2 emissions in 2021.

[8] Looney B. BP statistical review of world energy. 70th edition. July 2021. Available online: https://www.bp.com/content/dam/bp/business-sites/en/global/corporate/pdfs/energy-

economics/statistical-review/bp-stats-review-2021-full-report.pdf. [Accessed on 22 Feb 2022].

[9] Ibrahim H, Ilinca A, Perron J. Energy storage systems characteristics and comparisons. Renew Sust Energ Rev. 2008; 12(5):1221–1250.

[10] Koohi-Kamali S, Tyagi V, Rahim N, Panwar N, Mokhlis H. Emergence of energy storage technologies as the solution for reliable operation of smart power systems: a review. Renew Sust Energy Rev. 2013; 25: 135–65.

[11] Joerissen L, Garche J, Fabjan CH, Tomazic G, Possible use of vanadium redox-flow batteries for energy storage in small grids and stand-alone photovoltaic systems, J. Power Sources. 2004; 127: 98–104.

[12] Diam TU, Li X, Kim J, Simms S. Evaluation of energy storage technologies for integration with renewable electricity: quantifying expert opinions. J Environ Innov Soc Trans. 2012; 3: 29–49.

[13] Barton JP, Infield DG. Energy storage and its use with intermittent renewable energy, IEEE Trans. Energy Convers. 2004; 19: 441–448.

[14] Díaz-González F, Sumper A, Gomis-Bellmunt O, Villafáfila-Robles R. A review of energy storage technologies for wind power applications. Renew Sust Energ Rev. 2012;16(4): 2154–71.

[15] Hill CA, Such MC, Chen D, Gonzalez J, Grady WM, Battery energy storage for enabling integration of distributed solar power generation. IEEE Trans on Smart Grid vol. 2012; 3: 850–857.

[16] Divya K, Østergaard J. Battery energy storage technology for power systems—an overview. J Electr Power Syst Res. 2009; 79: 511–520.

[17] Veszpremi K, Schmidt I. Flywheel energy storage drive for wind turbines. Proceedings of IEEE 7th International Conference on power Electronics and Drive Systems; Nov 27-30; Bangkok, Thailand: IEEE; 2007. p. 916–923. doi.org/10.1109/PEDS.2007. 4487814.

[18] Kollimalla SK, Mishra MK, Narasamma NL. Design and analysis of novel control strategy for battery and supercapacitor storage system. IEEE Trans Sustainable Energy. 2014; 5: 1137–1144.

[19] Ongaro F, Saggini S, Mattavelli P, Li-Ion battery-supercapacitor hybrid storage system for a long lifetime, photovoltaic-based wireless sensor network. IEEE Trans Power Electron. 2012; 27: 3944–3952.

[20] Ineneji C.; Bamisile O.; Kusaf M. Super-Capacitors as an Alternative for Renewable Energy Unstable Supply. Acad. Perspect. Procedia. 2018; 1: 11–20.

[21] Orecchini F. The era of energy vectors. Int J Hydrogen Energ. 2006; 31; 1951–1954.

[22] Abdin Z, Zafaranloo A, Rafiee A, Merida W, Lipinski W, Khalilpour KR. Hydrogen as an energy vector. J Renewable Sust Energ Reviews. 2020; 120: 109620.

[23] Guilbert D, Vitale G. Hydrogen as a clean and sustainable energy vector for global transition from fossil-based to zero-carbon. Clean Technol. 2021; 3(4): 881–909.

[24] Mandal TK, Gregory DH. Hydrogen: future energy vector for sustainable development. Proceedings of the Institution of Mechanical Engineers, Part C: J of Mechanical Engineering Science. 224(3); 539–558. https://doi.org/10.1243/09544062JMES1774.

[25] De Saint Jean M, Baurens P, Bouallou C. Parametric study of an efficient renewable power-to-substitute-natural-gas process including high-temperature steam electrolysis. Int J Hydrogen Energ. 2014; 39: 17024–17039.

[26] Ramchandran R, Menon RK. An overview of industrial uses of hydrogen. Int J Hydrogen Energ. 1998; 23 (7): 593–598.

[27] Gotz M, Lefebvre J, Mors F, McDaniel K, Graf F, Bajohr S, et al. Renewable power-to-gas: a technological and economic review. J Renew Energ. 2016; 85: 1371–1390.

[28] Muller K, Fleige M, Rachow F, Schmeiber D. Sabatier based CO_2-methanation of flue gas emitted by conventional power plants. J Energ Procedia. 2013; 40: 240–248.

[29] NEDO. Environment D. NEDO's environmental technology activities in 2021. December 2021. Available online: https://www.nedo.go.jp/content/100900128.pdf. (Accessed on 28 February 2022).

[30] IEA. Japan 2021 energy policy review. Available online: https://iea.blob.core.windows.net /assets/3470b395-cfdd-44a9-9184-0537cf069c3d/Japan 2021_EnergyPolicyReview.pdf. [Accessed on 03 March 2022].

[31] Government of Japan (2020). Submission of Japan's nationally determined contribution. https://www4.unfccc.int/sites/ndcstaging/PublishedDocuments/Japan%20First/SUBMISSION%20OF%20JAPAN'S%20NATIONALLY%20DETERMINED%20CONTRIBUTION%20(NDC).PDF [Accessed on 03 March 2022].

[32] METI (2015) Long-term energy supply and demand outlook. Available online: https://www.meti.go.jp/english/press/2015/pdf/0716_01a.pdf [Accessed on 03 March 2022].

[33] Climate Policy. 2030 outlook for energy supply and demand. Available online: https://www.climatepolicydatabase.org/policies/2030-outlook-energy-supply-and-demand [Accessed on 03 March 2022].

[34] Nagashima M. Japan's hydrogen strategy and its economic and geopolitical implications. October 2018. Etudes de l'ifri, IFRI. Available online: https://www.ifri.org/sites/default/files/atoms/files/nagashima_japan_hydrogen_2018_.pdf. [Accessed on 03 March 2022].

[35] METI, Japan's energy 2020. Available online: https://www.enecho.meti.go.jp/en/category/brochures/pdf/japan_energy_2020.pdf [Accessed on 03 March 2022].

[36] Government of Japan (2019). The long-term strategy under the Paris Agreement. Available at: https://unfccc.int/sites/default/files/resource/The%20 Long-term%20Strategy%20under%20the%20Paris%20Agreement.pdf.

[37] Government of Japan (2020). The long-term strategy under the Paris Agreement. Available at: https://unfccc.int/sites/default/files/resource/Japan_LTS2021.pdf.

[38] IEA. Global energy and CO_2 status report. Available at: https://iea.blob.core.windows.net/assets/23f9eb39-7493-4722-aced-61433cbffe10/Global_Energy_and_CO2_Status_Report_2018.pdf.

[39] Iida S, Sakata K. Hydrogen technologies and developments in Japan. Clean Energ. 2019; 3(2): 105–113.

[40] Yamagata H. Carbon capture and storage activities in Japan. Feasibility study of the Ministry of Economy, Trade and Industry, Japan. 2006. Available online: https://www.cslforum.org/cslf/sites/default/files/documents/Japan_CCS.pdf. (Accessed on 28 February 2022).

[41] Japan METI. Japan's action toward public implementation of carbon recycling (progress over the past year). October 2021. Ministry of Economy, Trade, and Industry. Available online: https://carbon-recycling2021.go.jp/en/doc/211004e.pdf. (Accessed on 28 February 2022).

[42] IEA. The future of hydrogen, IEA, Paris, 2019. https://www.iea.org/reports/the-future-of-hydrogen.

[43] Arias J. Hydrogen and fuel cells in Japan. EU-Japan Center for Industrial Cooperation, Tokyo, 2019.

[44] Hydrogen and Fuel Cell Strategy Council J. The strategic road map for hydrogen and fuel cells: industry-academia-government action plan to realize a hydrogen society. March 2019. Available online: https://www.h2knowledgecentre.com/content/government620.

[45] Sterner M. Bioenergy and renewable power methane in integrated 100% renewable energy systems. Limiting global warming by transforming energy systems. Dissertation; 2009.

[46] Hollady JD, Hu J, King DL, Wang Y. An overview of hydrogen production technologies. Catal Today. 2019; 139: 244–260.

[47] Guo Y, Li G, Zhou J, Liu Y. Comparison between hydrogen production by alkaline water electrolysis and hydrogen production by PEM electrolysis. IOP Conf. Ser. Earth Environ. Sci. 2019; 371: 042022.

[48] Carmo M, Fritz DL, Mergel J, Stolten D. A comprehensive review on PEM water electrolysis. Int J Hydro Energ. 2013; 38: 4901–4934.

[49] Zeng K, Zhang D. Recent progress in alkaline water electrolysis for hydrogen production and applications. Prog Energ Combust Sci. 2010; 36: 307–326.

[50] Grigoriev SA, Porembsky VI, Fateev VN. Pure hydrogen production by PEM electrolysis for hydrogen production. Int J Hydrogen Energ. 2006; 31(2): 171–175.

[51] Feng Q, Yuan XZ, Liu G, Wei B, Zhang Z, Li H, Wang H. A review of proton exchange membrane water electrolysis on degradation mechanisms and mitigation strategies. J Power Sources. 2017; 366: 33–55.

[52] Marshall A, Borresen B, Hagen G, Tsypkin M, Tunold R. Hydrogen production by advanced proton exchange membrane (PEM) water electrolysers reduced energy consumption by improved electrocatalysis. Energy. 2007; 32: 431–436.

[53] Ayers KE, Capuano CB, Anderson EB. Recent advances in cell cost and efficiency for PEM-based water electrolysis. ECS Trans. 2012; 41: 15–22.

[54] Barbir F. PEM electrolysis for production of hydrogen from renewable energy sources. Sol Energ. 2005; 78 (5): 661–669.

[55] Ayers KE, Anderson EB, Capuano CB, Carter B, Dalton L, Hanlon G, et al. Research advances towards low cost, high efficiency, PEM electrolysis. ECS Trans. 2010; 33: 3–15.

[56] Rakousky C, Keeley GP, Wippermann K, Carmo M, Stolten D. The stability challenge on the pathway to high-current-density polymer electrolyte membrane water electrolyzers. Electochim Acta. 2018; 278: 324–331.

[57] Millet P, Andolfatto F, Durand R. Design and performance of a solid polymer electrolyte water electrolyzer. Int J Hydrogen Energ. 1996; 21: 87–93.

[58] Song S, Zhang H, Ma X, Shao Z, Baker RT, Yi B. Electrochemical investigation of electrocatalysts for the oxygen evolution reaction in PEM water electrolyzers. Int J Hydrogen Energ. 2008; 33: 4955–4961.

[59] Wambach J, Baiker A, Wokaun A. CO_2 hydrogenation over metal/zirconia catalysts. Phys Chem Chem Phys. 1999; 1: 5071–5080.

[60] Inayat A, Ahmad MM, Yusup S, Mutalib MIA. Biomass steam gasification with in-situ CO_2 capture for enriched hydrogen gas production: a reaction kinetics modelling approach. Energies. 2010; 3: 1472–1484.

[61] Zhang Q, Nurhayati, Cheng CL, Nagarajan D, Chang JS, Hu J, Lee DJ. Carbon capture and utilization of fermentation CO_2: integrated ethanol fermentation and succinic acid production as an efficient platform. Applied Energ. 2017; 206: 364–371.

[62] Salkuyeh YK, Adams II TA. Co-production of olefins, fuels, and electricity from conventional pipeline gas and shale gas with near-zero CO_2 emissions. Part I: process development and technical performance. Energies. 2015; 8(5): 3739–3761.

[63] Ramachandriya KD, Kundiyana DK, Sharma AM, Kumar A, Atiyeh HK, Huhnke RL, Wilkins MR. Critical factors affecting the integration of biomass gasification and syngas fermentation technology. AIMS Bioengineering. 2016; 3(2): 188–210.

[64] Ghaib K, Ben-Fares FZ. Power-to-methane: a state-of-the-art review. Renew Sust Energ Reviews. 2018; 81: 433–446.

[65] Gotz M, Koch AM, Graf F. State of the art and prospective of CO_2 methanation process concepts for power-to-gas applications. Proceedings of the International Gas Union Research Conference, 17-19 Sep; Copenhagen, Denmark: 2014. pp. 314-327.

[66] Turks D, Mena H, Armbruster U, Martin A. Methanation of CO_2 on Ni/Al_2O_3 in a structured fixed-bed reactor- a scale-up study. J Catalysts. 2017; 7: 152.

[67] Younas M, Kong LL, Bashir MJK, Nadeem H, Shehzad A, Sethupathi S. Recent advancements, fundamental challenges, and opportunities in catalytic methanation of CO_2. J Energ Fuels. 2016; 30: 8815–8831.

[68] Stageland K, Kalai D, Li H, Yu Z. CO_2 methanation: the effect of catalysts and reaction conditions. J Energy Procedia. 2017; 105: 2022–2027.

[69] Wieclaw-Solny L, Wilk A, Chwola T, Krotki A, Tatarczuk A, Zdeb J. Catalytic carbon dioxide hydrogenation as a prospective method for energy storage and utilization of captured CO_2. J. Power Technol. 2016; 96(4): 213–218.

[70] Gao J, Liu Q, Gu F, Liu B, Zhong Z, Su F. Recent advances in methanation catalysts for the production of synthetic natural gas. J RSC Adv. 2015; 5: 22759.

[71] Molina MM, Kern C, Jess A. Catalytic hydrogenation of carbon dioxide to methane in wall-cooled fixed-bed reactors. J Chem Eng Technol. 2016; 39(12): 2404–2415.

[72] Hoekman SK, Broch A, Robbins C, Purcell R. CO_2 recycling by reaction with renewably generated hydrogen. Int. J. Greenhouse Gas Control, 2010; 4: 44–50.

[73] Sun D, Khan FM, Simakov DSA. Heat removal and catalyst deactivation in a Sabatier reactor for chemical fixation of CO_2: Simulation-based analysis. J Chem Engg. 2017; 329: 165–177.

[74] Meng X, Wang T, Liu L, Ouyang S, Li P, Hu H, et al. Photothermal conversion of CO_2 to CH_4 with H_2 over Group VIII nano catalysts: an alternative approach for solar fuel production. Angew Chem Int Ed. 2014; 53: 11478-11482.

[75] Wei W, Jinlong G. Methanation of carbon dioxide: an overview. J Front Chem Sci Eng. 2011; 5(1): 2–10.

[76] Marinoiu A, Cobzaru C, Raceanu M, Varlam M, Carcadea E, Cernatescu C. Carbon dioxide conversion to methane over supported nickel base catalysts. J Rev Roum Chim. 2015; 60: 249–256.

[77] Da Silva DC, Letichevsky S, Borges LE, Appel LG. The Ni/ZrO_2 catalyst and methanation of CO and CO_2. Int J Hydrogen Energ. 2012; 37: 8923–8928.

[78] Schaaf T, Grunig J, Schuster Markus R, Rothenfluth T, Orth A. Methanation of CO_2-storage of renewable energy in a gas distribution system. J Energy Sustain Soc. 2014; 4: 1–14.

[79] Vance CK, Bartholomew CH. Hydrogenation of carbon dioxide on group VIII metals. III, effects of support on activity/selectivity and adsorption properties of nickel. J Appl Catal. 1983; 7: 169–177.

[80] Delmelle R, Duarte RB, Franken T, Burnat D, Holzer L, Borgschulte A, Heel A. Development of improved nickel catalysts for sorption enhanced CO_2 methanation. Int J Hydrogen Energ. 2016; 41: 20185–20191.

[81] Muroyama H, Tsuda Y, Asakoshi T, Masitah H, Okanishi T, Matsui T, Eguchi K. Carbon dioxide methanation over Ni catalysts supported on various metal oxides. J Catalysis. 2016; 343: 178–184.

[82] Takano H, Kirihata Y, Izumiya K, Kumagai N, Habazaki H, Hashimoto K. Highly active Ni/Y-doped ZrO_2 catalysts for CO_2 methanation. J Appl Surf Sci. 2016; 388: 653–663.

[83] Takano H, Shinomiya H, Izumiya K, Kumagai N, Habazaki H, Hashimoto K. CO_2 methanation of Ni catalysts supported on tetragonal ZrO_2 doped with Ca^{2+} and Ni^{2+} ions. Int J Hydrogen Energ. 2015; 40: 8347–8355.

[84] Pastor-Perez L, Sache EL, Jones C, Gu S, Arellano-Garcia H, Reina TR. Synthetic natural gas production from CO_2 over Ni-x/CeO_2-ZrO_2 (x=Fe,Co) catalysts: Influence of promoters and space velocity. J Catalysis Today. 2018; 317: 108–113.

[85] Ewald S, Kolbeck M, Kratky T, Wolf M, Hinrichsen O. On the deactivation of Ni-Al catalysts in CO_2 methanation. J Appl Catalysis A, General. 2019; 570: 376–386.

[86] Brooks KP, Hu J, Zhu H, Kee RJ. Methanation of carbon dioxide by hydrogen reduction using the Sabatier process in microchannel reactors. J Chem Engg Sci. 2007; 62: 1161–1170.

[87] Moioli E, Gallandat N, Zuttel A. Parametric sensitivity in the Sabatier reaction over Ru/Al_2O_3- theoretical determination of the minimal requirements for reactor activation. J React Chem Eng. 2019; 4: 100–111.

[88] Sun D, Simakov DSA. Thermal management of a Sabatier reactor for CO_2 conversion into CH_4: Simulation-based analysis. J CO_2 Utlization. 2017; 21: 368-382.

[89] El Sibai A, Rihko Struckmann LK, Sundmacher K. Model-based optimal Sabatier reactor design for power-to-gas applications. J Energy Technol. 2017; 5: 911-921.

[90] Steffi T, Ronsch S, Guttel R. Transient flow rate ramps for methanation of carbon dioxide in an adiabatic fixed-bed recycle reactor. J Energ. Technol. 2020; 8: 1901116.

[91] Jake C, Duyar MS, Hoskins M, Farrauto R. Catalytic and adsorption studies for the hydrogenation of CO_2 to methane. Appl Catal B. 2014; 152-153(1): 184-191.

[92] Kao YL, Lee PH, Tseng YT, Chien IL, Ward JD. Design, control and comparison of fixed-bed methanation reactor systems for the production of substitute natural gas. J Taiwan Inst Chem E. 2014; 45: 2346-2357.

[93] Ronsch S, Schneider J, Matthischke S, Schluter M, Gotz M, Lefebvre J, et al. Review on methanation-from fundamentals to current projects. Fuel. 2016; 166: 276-296.

[94] Hu J, Brooks KP, Holladay JD, Howe DT, Simon TM. Catalyst development for microchannel reactors for martian in situ propellant production. Catal Today. 2007; 125: 103-110.

[95] Frey M, Edouard D, Roger AC. Optimization of structured cellular foam-based catalysts for low-temperature carbon dioxide methanation in a platelet milli-reactor. C R Chim. 2015; 18: 283-292.

[96] Ohya H, Fun J, Kawamura H, Itoh K, Ohashi H, Aihara M, et al. Methanation of carbon dioxide by using membrane reactor integrated with water vapor permselective membrane and its analysis. J Membr Sci. 1997; 131(1-2): 237-247.

[97] Schlereth D, Hinrichsen O. A fixed-bed reactor modelling study on the methanation of CO2. Chem Eng Res Des. 2014; 92: 702-712.

[98] Lefebvre J, Gotz M, Bajohr S, Reimert R, Kolb T. Improvement of three-phase methanation reactor performance for steady-state and transient operation. Fuel Process Techno. 2015: 132: 83-90.

[99] Rostrup-Nielsen JR, Pedersen K, Sehested J. High temperature methanation sintering and structure sensitivity. Appl Catal, A 2007;330:134–8.

[100] Nguyen TTM, Wissing L, Skjøth-Rasmussen MS. High temperature methanation: catalyst considerations. Catal Today 2013; 215: 233–8.

[101] Bartholomew CH, Carbon Deposition in Steam Reforming and Methanation. Catalysis Reviews, 1982. 24: pp. 67-112.

Chapter 2

Evaluation of a Sabatier reaction utilizing hydrogen produced by concentrator photovoltaic modules under outdoor conditions

2.1 The concept of the system

In this chapter, we provided an outdoor solar-to-gas (StG) conversion installed at the University of Miyazaki, Japan. A highly efficient concentrator photovoltaic (CPV) module with an accurate and robust tracking system has been installed at the outdoor field of the University of Miyazaki, as shown in Fig. 2.1. An outdoor conversion from solar to hydrogen has been successfully carried out by InGaP/InGaAs/Ge triple-junction solar cells. The system is composed of electrochemical (EC) cells to perform water splitting to generate hydrogen, and the EC cells are connected to CPV cells. This demonstration set the highest global record for outdoor efficiency (24.4%) [1]. However, such conversion was instantaneous and carried out on CPV cells. Subsequently, the system was developed for CPV modules with a sub-kilowatt-scale power output and modified with the maximum power point tracking (MPPT) method and four sets of DC/DC converters combined with EC cells. The resulting system had advanced flexibility for variable radiation conditions. The system achieved the highest one-day solar to hydrogen (StH) efficiency (18.78%) for sunny days [2] and provided daily StH efficiencies of about 15% for partially cloudy days [3].

In this chapter, an outdoor attempt at the methanation reaction was conducted as the next step to the StG conversion. Hydrogen, produced by the EC cells, was consecutively applied to the reactors while pure carbon dioxide was supplied via a tank. The experimental procedures and attempts at the Sabatier reaction were conducted on sunny and cloudy days. The operation parameters were analyzed to achieve a high methane concentration. In addition, the power

consumption of the methanation system on a sunny day and a cloudy day is presented in this section.

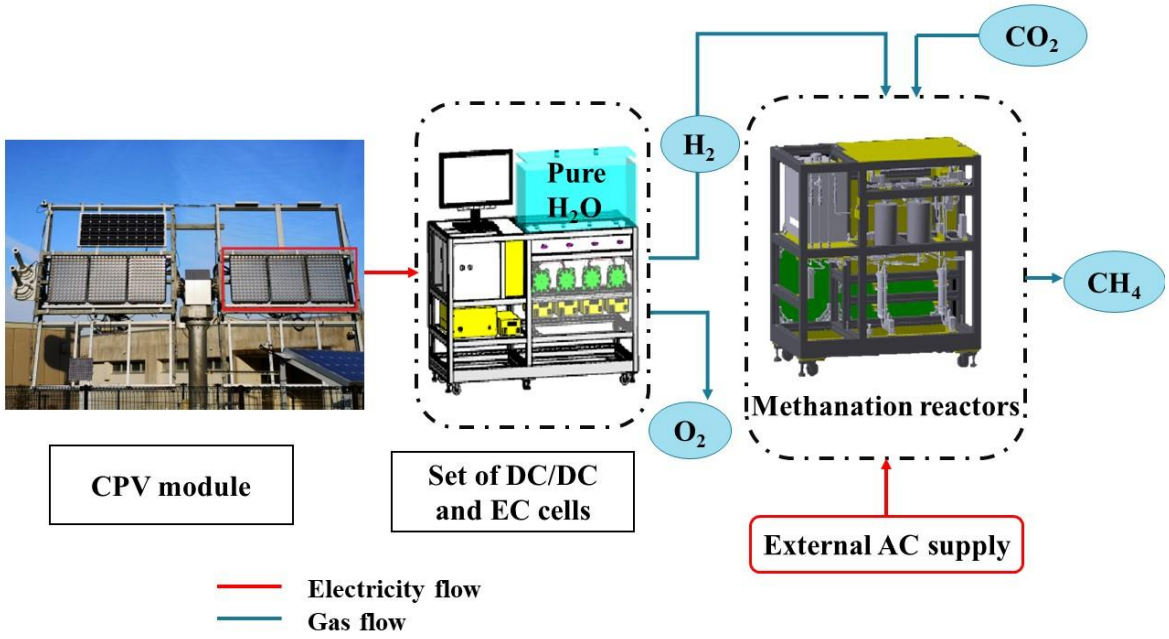

Fig. 2.1 Schematic illustration of outdoor solar-to-gas conversion framework, installed at the University of Miyazaki.

2.2 The system designs

2.2.1 CPV modules

As the first step to StG conversion, the solar cells with a highly efficient conversion are the primary core of the system. Multi-junction solar cells are currently trending to provide the highest conversion efficiency and developing in today's photovoltaic research society [4–7]. In multi-junction cells, p-n junctions of various semiconductor materials are designed to generate the current on different wavelengths. It increases the conversion efficiency of sunlight to electrical energy. They have been applied to the concentrator photovoltaic (CPV) cells and substantially improved their conversion efficiency under concentration operation [8]. In this approach, InGaP/InGaAs/Ge triple-junction solar cells with a high conversion efficiency are applied with a tracking system. The conversion efficiency of multi-junction cells has increased to 31% when they are lattice-matched to Ge [9, 10].

The multi-junction solar cells in this study utilized a concentration system, and the efficiency increased with increasing light intensity. Additionally, it provides higher annual output than flat-plate silicon solar cells under high-temperature operations [11]. The system can increase energy output and the cell's efficiency since the trackers are adaptable to the sun's location and designed to tilt the panels to the azimuth and zenith angles throughout the day. In addition, they provide peak output with an MPPT technique in which the panels are designed to be perpendicular to the sun while monitoring the panel's temperature and irradiance conditions. Moreover, the optimal concentration of a solar cell is influenced by the properties of a given solar cell. Accordingly, the conversion efficiency of the cells is a crucial aspect of the advanced solar system, such as solar to gas conversion.

At the outdoor field of the University of Miyazaki, three highly efficient CPV modules with a total output of 472 W under standard test conditions were installed, as shown in Fig. 2.2. They are connected to four sets of DC/DC converter-EC cells, as shown in Fig. 2.3. Direct

normal irradiance (DNI), the input power of the solar-to-gas conversion system, was gauged by a pyrheliometer (EKO, MS-56). Fig. 2.4 provides a view of the pyrheliometer installed at the University of Miyazaki.

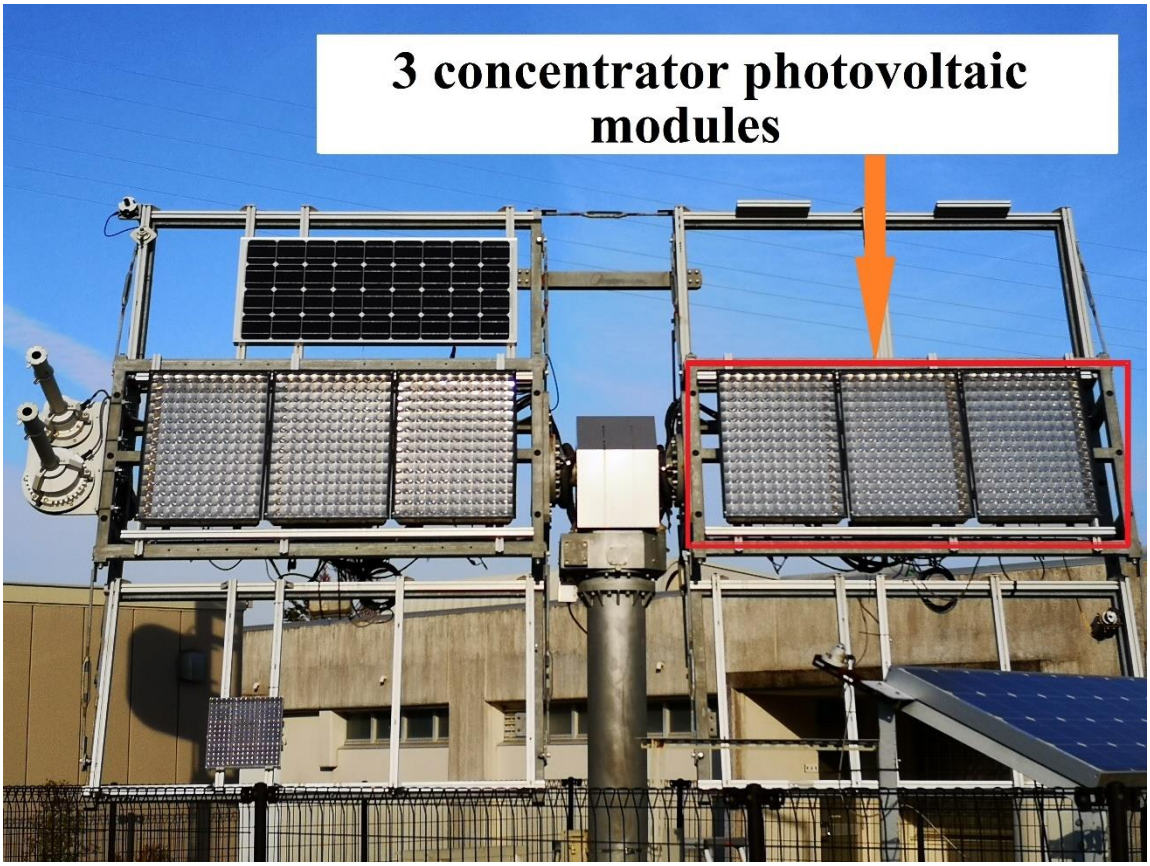

Fig. 2.2 View of the CPV configuration installed at the outdoor field of the University of Miyazaki.

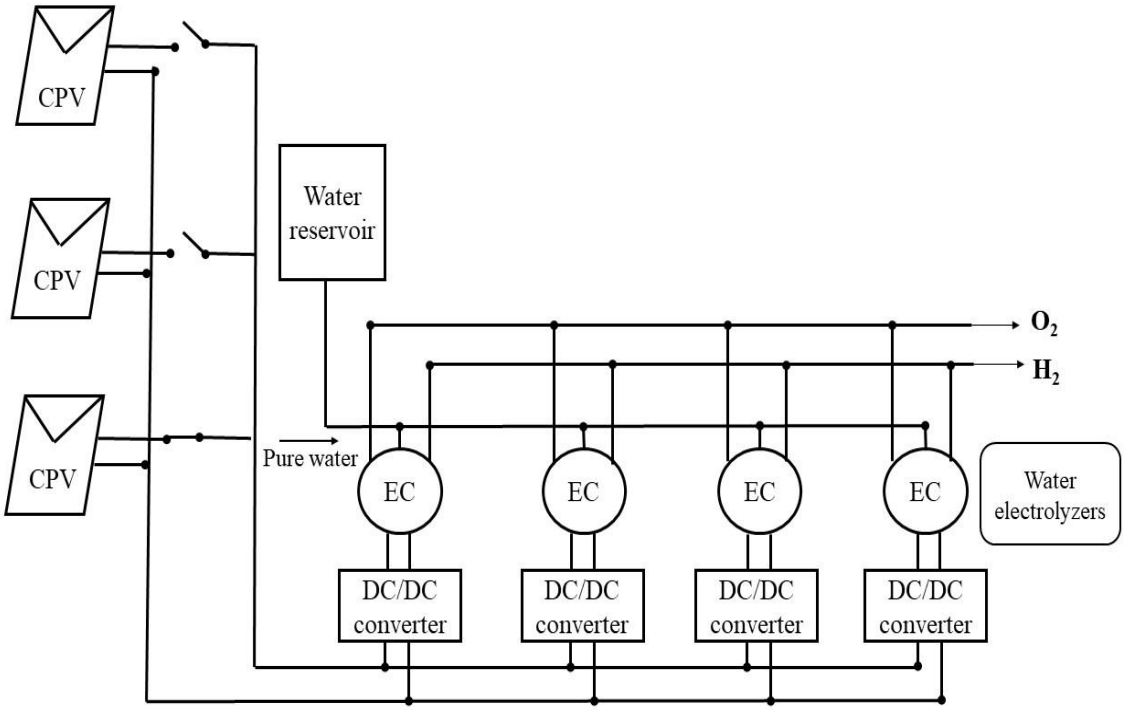

Fig. 2.3 Schematic layout of StH conversion system in which three CPV modules are connected to sets of DC/DC converters and EC cells.

Fig. 2.4. View of pyrheliometer to measure the DNI.

2.2.2 DC/DC converters

PV energy is intermittent in climate conditions, and solar-based hydrogen production is highly dependent on the maximum output extracted by the PV system. In solar-derived hydrogen production, there are two approaches to electrically connecting the photovoltaic system and hydrogen production system, such as EC cells. The first option is a direct coupling of PV and electrolyzer mechanically or electronically [12–19]. Such an approach is simple and provides high efficiency. However, there are technological challenges in sizing the electrolyzer with PV configuration, especially in extracting a maximum output of PV since the number of electrolyzers in series connection determines the PV voltage working point [13, 15, 18, 20]. The electrolyzers are designed for low operating voltage. Therefore, it is required to match the appliable voltage of the electrolyzer and the possible voltage range at MPP in PV configuration. Accordingly, it would decrease the whole system's performance unless the number of electrolyzer cells and PV are not optimized or controlled and do not match with the MPP of applied PV [13, 18, 21].

Another option is coupling with a DC/DC converter combined with an MPP tracking providing maximum PV power and higher efficiencies under any conditions. The system is more flexible to accommodate the voltage and current required for the electrolyzer. MPP tracking has been developed with several methods and algorithms [22]. State-of-the-art review of types of converters are buck-boost, push-pull, phase-shift full-bridge, and buck converters, respectively [23–27], and the proposed converter can differ depending on the system requirements. This converter-coupled method would be more cost-intensive, however, more advantageous than direct coupling.

In this study, we applied phase-shift full-bridge DC/DC converters made by Fujitsu Lab, proposed with an algorithm called "perturb and optimizing (P&O) with converter scoring." In our StG conversion, four DC/DC-EC cells were linked in parallel. They were connected with

three CPV modules. It achieved a maximum DC/DC conversion efficiency of 94.2% on a DC/DC output of 104.7W and provided a flexible performance on StH conversion on both a clear day and a cloudy day [2, 3, 28]. Additionally, it contributed converter efficiency of over 90% on a wide input voltage ranging from 60–300 V and a load power of 20–100% [2].

In this algorithm, some converters were designed to turn off while low output operation to reduce energy consumption at driver circuits, resulting in a high solar to hydrogen conversion. The converters calculate the current set point for PEM electrolyzers compared to the solar power reference and the measured stack voltage. The operation point is influenced by the climate conditions, EC temperature, hydrogen production, and other factors [28]. Fig. 2.5 and Fig. 2.6 shows the configuration of converter-electrolyzer sets to perform the water-splitting process.

Fig. 2.5 Photograph of a DC/DC converter applied for the solar-to-hydrogen conversion.

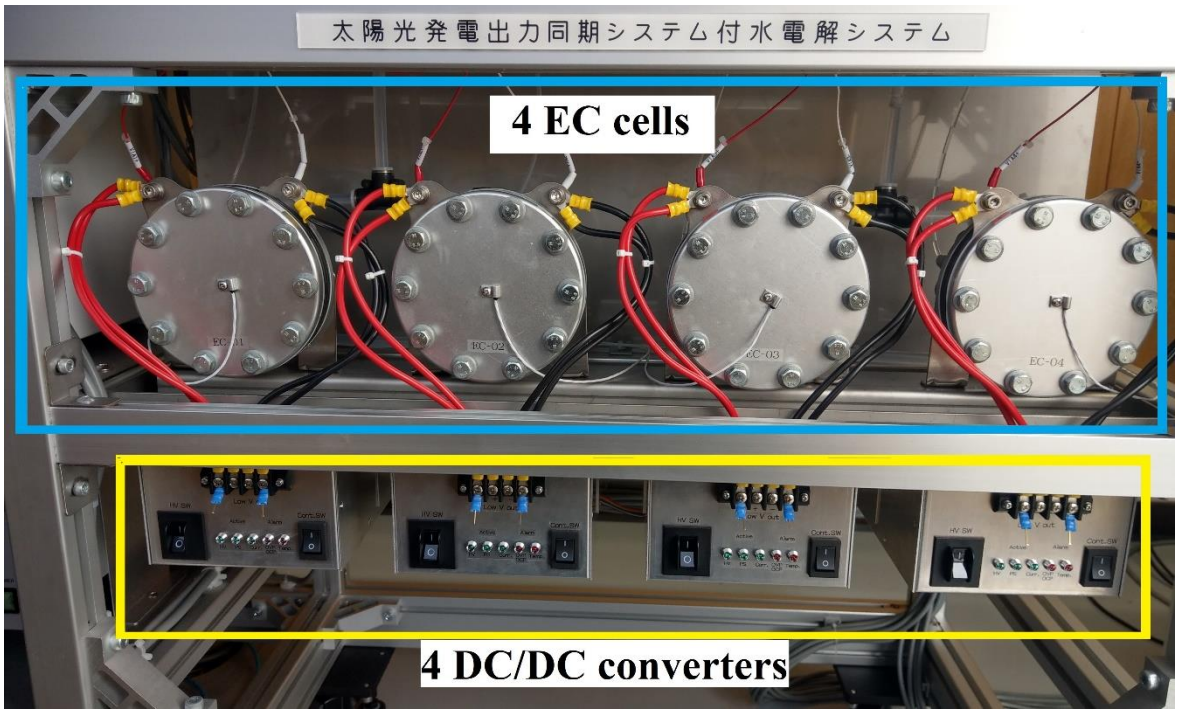

Fig. 2.6 View of the sets of EC-DC/DC configuration to perform water electrolysis, installed at the University of Miyazaki.

2.2.3 Electrochemical cells

Pure hydrogen can be extracted by simply applying electricity from renewable sources for water electrolysis. The kind of water electrolysis can be classified depending on the electrolyte, ionic agents, and operating parameters. Electrolyzers are the primary core of the water-splitting process in which water decomposes into hydrogen and oxygen when the electric current is applied. In solar-derived water electrolysis, the technology is limited to low-temperature electrolyzers [18]. The most widely used electrolyzers are alkaline (AEL) electrolyzer and polymer electrolyte membrane (PEM) electrolyzer. AEL is well-established and robust technology; however, its corrosive liquid electrolyte, less compact design, and gas permeation through the diaphragm attract attention to PEM as a promising technique [29–31].

A membrane electrode assembly (MEA) is the pivot of the PEM electrolyzer since its degradation seriously reduces the hydrogen production and performance of PEM. Nafion membrane is one of the main components in the MEA. Nafion membranes are widely used for PEM electrolyzers owing to their high adaptability and durability at high current densities. The electrodes (anode and cathode) are bonded to each side of the Nafion membrane. Therefore, the membrane of a PEM serves as an electrolyte and a gas separator for hydrogen and oxygen. Accordingly, its degradation can be affected by the deposition of impurities onto the membrane. In addition, these migrated cations could hinder hydrogen evolution and induce a rise in the operating voltage. The migrated cations reduce the proton transport properties from anode to cathode and severely affect the PEM degradation. Accordingly, the performance of MEA for cation contamination is a challenge to the overall cost.

Fig. 2.7 and Fig. 2.8 show the configuration of a PEM electrolyzer (Enoah Inc., EHC 070) that consists of MEA with a Nafion membrane and noble metal catalysts, a gas diffusion layer as a passage for reactant transport, current collectors, and end plates. A platinum catalyst was utilized at the cathode for the hydrogen evolution reaction, while IrO_2 was supported on the

anode side. Pure water is introduced at the anode and decomposed into oxygen, protons, and electrons. After passing through the electrolyte, protons move from the anode to the cathode through the cation exchange membrane. At the cathode, they combine with electrons to generate hydrogen gas.

There are four electrolyzers in our system, and each cell operates at a maximum capacity of approximately 20 A. The operating current of the electrolyzer increased by varying the number of CPV modules [2]. State-of-the-art StH conversions are carried out at a high current density (over 1A/cm^2) to reduce high capital costs. The higher the current density, the higher the overpotential losses that decrease in its efficiency [32]. Therefore, increasing overpotential and current density is a bottleneck to achieving high StH efficiency. It can be reduced approximately to a thermal neutral voltage of 1.48 V by optimizing the operating temperature and pressure of EC cells [33]. In our existing system, the current density of the electrolyzer is from 0.1–0.3 A/cm^2 by one-CPV or three-CPV configuration [2].

According to the outdoor results, the efficiency of electrochemical cells was over 70% and increased when the operating current was low, especially in the morning and evening when the output power of the CPV module was reduced [2]. The stored hydrogen energy was calculated by the free energy of hydrogen ($\Delta G° = -237$ kJ/mol) and hydrogen generation rate (GR_{H2}), which was measured by a mass flow meter (MFM, Alicat Scientific M-2SLM-D-25COMP).

Fig. 2.7 Photograph of a PEM electrolyzer manufactured by Enoah Inc., EHC 070, installed at the University of Miyazaki.

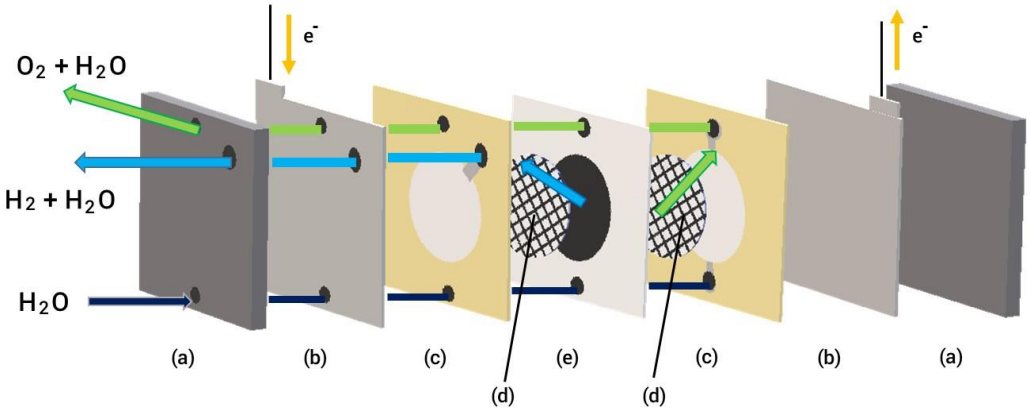

Fig. 2.8 Schematic of PEM electrolyzer assembly (a) end plates, (b) current collectors, (c) gaskets, (d) gas diffusion layers, (e) MEA.

2.2.4 Methanation reactors

Providing appropriate reactor design is the pivot of the methanation system to control the increasing temperature influenced by the reaction. The most established reactors for the methanation system are fixed-bed reactors. However, heat management in a fixed-bed reactor may be burdensome, resulting in localized hot spots. In contrast, cooled reactors transfer the released heat from the reaction to a cooling medium. This kind of reaction may be difficult to manipulate within a single reactor. Therefore, at least two adiabatic reactors are needed to connect in series for flexible control of reaction temperature in a fixed bed reactor [34]. The size of the reactors is a relevant factor in determining the contact time between the feed gas and the catalyst. The reaction performance was a function of the contact time of the reactant feed gas and the catalyst bed. If the contact time is too short, decreased CH_4 concentrations will result [35].

Additionally, the temperature is another essential parameter to achieving the highest CH_4 composition. Since low temperature provides the highest methane yield because of the reaction's exothermic nature, the operating temperature must be below 300 °C [36]. Increasing temperature is an undesirable condition for CO_2 methanation because of the strongly exothermic reaction of CO_2. Higher pressures and lower temperatures are more favorable in thermodynamic methanation. A high conversion can be maintained at high temperatures by increasing the pressures despite decreasing CH_4 generation and catalyst degradation. An active catalyst is required for lower-operating temperatures, while the high-pressure operation is often uneconomical [37]. As mentioned in the previous chapter, Ni-based catalysts are well-developed and low-cost materials for the methanation process. Additionally, ZrO_2 is the most suitable supporter of Ni-based to promote its CO_2 methanation reaction activity, and it was studied by several research groups [38–43]. Therefore, Ni-based ZrO_2 catalysts were used in our studies.

In the next step of the StM system, H_2 gas extracted from the electrolysis system was mixed with CO_2. The latter was introduced via a tank. The CO_2 hydrogenation or CO_2 reduction to CH_4 was developed using two adiabatic fixed-bed reactors provided with Ni-Y-doped ZrO_2 catalysts bed. They are attached in a series connection, as shown in Fig. 2.9. The two reactors were connected in series to maximize the CH_4 generation. The external electricity was applied to the heaters of reactors, and the reactor temperatures were controlled by a proportional, integral, derivative (PID) controller without cooling systems. The outside diameter of each reactor is 19.05 mm, the inside is 16.57 mm, and a height of 200 mm for each. The generated H_2 from water electrolysis was directly applied to reactors after passing through gas/liquid separators and dryers. It was intended to feed pure H_2 to the methanation system without resulting steam, while CO_2 was introduced from the outside source. The flow rate of H_2 fed into the methanation system was measured by MFM, whereas that of CO_2 was controlled by a mass flow controller (MFC, Alicat Scientific MC-500SCCM-D-25COMP). Gas/liquid separators were used to filter by-product H_2O and obtain pure CH_4. The additional pressure was not applied to the reactors in our system.

Since the reactors were connected in series, most reactions developed within the first reactor (reactor 1). Simultaneously, the residual and unreacted gases (such as H_2 and CO_2) travel from reactor 1 and maintain the reaction within the second reactor (reactor 2). Therefore, the output gas from reactor 2 was where system output was measured and analyzed. Fig. 2.10 illustrates the configuration of the methanation system. In this study, the composition of produced gases was quantitatively analyzed using a quadrupole mass spectrometer (QMS, MS 9600, Netzsch), as shown in Fig. 2.11. No H_2O was observed in our system due to filters and gas/liquid separators. The water was cooled and liquefied in the reactor after passing through the valves. The composition of methane was related to the feed mole ratio and feed temperature. Thus, the amount of CH_4 composition was concerned by various feed temperatures and

stoichiometric ratios. The volume of CH_4 gas was not directly measured. It was assumed that the volume of CH_4 gas corresponded to 1/4 times the fed H_2 gas volume and multiplied by the CO_2 to CH_4 conversion efficiency.

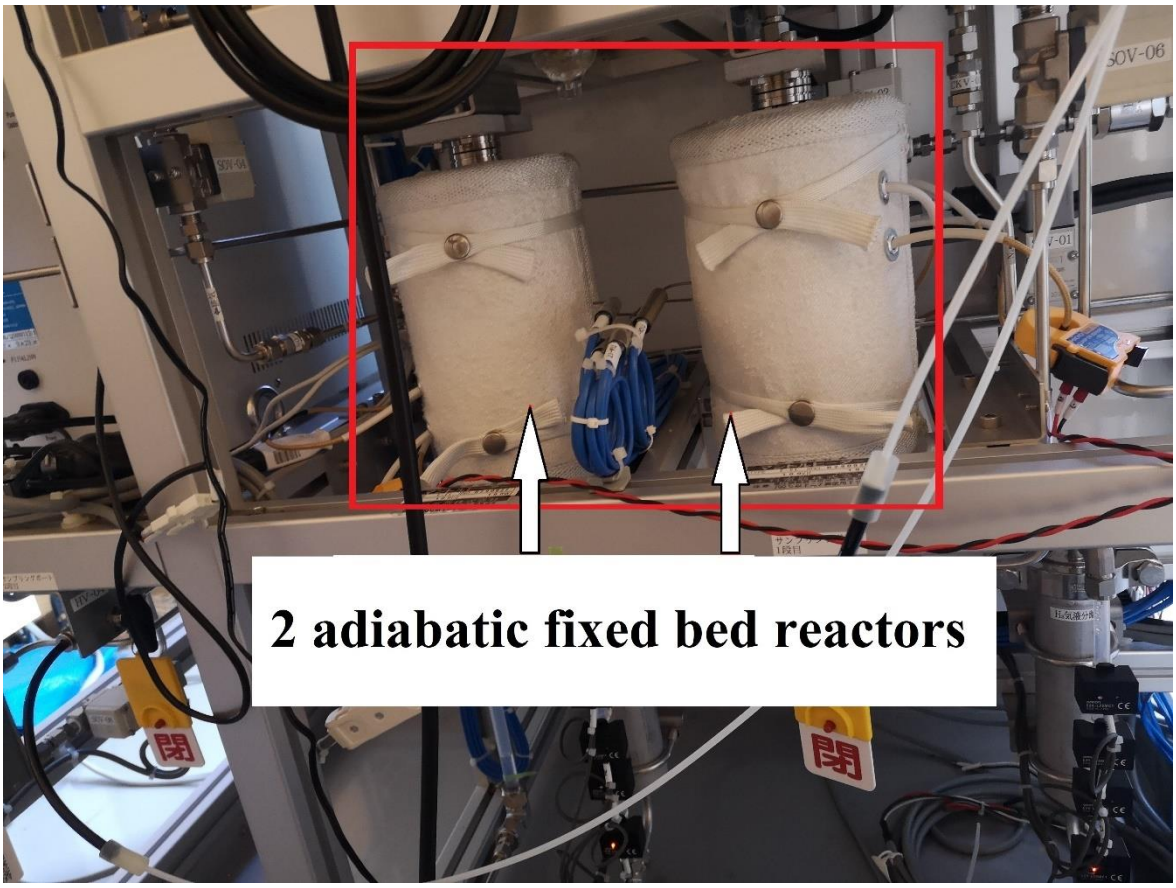

Fig. 2.9 Real image of two adiabatic fixed-bed reactors, used for methanation reaction.

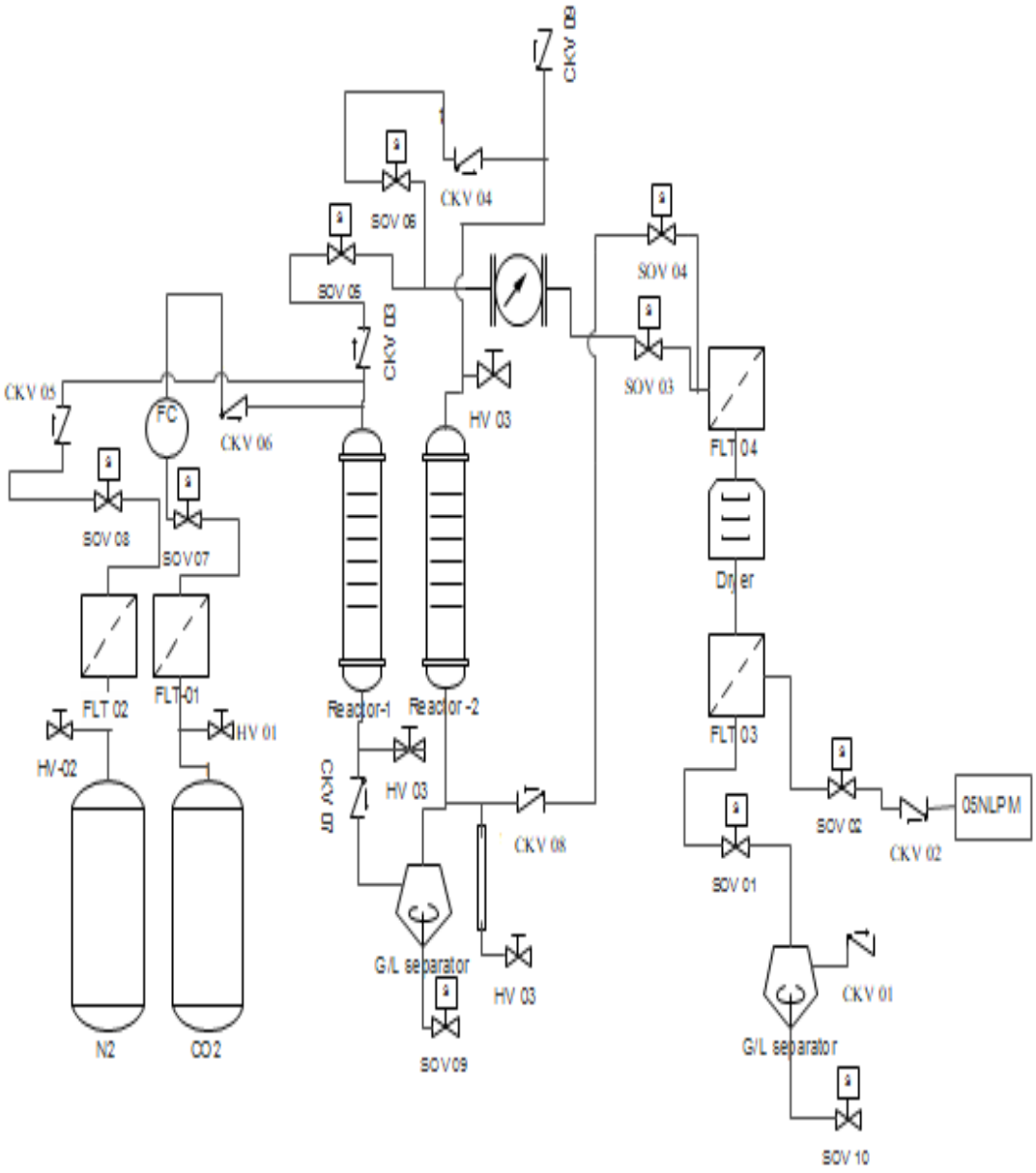

Fig. 2.10 Schematic diagram of methanation system.

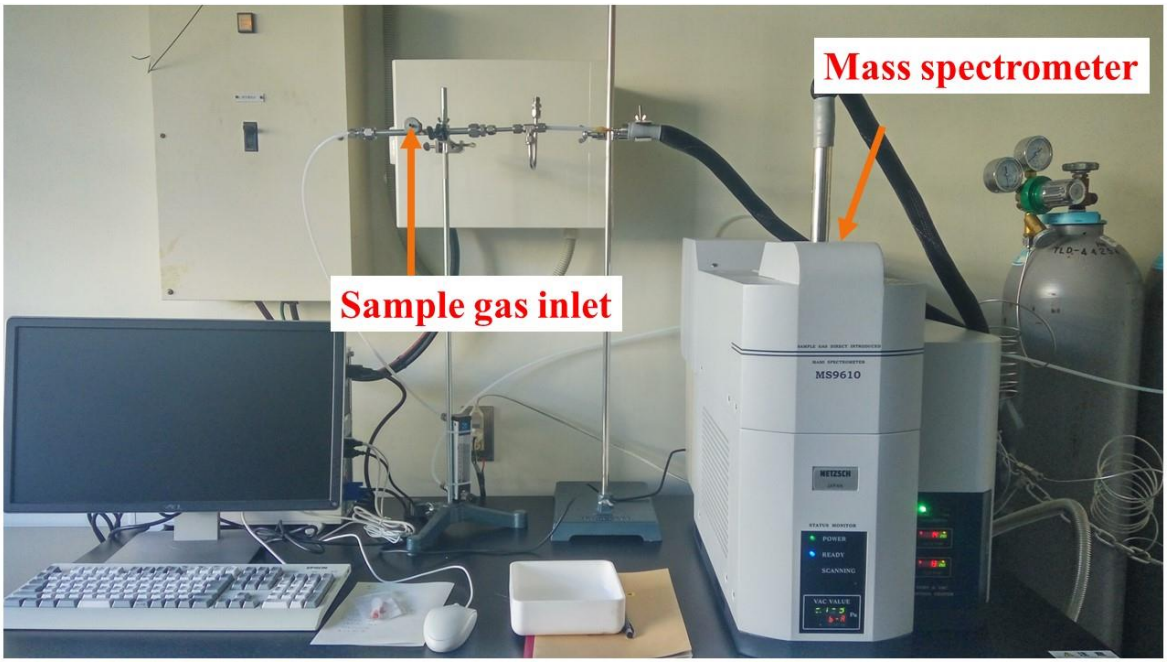

Fig. 2.11 View of quadrupole mass spectrometer (QMS, MS 9600, Netzsch) to measure the composition of methane, installed at the Nishioka Laboratory.

2.3 Results and discussion

2.3.1 Optimization for operation condition of reactors

This section outlines the method to determine the operating temperature of reactors that yields the highest conversion to CH_4 and consequently generates the highest CH_4 composition. The conversion and yield of CH_4 depend upon the operating temperature and the catalysts utilized. Moreover, catalyst deactivation, carbon, and coke formation are related to the high-temperature operation of the reactors. The preferred operating temperature must ensure catalyst productivity and hinder catalyst thermal deactivation. Ni-based ZrO_2 catalysts can perform higher CH_4 selectivity within the temperature range of 200–300 °C [38]. CO formation and catalyst deactivation will increasingly occur at temperatures higher than 320 °C [44, 45]. In

our system, the maximum allowable temperature for reactor 1 and reactor 2 is 400 °C and 300 °C, respectively.

The performance of methanation at temperatures ranging from 240 to 300 °C was analyzed in this study. The temperature of the gases generated from the catalytic reaction was measured. Fig. 2.12 indicates the quantity of CO_2 converted to CH_4 from both reactors. The CO_2 conversion to CH_4 was calculated as:

$$CO_2 \text{ conversion} = \frac{V_{CH_4}\text{output} \times 100\%}{V_{CH_4}\text{output} + V_{CO_2}\text{output}}, \quad (2.1)$$

where V_{CH4} output and V_{CO2} output are the volumes of CH_4 and CO_2 analyzed by QMS. The maximum conversion of CO_2 to CH_4 was 97.6%, which was achieved at a temperature of 260 °C. The reaction towards CH_4 can be controlled by varying the stoichiometric ratio of the reaction. Increased CO_2 conversion and CH_4 yields occur at the stoichiometric ratio of 1:4 depending upon the types of the catalyst used [46]. Additionally, carbon deposition and carbon monoxide formation also depend upon the stoichiometric of the reaction. The formation of carbon was observed when a molar ratio of 1:4 for CO_2/H_2 was not maintained [47–49]. This carbon generation may affect the catalyst performance and deactivate the catalyst. Consequently, it was necessary to determine the stoichiometric ratio that yielded the highest CO_2 conversion without negatively impacting the system. The CO_2 conversion to CH_4 was analyzed by changing the flow rate of CO_2 via MFC. As shown in Fig. 2.13, 1:4 was the best stoichiometric ratio for our system, which yielded a CO_2 conversion efficiency of 97.6%. The reactor temperatures were 260℃ for each reactor. When the stoichiometric ratio was changed to 0.9:4, the conversion was 91%, while it changed to 1.1:4, 89 % of CO_2 conversion was yielded, i.e., an efficiency lower than that of 1:4.

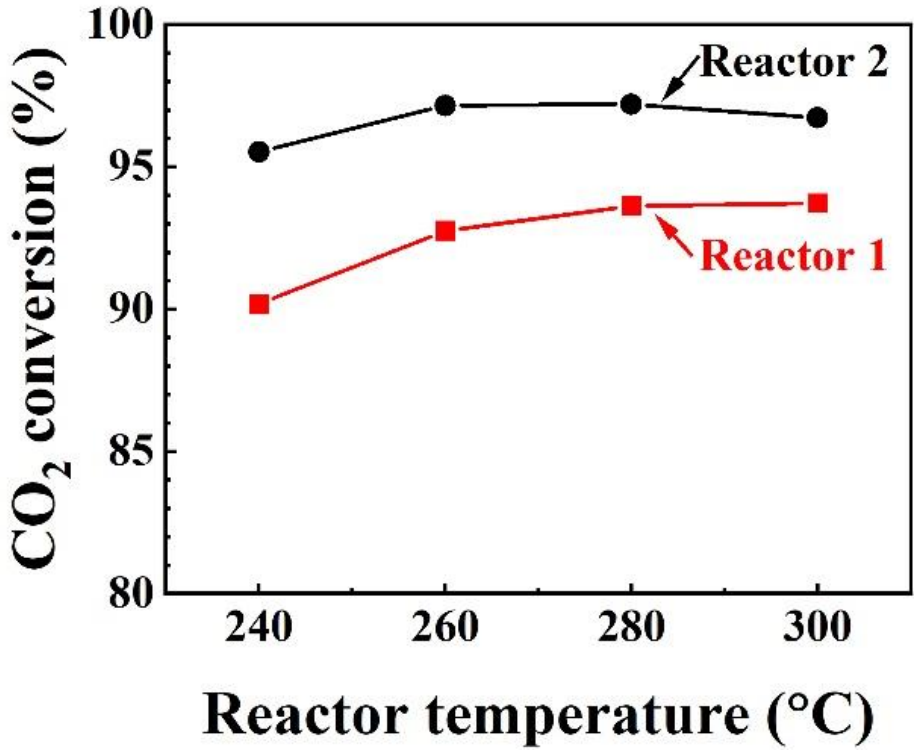

Fig. 2.12 Effect of reactor temperature on CO_2 conversion to CH_4.

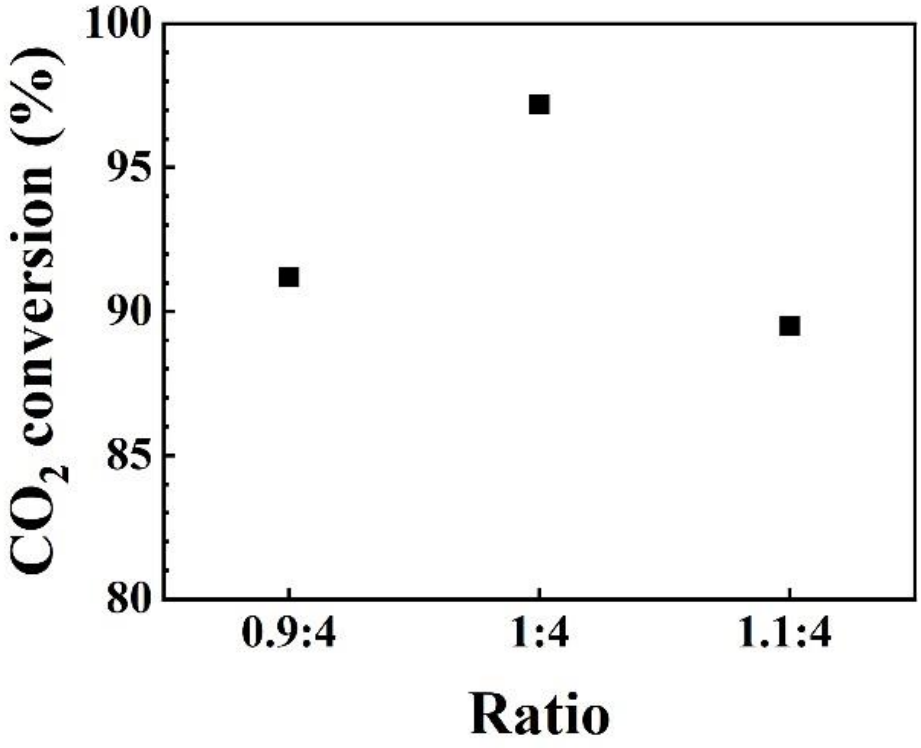

Fig. 2.13 Effect of ratio (CO_2:H_2) on CO_2 conversion to CH_4.

2.3.2 Validation of methane concentration during outdoor operation

Subsequent to determining the best feed ratio and reactor operating temperatures, the performance of methanation was examined. The methanation data to be analyzed was under operating conditions on a clear, sunny day between 10:00 AM to 2:00 PM. The target reactor temperature for both reactors was 260 °C. Gases were collected and calibrated each hour.

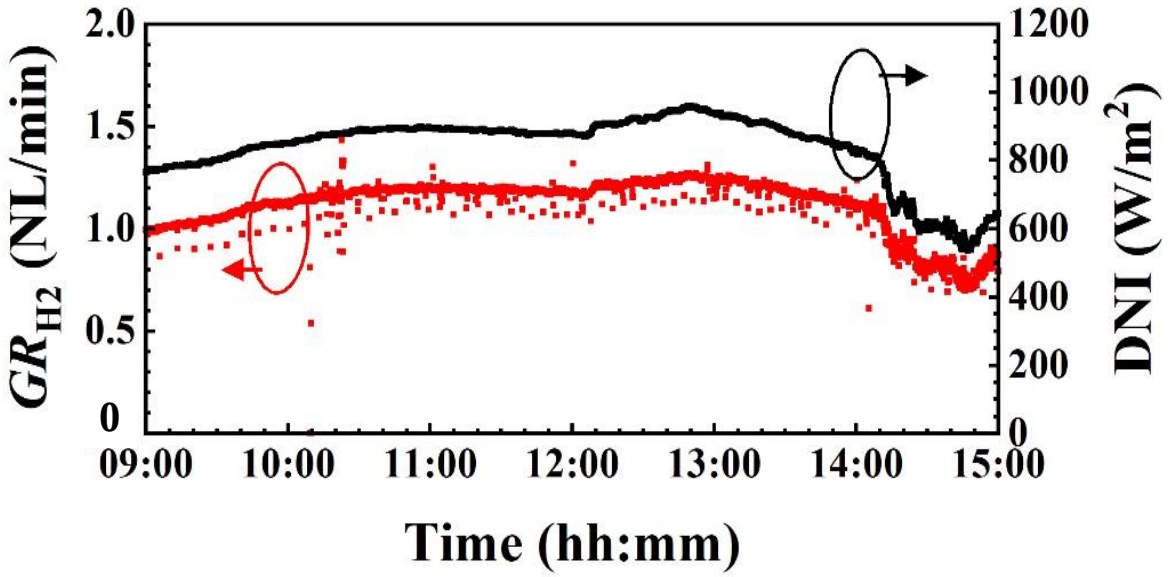

Fig. 2.14 Measured hydrogen generation rate (GR_{H2}) compared to DNI.

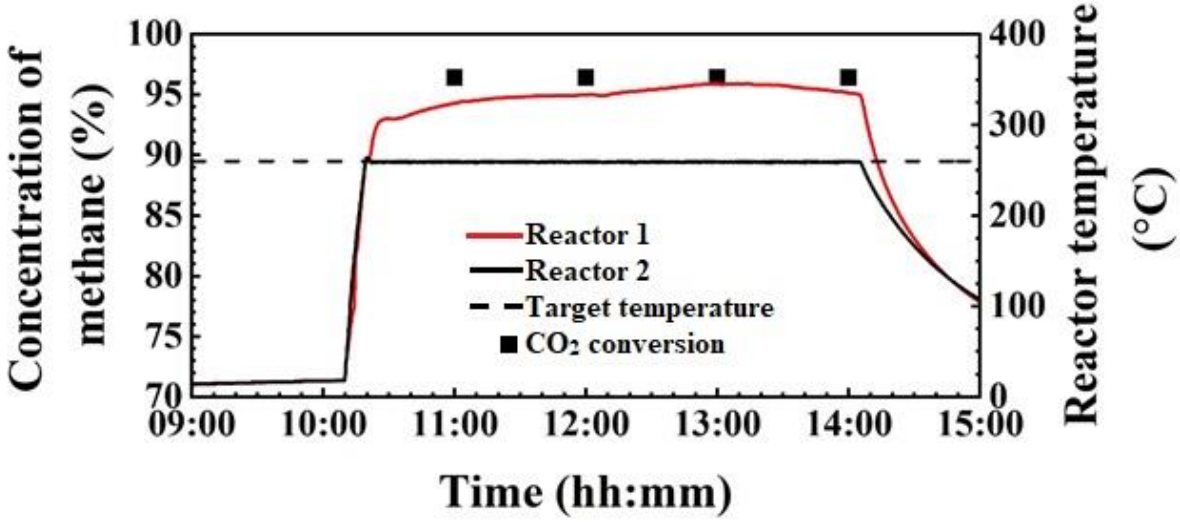

Fig. 2.15 Performance analysis on conversion of CO_2 to CH_4 compared to reactor temperature. Data in both plots were obtained on a clear, sunny day (15th Nov 2019).

Fig. 2.14 shows GR_{H2} compared to DNI. Fig. 2.15 shows the internal temperatures of the reactors compared to the concentration of CH_4. A CO_2 conversion efficiency of 97.6% was maintained for approximately 4 hours. Although the operating temperature was set to 260 °C, the inner temperature of reactor 1 increased over 260 °C. The cooling system was not utilized in this system. Therefore, the heat was released during the reaction. However, the temperature of reactor 2 was stable at the operating temperature (260 °C). It was because of the low reaction rates in the reactor 2. Most of the reaction were performed in the reactor 1 and thus, the temperature of the reactor 1 was higher than that of reactor 2 as a result. The average GR_{H2} was 1.19 NL/min in the experimental period (10:00 AM to 2:00 PM). CO_2 gas applied to the methanation system, which corresponds to 1/4 times the fed H_2 gas, was 0.30 NL/min. The total mixture gas, which fed to the system, was 1.48 NL/min. Due to the changing DNI during the experimental period, the generated H_2 gas changed. Therefore, mixture gas fed to the system and space velocity also changed. The degradation of catalysis could not seem in the experimental period.

2.3.3 Power consumption on the methanation system

Thermo-catalytic conversion of CH_4 is a highly exothermic reaction and consequently it may result in reactor overheating and a low conversion of CO_2. Reactor cooling is critical to the methanation process to avoid catalyst deactivation. Operating temperature is the most critical parameter to optimize the methanation system. Additional, critical operational factors such as catalyst deactivation, CO formation, CO_2 conversion, and CH_4 yield depend upon the operating temperature. The temperatures of the reactors should be maintained at a sufficiently high temperature to maintain catalytic reactions but also sufficiently low to avoid CO formation [50]. Heat management of the methanation system, specifically, reactor cooling and utilizing the reaction energy for power needs external to the reactors, is an active area of research in PtG systems. The heat released from the reaction must be removed from the system and

subsequently may be utilized in the electrolysis process [47, 50]. Optimization of Heat removal, to ensure uniform temperatures within the reactors is a currently unsolved concern.

The reaction is significantly exothermic. The reaction consumes 4 moles of H_2 for each mole of CH_4 produced; 2 moles of H_2O are generated as a byproduct. Energy is required to initiate the reaction. Increasing reaction time provides some heat to perpetuate the reaction. The energy required to maintain the reaction decreases from the initial amount once the reaction becomes stable. Reactor temperature is regulated by a PID controller. When reactor temperature increases because of the exothermic reaction, PID control switches regulate power depending upon reactor temperature. As a result, heat from the reactors provide the required reaction energy and the power consumption of the methanation system is reduced.

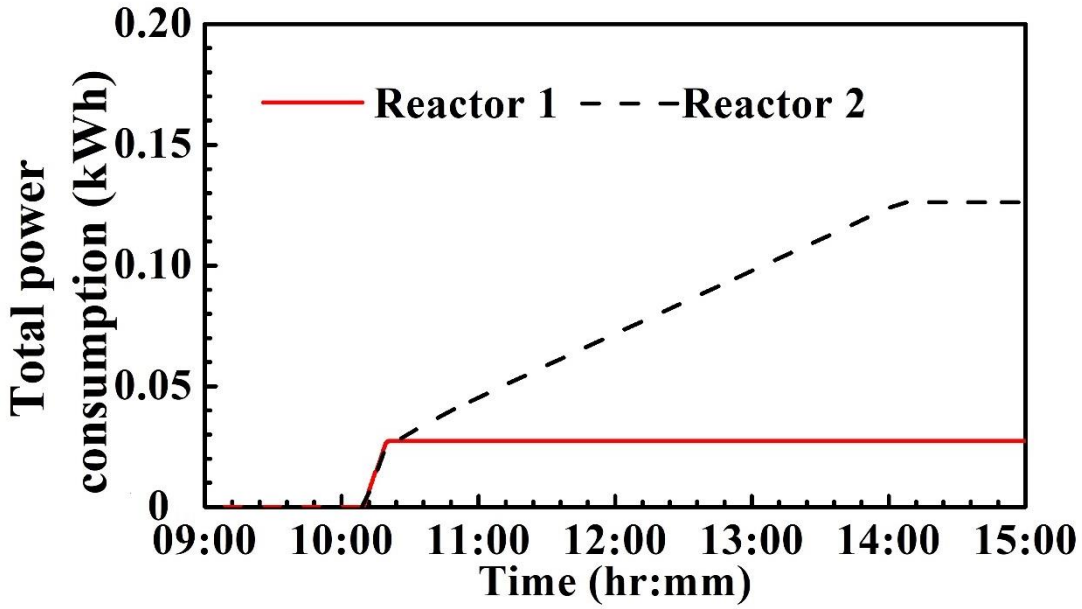

Fig. 2.16 Total power consumption of the reactors under a sunny condition (15th Nov 2019).

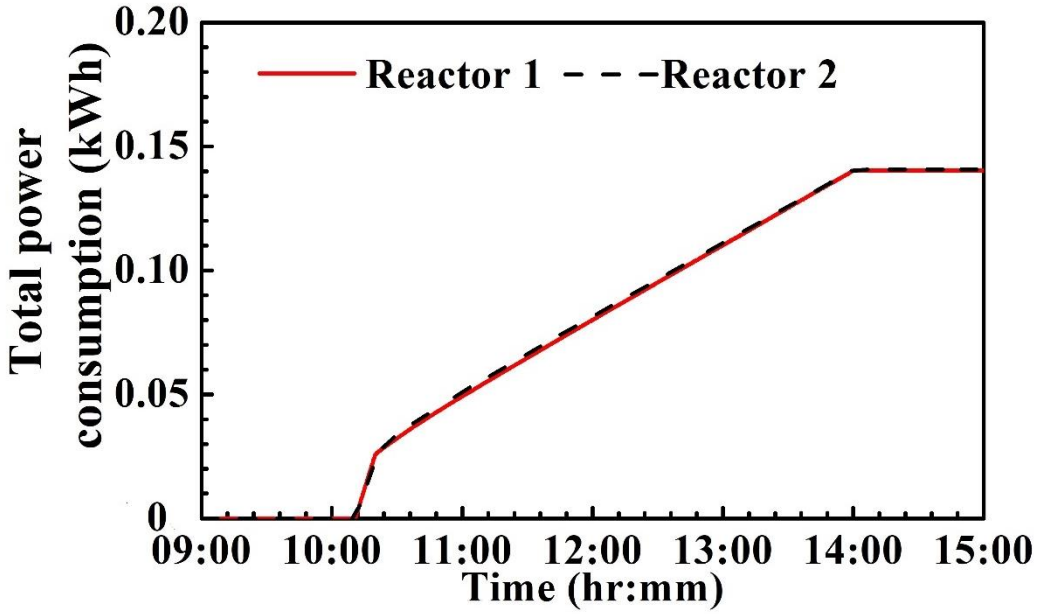

Fig. 2.17 Total power consumption of the reactors under an overcast condition (6th Dec 2019).

The total power consumption of the reactors was measured on a clear, sunny day from 10:00 AM to 2:00 PM local time. Fig. 2.16 shows the reactor total power consumption on a sunny day compared with time. Although the reaction initiates in reactor 1, generated gases, residual, and unreacted gases, maintain the reaction in reactor 2. The reaction rate of reactor 2 is lower than that of reactor 1. Therefore, the total power consumption of reactor 2 is higher than that of the reactor 1. It may be observed that after the initial energy is provided, the total power consumption of reactor 1 stabilizes as a result of the Sabatier effect. The heat of reaction for reactor 1 reduces power consumption of reactor 1, whereas for reactor 2, the reaction rate will be reduced because the majority of the reaction occurs in reactor 1. Therefore, more energy is consumed by reactor 2 to maintain the temperature and reaction. A total of 0.145 kWh is required for operation under sunny conditions. Fig. 2.17 indicates the total power consumption of the reactors under overcast conditions. The DNI was negligible as was the generation of H_2. The reactors required more energy under cloudy conditions due to low reaction rates. The total power consumption of 0.281 kWh was observed under overcast conditions.

Methanation process is a strongly exothermic reaction and requires external energy to initiate the reaction. Subsequent to initiation, the reaction can be maintained by the heat released. As a result, the energy requirements for the methanation system decrease significantly after reaction initiation. Energy consumption of the methanation system is a significant issue for the efficient conversion of solar energy to gas. It is important to note that a highly efficient PtG system is a result of highly efficient CPV modules, highly powerful DC/DC converters, and highly active catalysts. The PtG conversion system performed well and achieved high efficiency under variable weather conditions. This was a result of efficient CPV modules and active catalysts.

The stored chemical energy of CH_4 should be considered in PtG conversions because it is directly used in power generation via combustion. Fig. 2.18 shows a schematic illustration of

combustion energy of CH_4. CH_4 has a combustion energy of -802 kJ/mol. Solar to methane efficiency (η_{StM}) is defined as:

$$\eta_{StM} = \frac{\text{Combustion energy of Produced methane} \times \text{moles of produced methane}}{\text{Electrical energy required to generate } H_2 \text{ and } CH_4}, \quad (2.2)$$

$$\eta_{StM} = \frac{|\Delta H^\circ| \times \text{amount of } CH_4}{E_{DNI} + E_{reactors}}, \quad (2.3)$$

where the stored chemical energy of produced methane yields the combustion energy (ΔH° = -802 kJ/mol). The integrated irradiance is denoted as E_{DNI}, while the term $E_{reactors}$ represents the energy consumed by the reactors in the methanation system. Table 2.1 shows the summary of energy input and output for our system. The CH_4 generation rate was calculated based on mole fractions and generation rate of H_2 input into the reaction. The calculation assumes that the CH_4 generation rate corresponds to ¼ times the input of H_2. Subsequently, the CH_4 generation rate was multiplied with the calculated conversion of CO_2 to CH_4 (97.6%). The rate of H_2 input into the PtG system was evaluated by MFM. The conversion of CO_2 to CH_4 was analyzed and assessed by QMS. For sunny conditions (on 15th November 2019), an efficiency of 13.8% was achieved as shown in Table 1. In contrast, the system could not generate electricity from CPV modules under an overcast condition because the CPV modules use only the direct-beam component. Therefore, the hydrogen generation and Sabatier process did not operate under an overcast condition.

Table 2.2 shows the one day elementally efficiencies focused on solar to hydrogen conversion. The elementary efficiencies are defined as follows: η_{CPV} is the CPV module efficiency; η_{DCDC} is the conversion efficiency of the DC/DC converters; η_{EC} is the energy conversion efficiency from DC electricity into the free energy of hydrogen at the electrolyzer [2]. Especially, η_{EC} decreased in comparison with previous work [2]. The system in this study had consisted of three CPV modules and operated at the high operating current of the electrolyzer, which leads to reduce η_{EC}. The CO_2 conversion to CH_4 after passing thought

reactors 1 and 2 was 97.6% as shown in Fig 2.15. The StM efficiency could be improved by optimization of system configuration such as a number of CPV modules and operating current of the electrolyzer while considering space velocity.

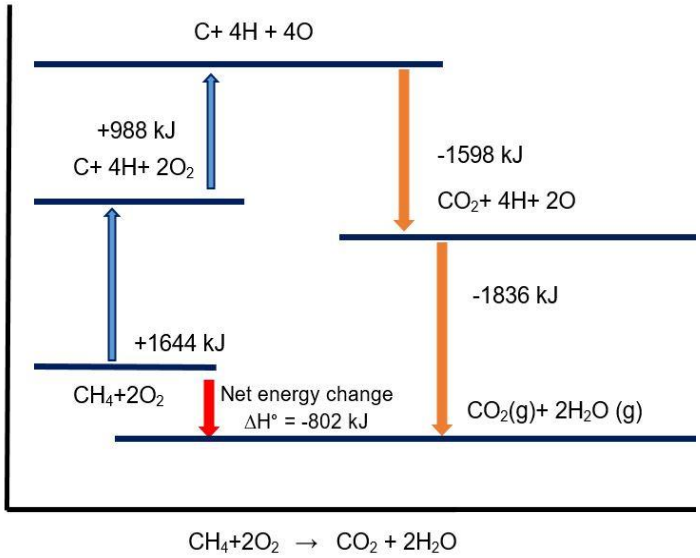

Fig. 2.18. Schematic illustration of the combustion energy contained in methane.

Table 2.1 Summary of energy input and output for the methanation system and conversion efficiency of solar energy to methane.

Input energies		Produced gases (output)			
E_{DNI} (kWh)	$E_{reactors}$ (kWh)	Amount of H_2 during experimental period (mol)	Amount of CH_4 during experimental period (mol)	Stored energy of produced methane (kWh)	η_{StM}
4.584	0.145	11.99	2.924	0.651	0.138 (13.8%)

Table 2.2 One day elementally efficiencies on the system.

	η_{CPV}	η_{DCDC}	η_{EC}
Sunny day 15th November 2019	27.4%	89.3%	70.2%

2.4 Conclusion

In a StG system, the hydrogenation of CO_2 was accomplished by utilizing the hydrogen extracted from solar power. An efficient StG system was operated outdoors during a field test at the University of Miyazaki, Japan. The solar to methanation performance was analyzed on a sunny day and an overcast day, respectively. Whereas the solar to hydrogen conversion was performed and measured daily except for the rainy days. Methanation is an exothermic reaction and a more complex system than the electrolysis process. The conversion was analyzed while the operating parameters were controlled.

Firstly, CO_2 to CH_4 conversion was analyzed at various operating temperatures (ranging from 240 to 300 °C) with a stoichiometric ratio of 1:4. The best operating temperature that provided maximum conversion efficiency was determined. After that, CO_2 to CH_4 conversion was analyzed by controlling the stoichiometric ratio to ensure its highest conversion. The reaction is a heat-released process. External electricity was provided to the rectors to initiate the methanation process in our system. Accordingly, the energy consumed by the reactors was measured and analyzed. As an overall system analysis, solar to methane conversion was estimated.

The results provided that the highest conversion of CO_2 to CH_4 (97.6%) was observed at a reactor temperature of 260 °C. These results indicated that the CO_2 hydrogenation reaction was favored at relatively low temperatures. Additionally, the results confirmed that the highest conversion was attained at the stoichiometric ratio of 1:4. Then, the total power consumption of the reactors was analyzed and concerned for the sunny and overcast conditions. The conversion efficiency of 13.8% for solar to methane was obtained in our system. These results led us to conclude that the highest global outdoor solar to methane conversion was achieved on highly efficient InGaP/InGaAs/Ge triple-junction modules associated with sets of DC/DC-EC cells at the University of Miyazaki, Japan. Natural gas composition often contains at least

80% of CH_4. Because our generated gas composition contains more than 80% of CH_4, the practical impact of our efficient PtG system is significant.

The previous results mentioned the total power consumption of the reactors during the reaction. This evaluation provided that the power consumption of reactor 2 was higher than that of reactor 1 due to the low reaction rate, and most of the reaction was conducted by reactor 1. Whereas the detailed analysis of the power consumption, such as hydrogen flow rate on the reaction, was not reviewed. Since the reaction rate is highly dependent on the feed gas flow and the main factor to the reaction heat. The factors increasing the methanation power consumption, especially on the hydrogen flow rate while improving the methane concentration, are expressed in the next chapter.

References

[1] Nakamura A, Ota Y, Koike K, Hidaka Y, Nishioka K, Sugiyama M, et al. A 24.4% solar to hydrogen energy conversion efficiency by combining concentrator photovoltaic modules and electrochemical cells. Appl Phy Exp. 2015; 8: 107101.

[2] Ota Y, Yamashita D, Nakao H, Yonezawa Y, Nakashima Y, Ebe H, et al. Highly efficient 470W solar-to-hydrogen conversion system based on concentrator photovoltaic modules with dynamic control of operating point. Appl Phys Express. 2018; 11: 077101.

[3] Wai SH, Ota Y, Yamashita D, Sugiyama M, Nishioka K. High efficiency solar to gas conversion system using concentrator photovoltaic and electrochemical cell. Proceedings of Grand Renewable Energy Conference, 17-22 June. Pacifico Yokohama, Yokohama. Japan: JCRE; 2018.

[4] Yamaguchi M. Super-high efficiency III-V multi-junction and multi-junction cells. 2nd ed. Archer MD, Green MA, Eds. Clean Electricity from photovoltaics. Imperial Collage Press. 2015; London, UK. 307-338.

[5] Yamaguchi M, Takamoto T, Araki K, Ekins-Daukes N. Multi-junction III-V solar cells: current status and future potential. Solar Energ. 2005; 79(1): 78–85.

[6] Green MA, Emery K, Hishikawa Y, Warta W, Dunlop ED, Levi DH, Ho-Baillie AWY. Solar cell efficiency tables (version 51). Prog. Photovolt. 2017; 25: 668–676.

[7] Bertness, K.A.; Kurtz, S.R.; Friedman, D.J.; Kibbler, A.E.; Kramer, C.; Olson, J.M. 29.5%-efficiency GaInP/GaAs multi-junction solar cells. Appl. Phys. Lett. 1994; 65: 989–991.

[8] Philipps SP, Bett AW. III-V Multi-junction solar cells and concentrating photovoltaic (CPV) systems. Adv. Opt. Technol. 2014; 3: 469–478.

[9] Olson JM, Kurtz SR, Kibbler AE. A 27.3% efficient Ga0.5In0.5P/GaAs tandem solar cell. Appl Phy Letters. 1990; 56: 623.

[10] Takamoto T, Agui T, Ikeda E, Kurita H. High efficiency InGaP/InGaAs tandem solar cells on Ge substrates. Proceedings of the 28th IEEE Photovoltaic Specialists Conference, 15-22 Sep; Anchorage, AK, USA: 2000. pp. 976–981.

[11] Nishioka K, Takamoto T, Agui T, Kaneiwa M, Uraoka Y, Fuyuki T. Annual output estimation of concentrator photovoltaic systems using high-efficiency InGaP/InGaAs/Ge triple-junction solar cells based on experimental solar cell's characteristics and field-test meteorological data. Solar Energ Mat Solar Cells. 2006; 90: 57–67.

[12] Solmecke H, Just O, Hackstein D. Comparison of solar hydrogen systems with and without power electronic DC/DC converters. Renew Energ. 2000;19(1–2): 333–338.

[13] Maeda T, Ito H, Hasegawa Y, Zhou Z, Ishida M. Study on control method of the stand-alone direct-coupling photovoltaic-water electrolyzer. Int J Hydrogen Energ. 2012; 37(6): 4819–4828.

[14] Clarke RE, Giddey S, Ciacchi FT, Badwal SPS, Paul B, Andrews J. Direct coupling of an electrolyser to a solar PV system for generating hydrogen. Int J Hydrogen Energ. 2009; 34(6): 2531–2542.

[15] Paul B, Andrews J. Optimal coupling of PV arrays to PEM electrolysers in solar hydrogen systems for remote area power supply. Int J Hydrogen Energ. 2008; 33(2): 490–498.

[16] Garrigós A, Blanes JM, Rubiato J, Ávila E, García CG, Lizán JL. Direct coupling photovoltaic power regulator for stand-alone power systems with hydrogen generation. Int J Hydrogen Energ. 2010; 35(19): 10127–10137.

[17] Arriaga LG, Martinez W, Cano U, Blud H. Direct coupling of a solar-hydrogen system in Mexico. Int J Hydrogen Energ. 2007; 32(13): 2247–2252.

[18] García-Valverde R, Espinosa N, Urbina A. Optimized method for photovoltaic-water electrolyser direct coupling. Int J Hydrogen Energ. 2011; 36(17):10575–10586.

[19] Kelly NA. The coupling factor: a new metric for determining and controlling the efficiency of solar photovoltaic power utilization. Int J Hydrogen Energ. 2013; 38: 2079–2094.

[20] Djafour A, Matoug M, Bouras H, Bouchekima B, Aida MS, Azoui B. Photovoltaic-assisted alkaline water electrolysis: basic principles. Int J Hydrogen Energ. 2011; 36: 4117–4124.

[21] Barbir F. PEM electrolysis for production of hydrogen from renewable energy sources. Solar Energ. 2005; 78(5): 661–669.

[22] Hohm DP, Ropp ME. Comparative study of maximum power point tracking algorithms. Prog Photovolt Res Appl. 2003; 11: 47–62.

[23] García-Valverde R, Miguel C, Martínez-Béjar R, Urbina A. Optimized photovoltaic generator-water electrolyser coupling through a controlled DC-DC converter. Int J Hydrogen Energ. 2008; 33: 5352–5362.

[24] Garrigós A, Blanes JM, Carrasco JA, Lizán JL, Beneito R, Molina JA. 5 kW DC/DC converter for hydrogen generation from photovoltaic sources. Int J Hydrogen Energ. 2010; 35: 6123–6130.

[25] Cavallaro C, Cecconi V, Chimento F, Musumeci S, Santonocito C, Sapuppo C. A phase-shift full bridge converter for the energy management of electrolyzer systems. Proceedings of 2007 IEEE International Symposium on Industrial Electronics. 4–7 June. Vigo, Spain: 2007. pp. 2649–2654.

[26] Agbossou K, Doumbia ML, Anouar A. Optimal hydrogen production in a stand-alone renewable energy system. Proceedings of IEEE 2005 Industry Applications conference. 2–6 Oct. Hong Kong, China: 2005. pp. 2932–2936.

[27] Sahin ME, Okumus HI, Aydemir MT. Implementation of an electrolysis system with DC/DC synchronous buck converter. Int J Hydrogen Energ. 2014; 39(13): 6802–6812.

[28] Yamashita D, Nakao H, Yonezawa Y, Nakashima Y, Ota Y, Nishioka K. A new solar to hydrogen conversion system with high efficiency and flexibility. Proceedings of IEEE 6th International Conference on Renewable Energy Research and Applications ICRERA; 5–8 Nov; San Diego, CA. USA: IEEE; 2017. pp. 441–446.

[29] Carmo M, Fritz DL, Mergel J, Stolten D. A comprehensive review on PEM water electrolysis. Int J Hydro Energ. 2013; 38: 4901–4934.

[30] Guo Y, Li G, Zhou J, Liu Y. Comparison between hydrogen production by alkaline water electrolysis and hydrogen production by PEM electrolysis. IOP Conf. Ser. Earth Environ. Sci. 2019; 371: 042022.

[31] Zeng K, Zhang D. Recent progress in alkaline water electrolysis for hydrogen production and applications. Prog Energ Combust Sci. 2010; 36: 307–326.

[32] Zhang H, Su S, Lin G, Chen J. Efficiency Calculation and Configuration Design of a PEM Electrolyzer System for Hydrogen Production. Int J Electrochem Sci. 2012; 7: 4143–4157.

[33] Onda K, Kyakuno T, Hattori K, Ito K. Prediction of production power for high-pressure hydrogen by high-pressure water electrolysis. J Power Sources. 2004; 132(1–2): 64–70.

[34] Schaaf T, Grunig J, Schuster MR, Rothenfluth T, Orth A. Methanation of CO_2-storage of renewable energy in a gas distribution system. Energy Sustain. Soc. 2014; 4: 1–14.

[35] Yingli, W.; Jiao, L.; Qiang, L.; Jian, Y.; Fabing, S. Performance comparison of syngas methanation on fluidized and fixed bed reactors. Proceedings of 13th International Conference on Fluidization New Paradigm in Fluidization Engineering, 16-21 May, Gyeong-ju, Korea: 2010, 102.

[36] Schlereth D, Hinrichsen O. A fixed-bed reactor modeling study on the methanation of CO_2. Chem Eng Res Des. 2014; 92: 702–712.

[37] Ghaib K, Ben-Fares FZ. Power-to-methane: a state-of-the-art review. Renew. Sust. Energy Rev. 2018; 81: 433–446.

[38] Takano H, Shinomiya H, Izumiya K, Kumagai N, Habazaki H, Hashimoto K. CO_2 methanation of Ni catalysts supported on tetragonal ZrO_2 doped with Ca_{2+} and Ni_{2+} ions. Int. J. Hydrogen Energ. 2015; 40: 8347–8355.

[39] Wang W, Gong J. Methanation of carbon dioxide: an overview. Front Chem Sci Eng. 2011; 5(1): 2–10.

[40] Takano H, Kirihat Y, Izumiya K, Kumagai N, Habazaki H, Hashimoto K. Highly active Ni/Y-doped ZrO_2 catalysts for CO_2methanation. Appl Sur Sci. 2016; 388: 653–663.

[41] Krämer M, Stöwe K, Duisberg M, Müller F, Resiser M, Sticher S, et al. The impact of dopants on the activity and selectivity of a Ni-based methanation catalyst. Appl Catal. 2009; 369: 42–52.

[42] Cai M, Wen J, Chu W, Cheng X, Li Z. Methanation of carbon dioxide on Ni/ZrO_2-Al_2O_3 catalysts: effects of ZrO_2 promoter and preparation method of novel ZrO_2-Al_2O_3 carrier. J of Natural Gas Chem 2011; 20: 318−324.

[43] Abate S, Mebrahtu C, Giglio E, Deorsola F, Bensaid S. Catalytic performance of γ-Al_2O_3−ZrO_2−TiO_2−CeO_2 composite oxide supported Ni-based catalysts for CO_2 methanation. Ind Eng Chem Res 2016; 55: 4451−4460.

[44] Ashok J, Ang ML, Kawi S. Enhanced activity of CO_2 methanation over Ni/CeO_2-ZrO_2 catalyst: influence of preparation methods. Catal Today. 2017; 281: 304–311.

[45] Zhen W, Li B, Lu G, Ma J. Enhancing catalytic activity and stability for CO_2 methanation on Ni@MOF-5 via control of active species dispersion. Chem Comm. 2015; 51: 1728–1731.

[46] Barbarossa, V.; Vanga, G. Methanation of carbon dioxide. Proceedings of XXXIV Conference Meeting of the Italian Section of the Combustion Institute, 24–26 October, Santa Maria di Galeria, Roma: 2011.

[47] Mendoza-Hernanda O.S, Shima A, Matsumoto H, Inoue M, Abe T, Matsuzaki Y, et al. Exergy valorization of a water electrolyzer and CO_2 hydrogenation tandem system for hydrogen and methane production. Sci Rep 2019; 9: 6470.

[48] Stageland K, Kalai D, Li H, Yu Z. CO_2 methanation: the effect of catalysts and reaction conditions. Energ Procedia. 2017; 105: 2022–2027.

[49] Gao J, Wang Y, Ping Y, Hu D, Xu G, Gu F, Su F. A thermodynamic analysis of methanation reactions of carbon oxides for the production of synthetic natural gas, RSC Advances 2012; 2: 2358–2368.

[50] Sun D, Simakov D.S.A. Thermal management of a Sabatier reactor for CO_2 conversion into CH_4: simulation-based analysis. J. CO_2 Util. 2017; 21: 368–382.

Chapter 3

Performance analysis of Sabatier reaction on direct hydrogen inlet rates based on power-to-gas conversion system

3.1 The concept of the system

In this chapter, we propose an improved conversion and a detailed analysis of the methanation power consumption for the hydrogen flow to the reaction. In the previous chapter, the energy consumption by the reactors performed on a sunny day and an overcast day has been introduced. Since there are two reactors in our system, the second reactor consumed more energy than the first one. Therefore, the factors increasing the consumption are reviewed and analyzed to improve the system with less energy consumption. To achieve a high solar-to-methane conversion efficiency, optimal conditions of the reactor temperature, and H_2 and CO_2 mixed gas flow rates are necessary.

In particular, since the Sabatier process is an exothermic reaction, the reactor temperature can be maintained at or above the optimal temperature without supplying external power by adjusting the flow rate of the mixed gas. Consequently, the power consumption of the reactors decreases, and the total energy conversion efficiency improves. Conversely, decreasing flow rate (or space velocity) reduces the heat generated during the Sabatier process; thus, external electric power is supplied to maintain the reactor temperature. In addition, the CO_2-to-CH_4 conversion efficiencies also decrease at low hydrogen generation rates. Under actual outdoor conditions, the flow rate of the mixed gas (or H_2 generation) fluctuates due to the changing irradiance. Therefore, maintaining optimal conditions, especially the flow rate, is difficult throughout the year. Consecutively, the energy loss by the system will be higher with an intermittent reaction rate. It is essential to identify the optimal conditions of the system when the input feed gas is low or if the input gas is maintained at a constant rate. To investigate this,

we applied DC electricity supply to the electrolysis process to smoothly control the hydrogen flow rate provided to the methanation reactors.

In the present study, we investigated the optimal operating conditions of reactors of the methanation system, especially the mixed gas flow rate, reaction temperature, and power consumption. Furthermore, we aimed to understand the required minimum flow rate while maintaining a high CO_2-to-CH_4 conversion efficiency since it is an important factor for designing the capacity (size of PV panels and EC cells) of the solar-based synthetic gas system. Additionally, optimal reactor temperatures were investigated due to their significance in minimizing energy loss. Optimum temperature of the reactor is important to avoid irrational kinetic barriers, such as reverse-water reaction and catalyst deactivation, which are mainly caused by catalyst sintering and carbon deposition on the catalyst [1–4]. These conditions can be accelerated at temperatures above 500 °C [5–13]. Catalyst deactivation is a common concern during the catalytic reaction process. It is associated with degradation of the catalyst performance activity and selectivity over the reaction period. Therefore, low reactor temperatures are favorable during operation.

Furthermore, controlling the heat of the reactors in the methanation system is critical as extreme heat can degrade the catalysts. CO_2-to-CH_4 conversion relies on catalyst performance; additionally, optimizing the reactor temperature is significant in investigating and identifying the performance of the methanation system. The inlet gas flow to the reactors is related to the reaction rates and temperature of the reactors. While the energy consumed by the reactors are influenced by the reaction rate in terms of feed gases flow. Therefore, the methanation performance was investigated and analyzed for different hydrogen generation rates along with monitoring of the operating temperature of the reactors.

3.2 The system designs

3.2.1 DC power supply

In our power-to-gas (PtG) conversion system, there are two main electricity options for the electrolyzers: electricity provided by the CPV modules and the DC electricity. The daily actual outdoor operation conditions for hydrogen conversion were provided by the electricity produced from the three CPV modules under actual outdoor operation. The output energy of the CPV modules and the daily hydrogen generation rates varied depending on the sunlight. The hydrogen generation rate was the highest on sunny days; however, it was zero during nights and cloudy days. The hydrogenation system performed spontaneously based on the applied solar energy, and the operating parameters of the system, such as the hydrogen generation rates (GR_{H2}).

The flow rate of hydrogen could not be controlled under actual outdoor conditions (using sunlight). GR_{H2} was dependent on sunlight, and the flow of hydrogen to the Sabatier reaction was also irregular and could not be performed during cloudy days. Currently, an efficient daily solar-to-methane conversion system is required for the energy sector. In this study, the required electricity for the hydrogenation system was applied using a DC power supply (Kikusui, PAS 320-2) to obtain a stable flow rate. The latter portion of the solar-to-gas conversion system and thermo-catalytical methanation was operated and analyzed using solar-based hydrogen on sunny days and using power supplied hydrogen on cloudy days. Fig. 3.1 shows the schematic configuration of electrolysis process supplied with DC supply and the methanation reactors to produce methane.

3.2.2 Operation system design and measurement equipment

The former portion of PtG conversion, hydrogen production was performed using the PEM method. DC/DC converters were applied to match the input and output voltage variabilities as

GR_{H2} was dependent on the electricity supplied to the DC/DC converters. Therefore, hydrogen production rate was controlled by varying the electric current of the DC power supply. After that, the hydrogen produced was consecutively transported to the reactors and combined with CO_2. Subsequently, methanation reaction was performed using catalysts. Fig. 3.2 illustrates the system configuration of DC-supplied electrolysis system in a consecutive connection with methanation system. The generation rates of produced hydrogen were measured using a mass flow meter (MFM, M-2SLM-D-25COMP), while the flow rate of CO_2 was controlled by a mass flow controller (MFC, Alicat Scientific MC-500SCCM-D-25COMP). The generated gas mixtures were analyzed using gas chromatography (GC) (J-SCIENCE LAB, GC 7100), as shown in Fig. 3.3. GC measurement device is directly connected to the outlet of methanation reactors via pipes. The byproduct, water (from electrolysis process), was filtered using gas/liquid separators; however, GC analysis could not detect peaks of water during the operation period. Argon (Ar) was used as the carrier gas for the mixture of gases during the measurement. The two reactors were attached sequentially; the reaction initially occurred in the first reactor, while the produced and unreacted gases proceeded in the second reactor.

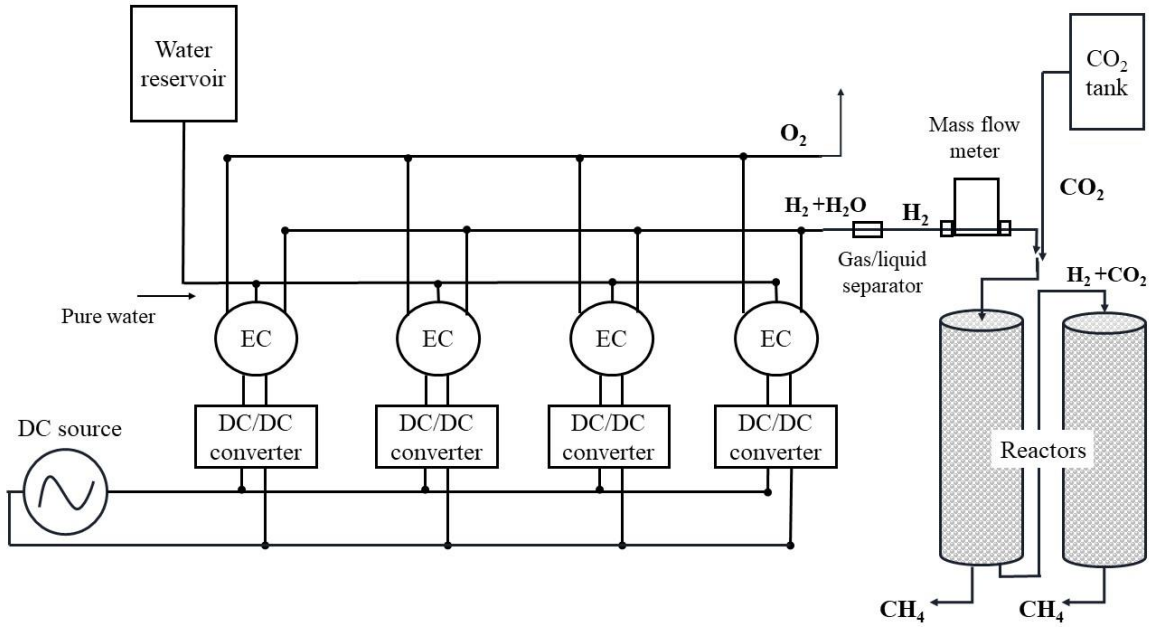

Fig. 3.1 Schematic illustration of hydrogen production from DC electricity and methanation system.

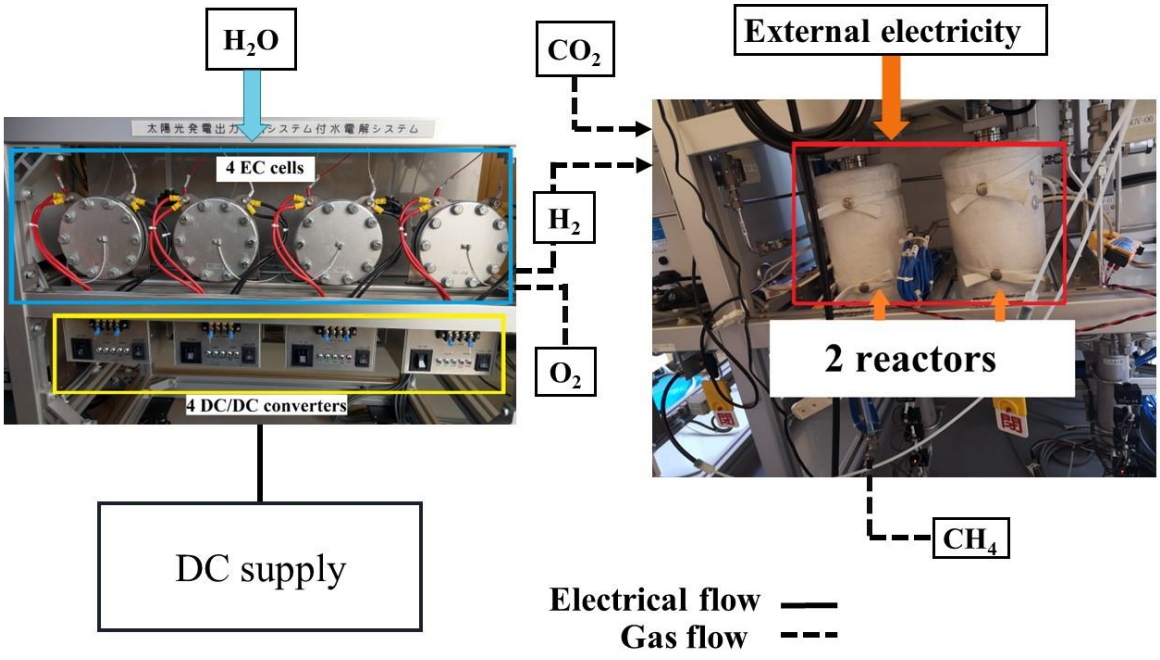

Fig. 3.2 Configuration of power-to-gas conversion in which DC supply is provided to the electrolysers through DC/DC converters and consecutive methanation system.

Fig. 3.3 Photograph of gas chromatography, (GC) (J-SCIENCE LAB, GC 7100), installed at the outdoor solar-to-gas conversion field test area of the University of Miyazaki.

3.3 Results and discussion

3.3.1 Evaluation of methane concentration based on hydrogen generation rates

Controlling the reactor temperature is critical during the Sabatier reaction to overcome thermodynamic constraints related to catalysts [12, 14]. The residence time of the feed gas and catalyst, and the optimal operating conditions such as feed gases flow and temperature for the reaction are dependent on the size of the reactors. The reactor was thus, designed accordingly. A methanation system with a series of multiple reactors and complicated cooling system leads to the system more complex, and results in high initial cost [15–17]. Presently, a series of adiabatic reactors are in demand to optimize thermal control in fixed-bed reactors [15, 18]. In this study, a couple of adiabatic fixed-bed reactors were used while Ni-based catalysts are attached inside the reactors. The parameters of the rectors presented here are 19.05 mm for its outside diameter, 16.57 mm for inside diameter with the length of 200 mm for each reactor. The output hydrogen was subsequently applied to the reactors. The intermittent hydrogen production due to variable solar irradiance generates an unsteady flow feed to the methanation system. Consequently, the unsteady flow of hydrogen in the Sabatier reaction produces variability in the reaction rate between the feed gases (CO_2 and H_2). The transient feed flow of reactant gases can develop hot spots in the reactors [19]. Therefore, the performance of the Sabatier reaction was analyzed to optimize methane production based on operating parameters, such as GR_{H2}.

This section outlines the effect of methane concentration on GR_{H2}. Initially, a high setting temperature (260 °C) was induced in Reactor 1 [20] because the exothermic Sabatier reaction mainly occurred in Reactor 1. GR_{H2} depends on the performance of EC cells, which is a function of the input current of the DC/DC converter. Correspondingly, Higher the input current, greater is the generation of hydrogen from the electrolysis process. The produced hydrogen was not stored and was subsequently fed into the reactors. Consequently, the

intermittent hydrogen flow in the inlet reduced the residence time between the reactant gases (CO_2 and H_2) and the catalyst. Thus, the operating temperature of Reactor 1 increased with increasing GR_{H2}. Alternatively, a short residence time lowers the methane concentration [11, 21–23]. The Sabatier reaction was completed, and the composition of methane was measured at different GR_{H2} by setting the input current of the DC/DC converters. As mentioned above, the input current to the DC/DC converters was supplied and manually controlled through DC power supply device.

Fig. 3.4 shows the test results on the concentration of methane at varying GR_{H2}. The operating temperature of the two reactors was set to 260 °C (previously optimized temperature) [20]. The current of DC/DC converters ranged from 0.2 A to 1.6 A and subsequently, the GR_{H2} were calculated. The average GR_{H2} of a sunny day under the highest direct normal irradiance (900 W/m^2) is 1.19 NL/min, and it was generated at 1.6 A of the average input current of DC/DC converters. The generation rate was lower than this and could not perform well during overcast and cloudy days. Therefore, the average GR_{H2} on a sunny day was considered in this study. The highest methane concentrations, measured at 30 min intervals for each GR_{H2}, were achieved at 0.337 and 0.449 NL/min of GR_{H2}. Furthermore, observing the stability of the methane composition during long-term measurements is significant. Subsequently, the Sabatier reaction was analyzed by varying the temperature from 180 °C to 340 °C (Fig. 3.5), with each operation maintained for 4 h. Consequently, high methane composition (98.4%) was observed at 220 °C and 0.449 NL/min of GR_{H2}.

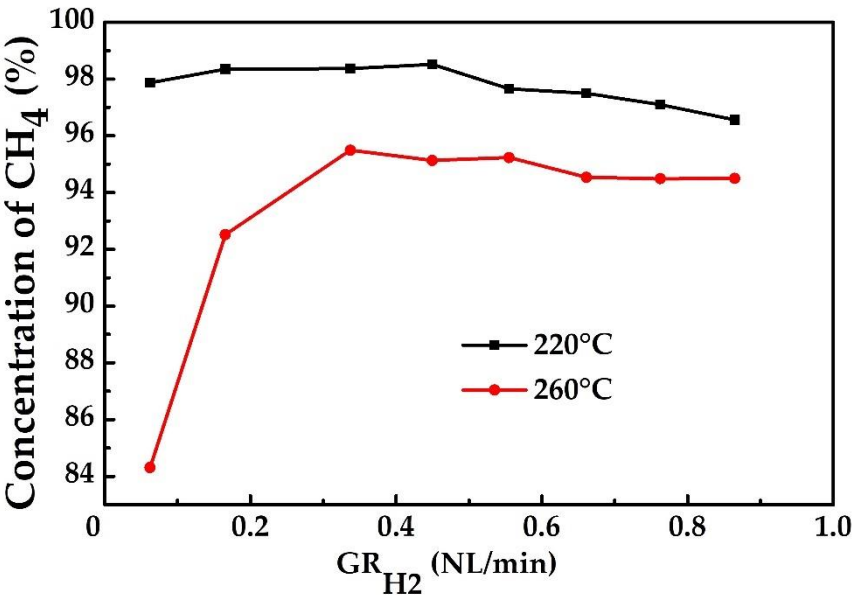

Fig. 3.4 Analysis of methane concentration on different hydrogen generation rates.

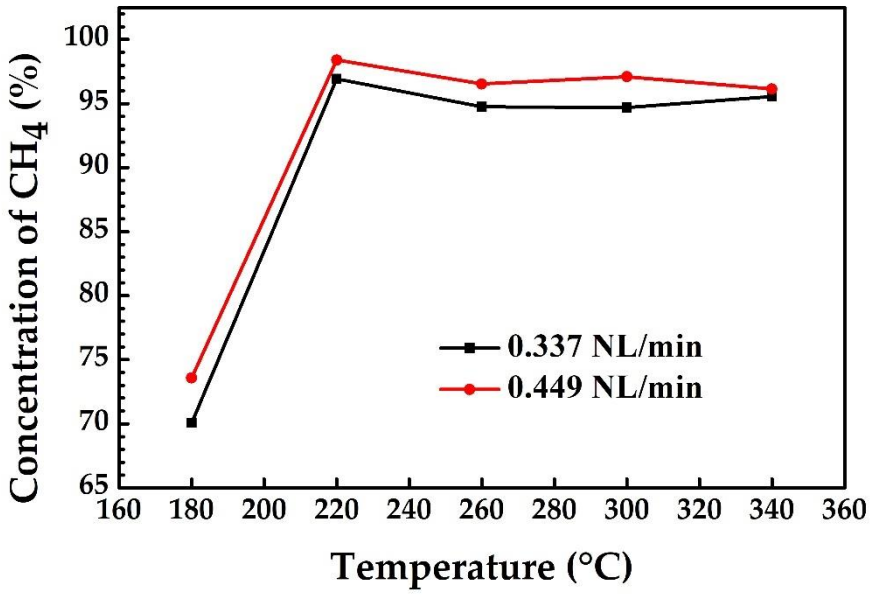

Fig. 3.5 Analysis of methane concentration on different operating temperatures ranging from 180 °C to 340 °C.

3.3.2 System performance on a 4 h period

The stability of the system performance in terms of methane composition was analyzed and evaluated for a 4 h operation. The Sabatier reaction was evaluated at a low GR_{H2} (0.339 NL/min) and a high GR_{H2} (0.449 NL/min). The methane composition was measured every 30 min during the experimental period from 10:00 a.m. to 2:00 p.m., and the corresponding GR_{H2} was measured on two different days, as shown in Fig. 3.6.

The highest concentration of methane (98.4%) was observed at 220 °C and high GR_{H2} (0.449 NL/min). Similarly, 97.2% of methane was obtained at the same temperature, but lower GR_{H2} (0.337 NL/min), indicating that methane concentration was high at a higher GR_{H2}, whereas it decreased at a lower GR_{H2}. Since maintaining a high performance over a long duration is necessary to achieve high methane concentrations, a low operating temperature (220 °C) and a high GR_{H2} were selected as the optimal operating parameters for the operation test.

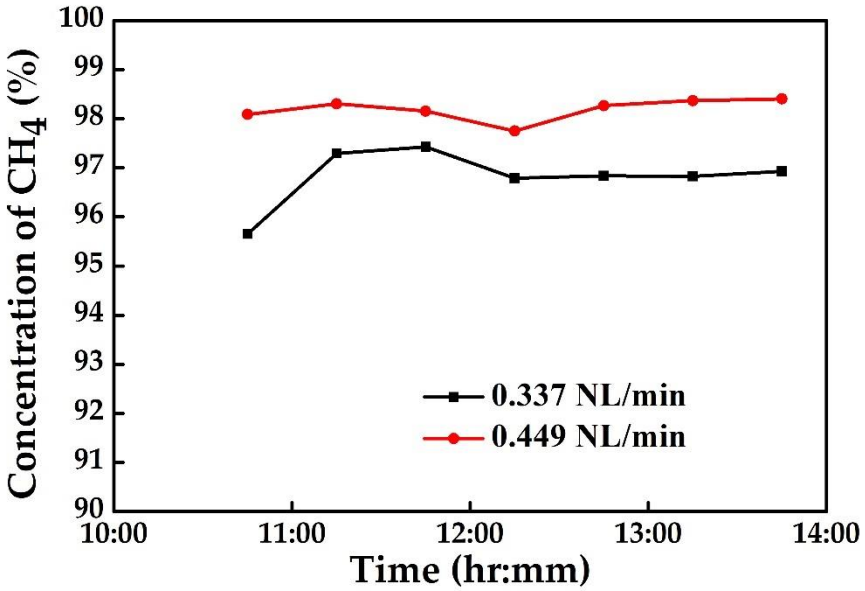

Fig. 3.6 Analysis of methane concentration during the 4 h operation at an operating temperature of 220 °C and measured on July 21, 2020 and August 6, 2020.

3.3.3 Optimization of the reactor operating conditions: operating temperature of the reactors

The performance of the reactors was analyzed under controlled operating conditions of DC/DC converters. Based on the previous results, both reactors were set at 220 °C and an input GR_{H2} of 0.449 NL/min. External power was supplied to the reactors; subsequently, the inner and outer temperatures of the reactors during the study period were measured using heat sensors.

Fig. 3.7 presents the inner temperatures of the two reactors against the target set temperature. Subsequently, the inner temperatures of the reactors reached and were maintained at the target set temperature of 220 °C for 4 h. The controlled performance of the DC/DC converters and EC cells provided a low hydrogen feed flow to the reactors, thus, contributing to a longer residence time between the gas mixture and the catalyst bed. Consequently, stable reaction rates within the reactors maintained uniform operating temperatures. The uniform reactor temperature occurs because of low inlet hydrogen rate [24]. Moreover, the concentration of methane increased.

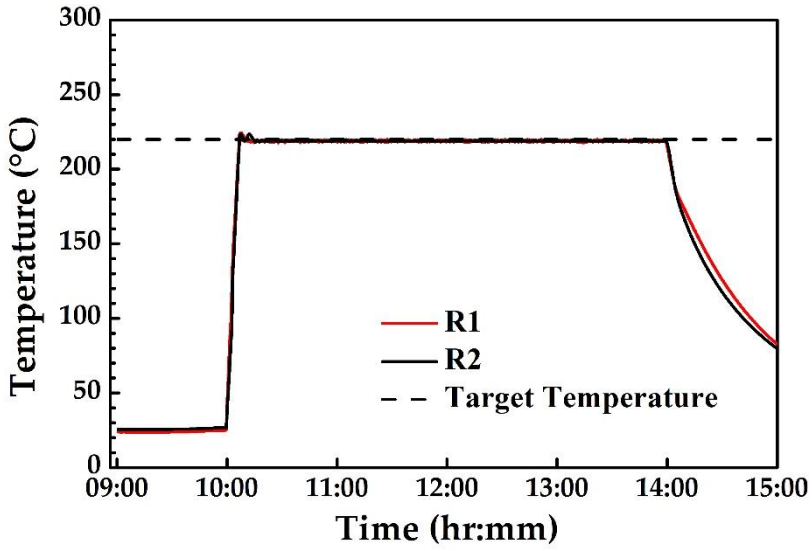

Fig. 3.7 Measurement on operation temperatures of the reactors compared with the set temperature (220 °C).

3.3.4 Optimization of the reactor operating conditions: power consumption of methanation system based on the two GR_{H2}

A cost-effective system having a high methane composition and low total power consumption is desirable for conventional gas-grid infrastructures. Increased heating of the reactors caused by the Sabatier reaction can influence the performance and shelf life of the catalysts [6, 25]. Additionally, low reaction rate consumes more power to initiate the reaction. Since external power was supplied to the methanation system in this study, power consumption of the reactors was analyzed.

The total power consumption of the reactors was evaluated under two GR_{H2} conditions (Fig. 3.8). At high GR_{H2} (0.449 NL/min), the total power consumption (0.156 kWh) was low, whereas the total power consumption (0.161 kWh) was high at low GR_{H2} (0.337 NL/min). A stable flow rate with sufficient amount of H_2 and CO_2 contributed to uniform reaction rates of the gases with the catalyst bed. Furthermore, a constant temperature was maintained to sustain the reaction. Consequently, the total power consumption was low at high GR_{H2} and uniform reactor temperature.

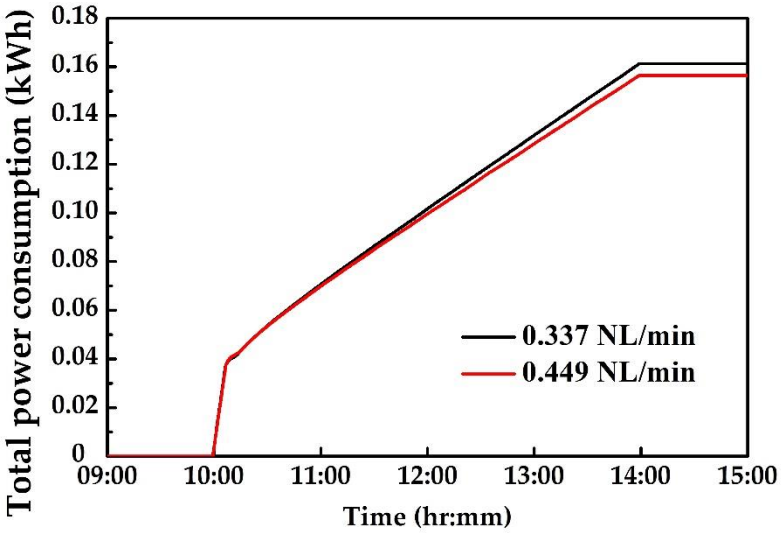

Fig. 3.8 Analysis on total power consumption of the reactors operating in two GR_{H2} conditions (on July 21, 2020 and August 6, 2020).

Solar-to-methane conversion with high methane conversion rates and low power consumption promotes an economic and effective system. The Sabatier reaction is highly exothermic, releasing 165 kJ of energy to produce 1 mol of methane during the reaction. The heat released during the reaction can affect the catalyst performance, and thus, the temperature of the reactor needs to be controlled. Furthermore, a transient inlet flow in the reactors can affect the reaction rates, consequently, requiring a high temperature to maintain the reaction. High operating temperatures and subsequent extreme heating in the reactors are undesirable conditions. Thus, the methanation system was evaluated in this study to maintain a constant temperature.

Solar-to-methane production could provide a carbon-free clean energy production mechanism with constant production of hydrogen and methane. Solar-based hydrogen provides intermittent and unsteady GR_{H2} to the methanation system due to its dependence on solar irradiance. Additionally, the solar-to-gas conversion fluctuates under varying weather conditions. Furthermore, the use of batteries to store solar energy not only decreases the efficiency of the methanation system, but also increases the cost. However, if solar energy is used for hydrogenation and simultaneously stored in the batteries, a constant solar-to-gas conversion rate could be provided throughout the year. Subsequently, hydrogen generated during the day could be stored and provided to the methanation system, especially during night and cloudy days.

GR_{H2} is known to fluctuate during actual outdoor operation and thus, cannot be controlled. Additionally, it depends on the current applied to the ECs and the amount of electricity produced by the CPV modules or supplied by the DC power. A moderate inlet hydrogen flow is required to maintain a steady reaction of the methanation system while maintaining a constant feed temperature. Conversely, a stable H_2 generation rate can be supplemented with a DC supply, in the form of a battery. Subsequently, the battery can store solar energy from the

CPV modules. In this study, the methanation system was analyzed based on the hydrogen inlet rates generated by the DC supply. It highlighted the methane concentration with respect to GR_{H2}, constant temperature, and low power consumption of the system.

We discussed the assumption that the system consisted of a CPV module and a battery that stored hydrogen from the solar energy. The total power consumption of the methanation system was evaluated and compared between the fully operated GR_{H2} (1.19 NL/min) [20] and controlled GR_{H2} (0.449 NL/min). The results are summarized in Table 1. In the former case, 0.145 kWh and 0.281 kWh of power was consumed on sunny and cloudy days, respectively. Therefore, the percentage of energy loss was computed as follows:

$$\text{Energy loss}(\%) = \frac{E_{\text{r con}} - E_{\text{r app}}}{E_{\text{r app}}} \times 100, \tag{3.1}$$

where, $E_{\text{r con}}$ and $E_{\text{r app}}$ are the total power consumptions on two days under the conventional system and assumed system, respectively. In the conventional system, the required energy to maintain the reactor's temperature decreased to 48.3% on a sunny day, however, an energy loss (36.5%) was incurred from impractical H_2 production on cloudy days. Conversely, a stable H_2 flow provided a stable operating temperature and resulted in decreasing power consumption. If maintaining the high GR_{H2}, the energy loss could be reduced. Thus, an efficient methanation system can be developed in the presence of sufficient storage of electricity produced by CPV modules and a moderate GR_{H2}. Consequently, energy losses would be significantly reduced while ensuring constant generation of hydrogen throughout the year. The findings of this study could provide a flexible performance of a methanation system under any weather conditions, especially during night and cloudy days. We are continuously measuring the stored energy of produced methane and power consumption of the reactors and analyzing the optimal condition with high methane concentration and low energy loss for the long-term operation of methanation throughout the year based on it.

Table 3.1 Summary of the total power consumption, and percentage of energy losses on fully operated GR_{H2} and controlled GR_{H2}.

System configuration	Operation Temperature (°C)	Total power consumption (kWh)		Energy loss (%)
		Sunny day	Overcast day	
Directly applied by CPV module (conventional system)	260 °C	0.145 kWh GR_{H2} (1.19 NL/min)	0.281 kWh GR_{H2} (0.00 NL/min)	36.5%
Applied by CPV module with battery (as an assumption)	220 °C	0.156 kWh GR_{H2} (0.449 NL/min) (H_2 generated by CPV module energy)	0.156 kWh GR_{H2} (0.449 NL/min) (H_2 generated by battery energy)	–

3.4 Conclusion

The power-to-gas conversion was approached from CO_2 hydrogenation in which DC-derived hydrogen was consecutively supplied to the reactors. The Methanation process releases extreme heat during the reaction. It would result in catalyst degradation. The reactors in the study were provided with external electricity to initiate the reaction process. Subsequently, the reaction itself was maintained by the heat released. However, in our previous study, reactor 2 consumed more energy than reactor 1, although the temperature of reactor 2 maintained at the operating set temperature (260 °C). Therefore, it is crucial to reduce the power consumption of the reactors while maintaining the operating set temperature and improving the methane concentration.

In this chapter, we analyzed the power consumption of the methanation reactors at various hydrogen generation rates, which was the reactant of the methanation reaction). To investigate and manage the hydrogen generation rates, we controlled the electricity provided to the DC/DC converters, which is the input of the electrolyzers. Regulating hydrogen generation rates using solar energy outdoor is difficult due to the intermittent irradiance. Accordingly, the DC electricity supply was applied to control the hydrogen flow rate to the reactors. DC electricity was varied from 0.2 A to 1.6 A while the hydrogen generation was automatically measured by the mass flow meter. It is required to analyze the operating temperature on varied hydrogen flow rates to observe the maximum methanation concentration. Therefore, concentration of methane, total power consumption, and optimized reactor temperatures was reviewed and highlighted.

The results indicated that the reactors maintained a constant temperature because of moderate hydrogen flow rates; additionally, low power consumption at increased GR_{H2}. The results also provided that the higher the hydrogen generation, the higher the methanation concentration. Additionally, it was found that a stable hydrogen flow could reduce increasing

reactors' temperature and maintain the set temperature. Whereas the results showed that a low hydrogen flow feed or hydrogen generation required more energy consumption than a high hydrogen generation. Additionally, the concentration of methane improved at a stable and moderate hydrogen flow rate.

The solar-based hydrogen generation was inefficient during cloudy days and nights. Therefore, we discussed the assumption and comparison on two systems: fully operated GR_{H2} on CPV-derived system and controlled moderate GR_{H2} using a battery storing energy from the CPV. The results provided that the energy loss was incurred in the former case due to impractical hydrogen production on cloudy days while the required energy for the reactors decreased on sunny day. Whereas in the latter case, energy loss would be reduced with a constant and moderate hydrogen generation throughout the year. The findings of this study could provide a flexible performance of a solar-based methanation system under any weather conditions, especially during night and cloudy days.

References

[1] Mendoza-Hernanda OS, Shima A, Matsumoto H, Inoue M, Abe T, Matsuzaki Y, Sone Y. Exergy valorization of a water electrolyzer and CO_2 hydrogenation tandem system for hydrogen and methane production. J Sci Rep. 2019; 9: 6470.

[2] Bartholomew CH. Carbon deposition in steam reforming and methanation. J Catal Rev Sci Eng. 1982; 24(1): 67-112.

[3] Ewald S, Kolbeck M, Kratky T, Wolf M, Hinrichsen O. On the deactivation of Ni-Al catalysts in CO_2 methanation. J Appl Catalysis A, General. 2019; 570: 376–386.

[4] P.Brooks K, Hu J, Zhu H, Kee RJ. Methanation of carbon dioxide by hydrogen reduction using the Sabatier process in microchannel reactors. J Chem Engg Sci. 2007; 62: 1161–1170.

[5] Turks D, Mena H, Armbruster U, Martin A. Methanation of CO_2 on Ni/Al_2O_3 in a structured fixed-bed reactor- a scale-up study. J Catalysts. 2017; 7: 152.

[6] Younas M, Kong LL, Bashir MJK, Nadeem H, Shehzad A, Sethupathi S. Recent advancements, fundamental challenges, and opportunities in catalytic methanation of CO_2. J Energ Fuels. 2016; 30: 8815–8831.

[7] Stageland K, Kalai D, Li H, Yu Z. CO_2 methanation: the effect of catalysts and reaction conditions. J Energy Procedia. 2017; 105: 2022–2027.

[8] Wieclaw-Solny L, Wilk A, Chwola T, Krotki A, Tatarczuk A, Zdeb J. Catalytic carbon dioxide hydrogenation as a prospective method for energy storage and utilization of captured CO_2. J. Power Technol. 2016; 96(4): 213–218.

[9] Gao J, Liu Q, Gu F, Liu B, Zhong Z, Su F. Recent advances in methanation catalysts for the production of synthetic natural gas. J RSC Adv. 2015; 5: 22759.

[10] Molina MM, Kern C, Jess A. Catalytic hydrogenation of carbon dioxide to methane in wall-cooled fixed-bed reactors. J Chem Eng Technol. 2016; 39(12): 2404–2415.

[11] Hoekman SK, Broch A, Robbins C, Purcell R. CO_2 recycling by reaction with renewably-generated hydrogen. Int. J. Greenhouse Gas Control, 2010; 4: 44–50.

[12] Sun D, Khan FM, Simakov DSA. Heat removal and catalyst deactivation in a Sabatier reactor for chemical fixation of CO_2: Simulation-based analysis. J Chem Engg. 2017; 329: 165–177.

[13] Gotz M, Koch AM, Graf F. State of the art and prospective of CO_2 methanation process concepts for power-to-gas applications. Proceedings of the International Gas Union Research Conference, 2014 Sep 17-19; Copenhagen, Denmark: 2014. p. 314-327.

[14] Moioli E, Gallandat N, Zuttel A. Parametric sensitivity in the Sabatier reaction over Ru/Al_2O_3- theoretical determination of the minimal requirements for reactor activation. J React Chem Eng. 2019; 4: 100–111.

[15] Schaaf T, Grunig J, Schuster Markus R, Rothenfluth T, Orth A. Methanation of CO_2-storage of renewable energy in a gas distribution system. J Energy Sustain Soc. 2014; 4: 1–14.

[16] Sun D, Simakov DSA. Thermal management of a Sabatier reactor for CO_2 conversion into CH_4: Simulation-based analysis. J CO_2 Utlization. 2017; 21: 368-382.

[17] El Sibai A, Rihko Struckmann LK, Sundmacher K. Model-based optimal Sabatier reactor design for power-to-gas applications. J Energy Technol. 2017; 5: 911-921.

[18] Toro C, Sciubba E. Sabatier based power-to-gas system: heat exchange network design and thermoeconomic analysis. J Appl Energ. 2018; 229: 1181–1190.

[19] Steffi T, Ronsch S, Guttel R. Transient flow rate ramps for methanation of carbon dioxide in an adiabatic fixed-bed recycle reactor. J Energ. Technol. 2020; 8: 1901116.

[20] Wai SH, Ota, Y, Sugiyama M, Nishioka K. Evaluation of a Sabatier reaction utilizing hydrogen produced by concentrator photovoltaic modules under outdoor conditions. Appl Sci. 2020; 10: 3144.

[21] Yingli W, Jiao L, Qiang L, Jian Y, Fabing S. Performance comparison of syngas methanation on fluidized and fixed bed reactors. Proceedings of 13th International Conference on Fluidization New Paradigm in Fluidization Engineering, 2010 May 16-21; Gyeong-ju, Korea, ECI Symposium Series; 2010.

[22] Chein RY, Chen WY, Yu CT. Numerical simulation of carbon dioxide methanation reaction for synthetic natural gas production in fixed-bed reactors. J Nat Gas Sci Eng. 2016; 29: 243–251.

[23] Jaffar MM, Nahil MA, Williams PT. Parametric study of CO_2 methanation for synthetic natural gas production. J Energ Technol. 2019; 7: 1900795.

[24] Currie R. Design and simulation of novel Sabatier reactors for the thermocatalytic conversion of CO_2 into renewable natural gas [Dissertation]. Waterloo, Ontario, Canada: University of Waterloo, 2019.

[25] Matthisschke S, Kruger R, Ronsch S, Guttel R. Unsteady-state methantion of carbon dioxide in a fixed-bed recycle reactor- experimental results for transient flow rate ramps. J Fuel Processing Technol. 2016; 153: 87–93.

Chapter 4

Forecasting solar-to-hydrogen and solar-to-methane energy conversion efficiency using Si and IMM PV-modules: a case-study in Japan

4.1 The concept of the system

In our previous studies, the outdoor solar-to-gas (StG) conversion has been successfully accomplished from triple-junction concentrator photovoltaic (CPV) modules. The system achieved the highest performance with the sets of DC/DC converters and electrochemical (EC) cells. In this chapter, we aimed to estimate the prospective StG conversion from flat PV systems based on our outdoor CPV-based results.

Currently, power-to-gas (PtG) conversion is drawing attention in Japan and the Japanese government is promoting cost-effective renewable energy generation and efficient PtG conversion (especially for hydrogen production, decarbonization, and storage). Considering the SDGs and growing energy demands, it could provide promising benefits for curtailing fossil fuels. Besides, methane is another feasible option that can be directly integrated into the current gas grid [1], while the infrastructure for hydrogen production and distribution is under development [2–6].

The energy conversion efficiency is one of the main factors in determining the long-term PtG implementation and addressing the capital cost of the efficient system [7–10]. To establish and realize an efficient PtG plant in the future, it is necessary to identify power generation and predict the potential energy conversion efficiency in the proposed regions. Accordingly, forecasting technologies play an essential role in addressing the challenges of implementing an efficient energy network. Various forecasting technologies for the solar system have been developed to accurately predict solar radiation and PV output [11–17]. In addition, the

estimation of potential solar-based hydrogen production concerning techno-economic analysis has been investigated by numerous researchers [8–10, 18, 19]. However, a detailed forecasting method related to the StG energy conversion technology is currently lacking.

In our previous studies, we demonstrated the world record solar-to-hydrogen (StH) conversion efficiency (24.4%) of concentrator photovoltaic (CPV) cells [20]. Additionally, the system was developed from CPV cells to CPV modules (sub-kilowatt output power) and an effective combination of electrochemical (EC) cells with DC/DC converters. The system provided the highest one-day StH conversion efficiency (18.78%) on a sunny day [21] and approximately 15% efficiency on a partial-cloudy day under outdoor operations [22] owing to the efficient cooperative performance of EC cells with converters [23]. Subsequently, StG conversion was expanded to solar-based methane production. The system achieved 96.1% methane composition and 97.6% CO_2-to-CH_4 conversion efficiency, respectively [22, 24]. Moreover, we obtained the highest outdoor solar-to-methane (StM) conversion efficiency record (13.8%) on a sunny day [24].

Additionally, a power generation prediction model considering all-climate conditions, called Miyazaki Spectrum to Energy (MS2E), has been developed from the meteorological test data for photovoltaic systems, METPV-11 database at the University of Miyazaki, Japan [17]. Accordingly, the amount of energy generated by various PV systems can be forecasted nationwide. In this study, we applied this MS2E PV energy prediction method and approached the potential StG conversion efficiency from Silicon-PV and inverted metamorphic (IMM) PV across Japan. Based on our actual StG measurement data, we approximated the conversion of each sub-system, as shown in Fig. 4.1.

In general, the application of tracking CPV systems is challenging, and the capital cost is slightly higher than that of traditional fixed-type PV systems [25, 26]. However, CPV has the potential to enable technological improvements with a reduction in cost. Various studies have

focused on technical improvements to provide highly efficient and cost-effective CPV systems [25, 27, 28]. Whereas silicon-PV types are well-established and commercially available, despite their low efficiency. Currently, multijunction cells are promising for improving the efficiency of both CPV and PV systems [29–33]. Additionally, these cells are being developed with a cost reduction prospect [27, 34–36]. Using the outdoor results as a benchmark, we approximated the conversion efficiency of two types of fixed PV modules: Silicon (Si) and highly efficient triple-junction inverted metamorphic modules (IMM). In this study, we only emphasized the prospective annual conversion efficiency in Japan by two types of flat PV. Economic aspects were not discussed in this approach. Additionally, we discuss an efficient type of PV module to realize StG conversion in Japan.

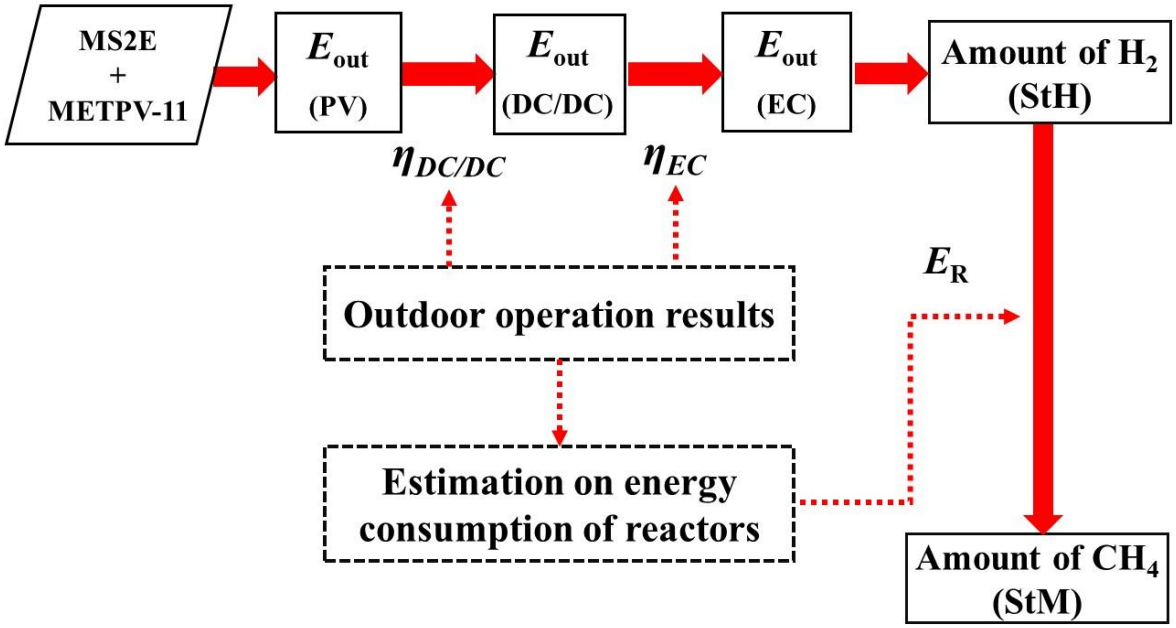

Fig. 4.1 Diagram layout for the estimation of energy yield of each system and conversion efficiencies. Based on the outdoor results, potential efficiencies of converter, EC cells and power consumption of reactors were predicted.

4.2 The system designs

4.2.1 Outdoor measurement data

In our previous studies, a StG conversion was performed using InGaP/GaAs/Ge triple-junction CPV modules with a tracking system under outdoor test field. Daily solar radiation was measured using a pyrheliometer during actual outdoor operations. The input/output voltages and current of the CPV modules, DC/DC converters and EC cells were automatically measured and monitored. The hydrogen generation rates (GR_{H2}) were determined using a mass flow meter (MFM), whereas carbon dioxide flow was controlled by a mass flow controller (MFC). The amount of produced gas was directly connected to the gas chromatography through pipes and analyzed its amount of concentration in percentage. The amount of methane produced was calculated on GR_{H2} and concentration of produced methane [24], and the energy consumption was measured during the experimental periods. The StH conversion was performed on sunny and cloudy days, whereas the StM conversion was performed only on sunny days. Based on the measured data, we approximated the conversion profiles from the input power of each system.

4.2.2 Simulation databases: irradiance and solar spectrum databases

To predict the energy yield by the PV system accurately, it is crucial to identify the precise solar spectrum in the proposed regions. The meteorological database for Japan (including 837 sites) was reported by the New Energy and Industrial Technology Development Organization (NEDO) [37]. This database is known as meteorological test data for photovoltaic systems (METPV-11). METPV-11 provides direct horizontal irradiance (DHI), scatter irradiance (SI), and ambient temperature (T_{amb}). We used these databases for the simulation. Japan has five regional solar spectrum databases classified by the NEDO [38]. Based on Bird's model, the Miyazaki-Spectrum-to-Energy (MS2E) method modified the solar spectrum estimation for all-

weather conditions considering atmospheric parameters (aerosol density and water precipitation) [17]. This method provides improved forecasting accuracy for both clear and overcast spectra. The accurate PV-output forecasting methods and simulation results have been established [17]. We employed this energy forecasting method to estimate the potential StG conversion in Japan.

4.2.3 Characteristics of Si and IMM modules

In this study, fixed-type Si (KIS AS-140) and InGaP/GaAs/InGaAs IMM (fabricated by SHARP) flat-PV modules were proposed to perform the StG conversion. Potential StG conversion efficiencies were approximated using these two modules. This flat-type IMM PV-module was installed at the University of Miyazaki and its high outdoor performance was tested and demonstrated [33, 39]. Therefore, we predicted the energy output of these modules using the MS2E method and the METPV-11 data. Subsequently, the potential StG conversion efficiencies of these modules were estimated.

4.2.4 Estimation of energy output by the modules

To predict the accurate energy yield by the PV system, it is crucial to identify the precise solar spectrum on the proposed regions. To determine the energy conversion efficiency of StG in Japan, the potential energy yield of the PV modules in t 837 locations was first evaluated. Since the crystalline silicon module consists of a single cell, estimation of the short circuit current (Isc), open-circuit voltage (Voc), and fill factor (FF) is simple. However, an IMM module consists of a combination of semiconductors in a layered structure, and luminescence coupling is a case matter for multi-junction solar cells. Therefore, it is necessary to include luminescence coupling to estimate the short-circuit current [17, 40]. In multi-junction solar cells, the fill factor is improved by the current-mismatching design. The FF was calculated by considering the current mismatching ratio between the sub-cells. According to the previously

established equations [17], the short-circuit current, open-circuit voltage, fill factor were calculated. After that, the annual energy output of a proposed PV module was calculated as follows:

$$E_{\text{out-PV}_{i,j}}(\text{kWh}) = \sum_{i=0}^{23}\sum_{j=0}^{364} P_{PV_{i,j}} \times t = \sum_{i=0}^{23}\sum_{j=0}^{364} \left[J_{sc_{i,j}} \times V_{oc_{i,j}} \times FF_{i,j} \times A_{mod} \times \eta_{sys} \times t \right], \quad (4.1)$$

where P_{PV} is the power output of the proposed PV module, J_{sc} is the estimated short-circuit current density, V_{oc} is open-circuit voltage, FF is estimated fill factor, A_{mod} is the area of proposed PV module, η_{sys} is the system efficiency and t is the duration in hour. The number, 0, represents the day number for 1st January and 364 is for 31st December. Similarly, the number of hours for a day is expressed from 0 to 23.

In our outdoor system, three CPV modules were connected in series to perform the StG conversion, in which the total output was about 470W (a sub-kilowatt PV system) under standard test condition. Four sets of DC/DC-electrochemical cells were attached in parallel to the CPV modules. Accordingly, the total electricity output could be increased by manually adjusting the number of connected CPV. Regardless of the number of modules, the efficiency of CPV was almost similar, whereas the converters' efficiency increased with increasing number [21]. The simulation results were similar to those of the outdoor performance. Since the area of the IMM module for the simulation model was smaller than the installed CPV, the total output energy yield of the IMM was lower than that of the CPV. Consequently, the efficiency of the DC/DC converter decreases in the IMM module. Similarly, the Si module provided a low energy yield even though it had the same module area as the CPV. To make a fair comparison and identify an efficient conversion, the module numbers of the simulation model were increased to match the output values provided by the outdoor system. Therefore, three Si-modules and 15 IMM-modules were considered in the simulation to achieve the highest conversion efficiency with respect to the actual outdoor conditions.

4.2.5 Calculation of converter efficiency and its integrated output power

Since electrochemical cells require a DC supply, DC/DC converters were applied to the EC cells to efficiently convert the electrical output from the PV modules. The daily input/output currents and voltages were measured under actual outdoor conditions, and the conversion efficiency of DC/DC converters was calculated. Based on the outdoor measurement results, the efficiency curve profile was identified for the output of PV-modules (which is also the DC/DC input). In this simulation model, we approximated the converters' efficiency and analyzed the relationship between the efficiency and energy input of the DC/DC converter. Accordingly, the integrated output power of the DC/DC converter was computed as below:

$$E_{\text{out-DC/DC}_{i,j}}(\text{kWh}) = \text{f}_{\text{DC/DC}} \times \sum_{i=0}^{23} \sum_{j=0}^{364} E_{\text{out-PV}_{i,j}}, \tag{4.2}$$

in which $\text{f}_{\text{DC/DC}}$ is the conversion efficiency approximated from the curve as a function of input energy, and $E_{\text{out-PV}}$ represents for the energy yield from the PV-modules.

4.2.6 Calculation of EC conversion efficiency and its energy output

The efficiency of EC cells in today's technologies is between 60-80%, depending on the installed type and load factor. PEM-type EC cells are attractive because of their compact design and their ability to provide pure hydrogen. PEM electrolyzers (fabricated by Enoah Inc., EHC-750) were used in our study. The EC cells used in our previous studies were efficient about 70% under outdoor conditions [21, 24]. The detailed outdoor performance on sunny and cloudy days was demonstrated in our previous work [22]. The daily input and output data were automatically monitored by the system. The daily conversion efficiency was estimated over the years. Since the electricity output was directly applied to the electrochemical cells through DC/DC converters, the outputs of DC/DC converters are the input to the EC cells. Based on our previous outdoor results, we constructed an approximation curve between the conversion

efficiency of EC cells and energy input of the EC cells. The annual integrated output of EC cells was estimated as:

$$E_{\text{out-EC}_{i,j}}(\text{kWh}) = f_{EC} \times \sum_{i=0}^{23} \sum_{j=0}^{364} E_{\text{out-DC}_{i,j}}, \quad (4.3)$$

where f_{EC} is the conversion efficiency approximated from the curve as a function of the output energy of the DC/DC converters.

4.2.7 Calculation of hydrogen generation rates and StH conversion

The energy required to generate hydrogen is the output energy of the EC cells. The potential numbers of generated hydrogen were estimated on the output energy produced by the EC cells divided by the Faraday constant, number of moles of hydrogen electrons, and the theoretical voltage required to split the water molecules. The amount of produced hydrogen and the StH conversion efficiency was calculated using the following equations.

$$\eta_{StH}(\%) = \sum_{i=0}^{23} \sum_{j=0}^{364} \frac{E_{\text{out-EC}_{i,j}}}{E_{\text{TSI}_{i,j}}} = \sum_{i=0}^{23} \sum_{j=0}^{364} \frac{E_{\text{H2}_{i,j}}}{E_{\text{TSI}_{i,j}}}, \quad (4.4)$$

where, $E_{\text{out-EC}}$ is the energy produced by the electrolyzer, E_{TSI} is the integrated annual solar irradiance on the proposed module and E_{H2} is the total energy stored by the generated hydrogen.

4.2.8 Calculation of energy consumption of the reactors and StM conversion

As previously mentioned, hydrogen generation is based on sunlight and fluctuates on cloudy days [24, 41]. However, a stable flow rate is required to produce methane thermodynamically. Since the generated hydrogen was not stored and spontaneously applied to the methanation system, the solar-based Sabatier reaction was performed only on sunny days, whereas the power-supplied reaction was operated on cloudy days. In this simulation study, we used solar-derived methanation results to approximate the reactor power consumption under actual conditions. Outdoor methanation analysis was performed on 15th

Nov 2019, [(17th/23rd/24th Mar), 2nd Apr, (3rd/8th/10th/18th/23rd/24th Jun), 3rd Jul in 2020], [(21st/25th/28th/29th Jan), (3rd/18th Feb), (8th Mar) in 2021. During measurements, the operating temperature of the reactors was 260 °C. These 19-days results were used to analyze the approximation profile of the reactors' energy consumption and hydrogen generation. Since the reactors were supplied with external electricity, it was necessary to identify the energy consumed by the reactors. The energy stored by the generated methane and the StM conversion efficiency were calculated as follows:

$$n_{H2}(\text{mol}) = \frac{\sum_{i=0}^{23}\sum_{j=0}^{364} E_{\text{out-EC}_{i,j}}}{1.23\ (\text{V})\times 2\times \text{F(C/mol)}}, \tag{4.5}$$

$$\eta_{StM}(\%) = \sum_{i=0}^{23}\sum_{j=0}^{364}\left[\frac{E_{CH4_{i,j}}}{E_{TSI_{i,j}} + E_{reactors_{i,j}}}\right] = \sum_{i=0}^{23}\sum_{j=0}^{364}\left[\frac{1/4 \times n_{H2} \times \eta_{CO_2\rightarrow CH_4} \times |\Delta H|}{E_{TSI_{i,j}} + E_{r1_{i,j}} + E_{r2_{i,j}}}\right], \tag{4.6}$$

in which, n_{H2} is the amount of hydrogen in moles produced by the electrolysis process, F is the Faraday's constant, E_{CH4} is the energy stored by the generated synthetic methane, $\eta_{CO2\rightarrow CH4}$ is the percentage of CO_2 to CH_4 conversion, and ΔH is the combustion energy of methane. $E_{reactors}$ is the energy consumed during the reaction, in which E_{r1} and E_{r2} are estimated as a function of hydrogen flow. E_{r1} and E_{r2} are the energy consumption of first reactor and second reactor, respectively. The amount of methane generated was correlated to one-fourth of the amount of hydrogen flow to the reaction and multiplied by the CH_4 concentration percentage [24]. In our study, we obtained 97.6 % as the CO_2 to CH_4 conversion rate at an operating temperature of 260 °C and the molar ratio of 1:4 (CO_2:H_2) [24]. We observed that the energy consumed by the reactors depended on the hydrogen feed flow to the reaction [24, 41]. A stable and moderate hydrogen flow provided a lower power consumption. Accordingly, the energy consumption by the Sabatier reaction was approximated based on the hourly amount of integrated hydrogen feed during the experimental period.

4.3 Results and discussion

4.3.1 Approximation curves of DC/DC converters and EC cells under outdoor performance

As the conversion efficiency of DC/DC converters is determined by the output of PV modules, it is important to identify the total energy output of the PV system. The converter efficiency was approximated from the outdoor results.

As shown in Fig. 4.2, the efficiency was fluctuated and low when the input energy ($E_{in\text{-}DC/DC}$) was low. However, the efficiency was steady at approximately 90% if the input was high. Using the localized polynomial regression method, we approached the potential hourly conversion efficiency as a function of DC/DC input provided by the PV system. Then, the integrated power output of DC/DC converters was estimated, and the annual conversion efficiency was evaluated on the total energy yield of DC/DC and PV.

As shown in Fig. 4.3, the conversion efficiency of the EC cell decreases with increasing input energy (which is the energy output of DC/DC). Similarly, the potential EC cell efficiency was approximated using a linear regression method. The energy produced by the EC cells was estimated as a function of DC/DC output. Subsequently, the potential amount of hydrogen generation was predicted. Finally, the yearly conversion efficiency of EC cells was estimated on the potential energy yield by the EC cells and the energy produced by the DC/DC.

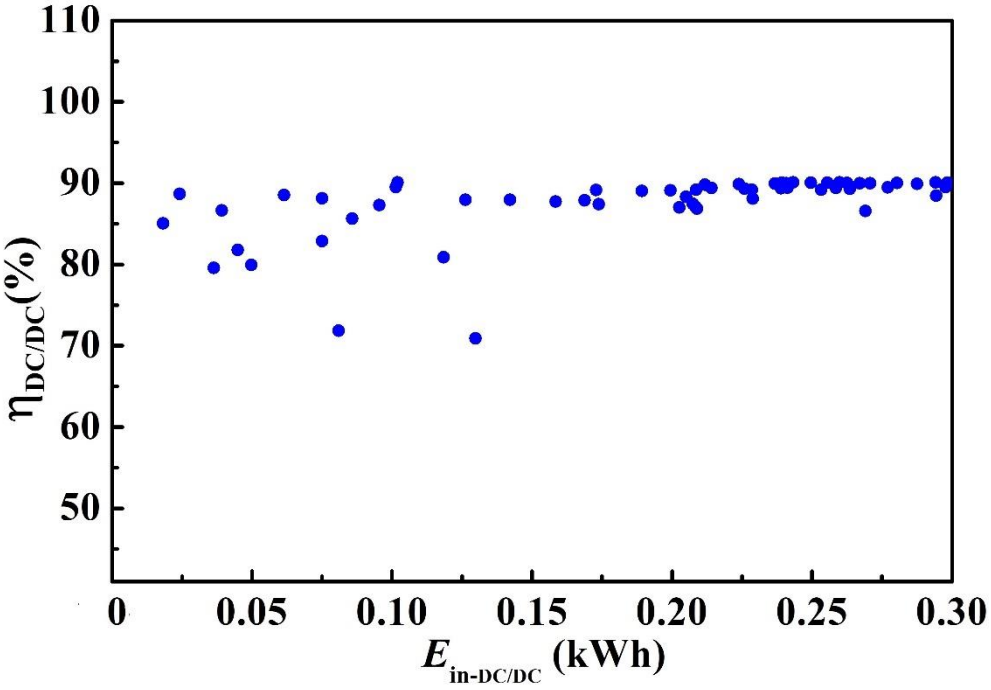

Fig. 4.2 Approximation curve profile of DC/DC converters efficiency with respect to DC/DC input energy.

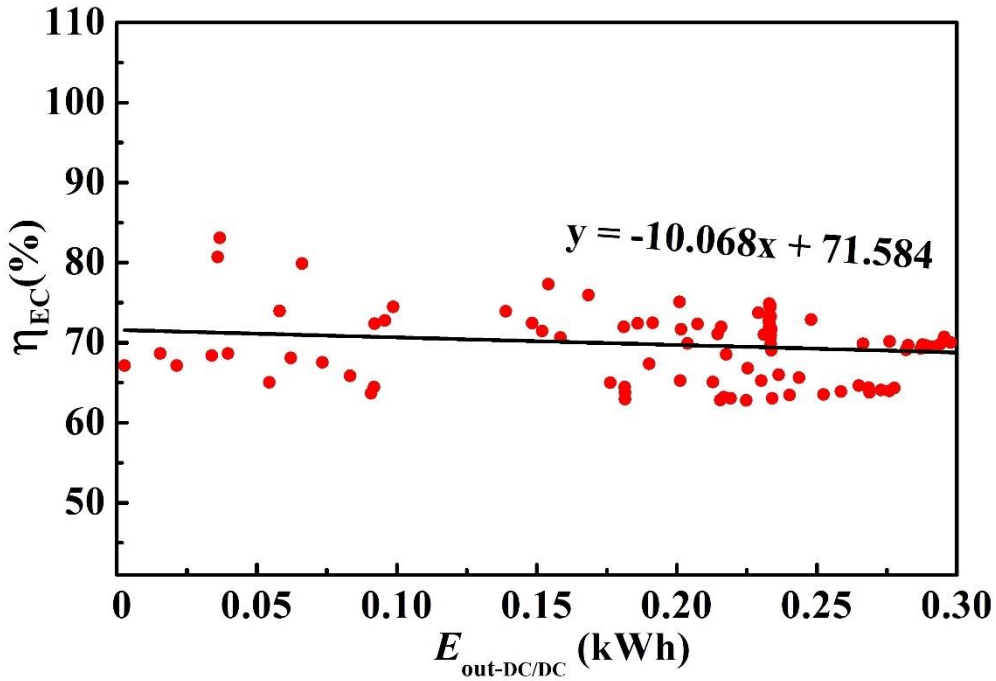

Fig. 4.3 Approximation curve profile of EC cells efficiency with respect to DC/DC output.

4.3.2 Energy consumption of the reactors under actual hydrogen generation

Since the methanation system involves a heat-released process, it is important to provide a moderate inlet feed at a suitable temperature to achieve low energy consumption. Therefore, we used outdoor data at 260 °C, which provided a high concentration of methane. Based on the actual outdoor hydrogen flow, the energy consumed by the reactors was approximated using the localized polynomial regression method.

Since we used two reactors in a series connection, the Sabatier reaction was more favorable in the first reactor and subsequently, it maintained the required energy owing to its exothermic nature. As shown in Fig. 4.4, the power consumption increased and fluctuated with low hydrogen generation. Additionally, the reactor requires energy to initiate the reaction. Subsequently, the reaction is maintained, and the energy consumption decreases. The energy consumption of the second reactor is higher than that of the first reactor, as shown in Fig. 4.5. Based on this data, the potential power consumption of the reactors was approximated using a localized polynomial regression method. During outdoor measurements, the hydrogen flow was measured every 10s. In the simulation model, we approached the energy consumption from the hourly integrated amount of hydrogen. The maximum amount of hydrogen flow under outdoor performance was 3.26 mol. The potential amount of hydrogen generation for this simulation was provided by equation (4.5), and energy consumption was approximated based on the estimated amount of hydrogen.

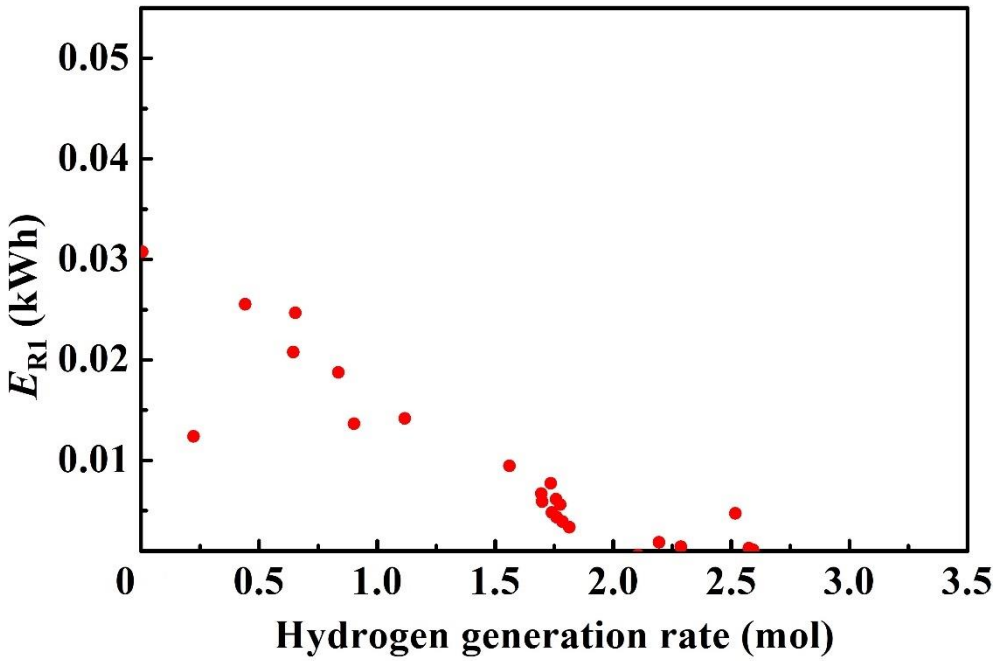

Fig. 4.4 Approximation curve profile of the effect of energy consumption on amount of hydrogen generation for first reactor.

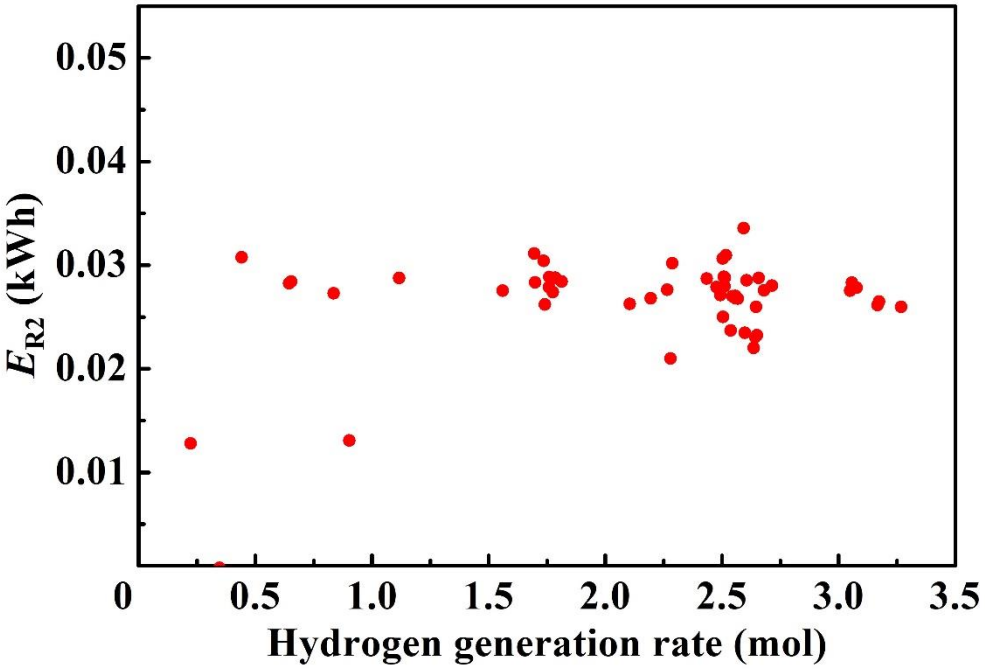

Fig. 4.5 Approximation curve profile of the effect of energy consumption on amount of hydrogen generation for second reactor.

4.3.3 Potential StH and StM conversion efficiency in Japan

We estimated the annual StH energy conversion efficiency at 837 sites in Japan. Figures 4.6 and 4.7 show the nationwide StH conversion and StM conversions, respectively.

Fig. 4.6 (a) and (b) show the estimated annual StH conversion from the Si and IMM PV modules. The crystalline Si module provided low StH conversion in the southwest region and showed the highest value in the northeast region. However, the conversion was double for the IMM module compared to that of the Si Module. Additionally, a high conversion was achieved nationwide because of the multi-junction PV and the efficient sets of DC/DC converters and EC cells. Similar to the Si-module, the highest conversion was obtained in the northern part of Japan. It means that the module's conversion efficiency (which is affected by the module's temperature) is one of the dominant factors for achieving a high StH conversion.

Similarly, the solar-to-methane conversion efficiency was estimated at 837 locations. Fig. 4.7 provides the nationwide potential StM conversion efficiencies. A high StM conversion was achieved in the northeastern parts of Japan and provided the lowest value in the southern part, where the conversion was proposed from the Si-PV module. A pattern similar to that of the Si-PV system was achieved for the proposed IMM module system. In both StH and StM conversions, the IMM modules provided the highest value (two times higher than that of the Si module).

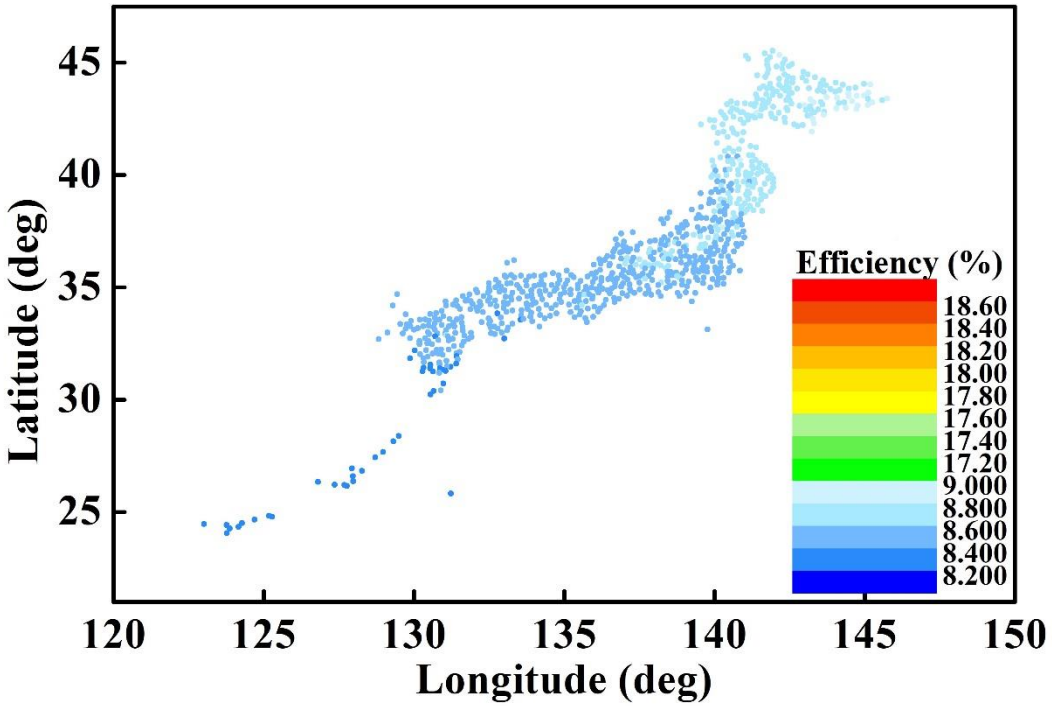

Fig. 4.6 Forecasted graphs of nationwide annual solar-to-hydrogen conversion efficiency (a) from the Si-PV module.

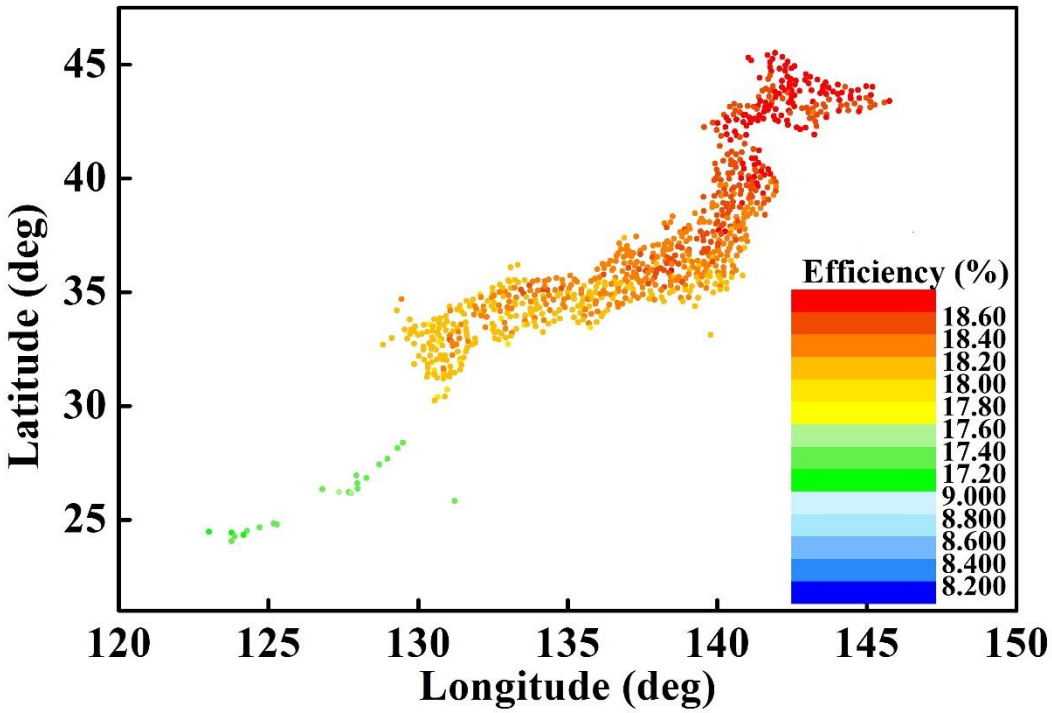

Fig. 4.6 (b) from the IMM-PV module.

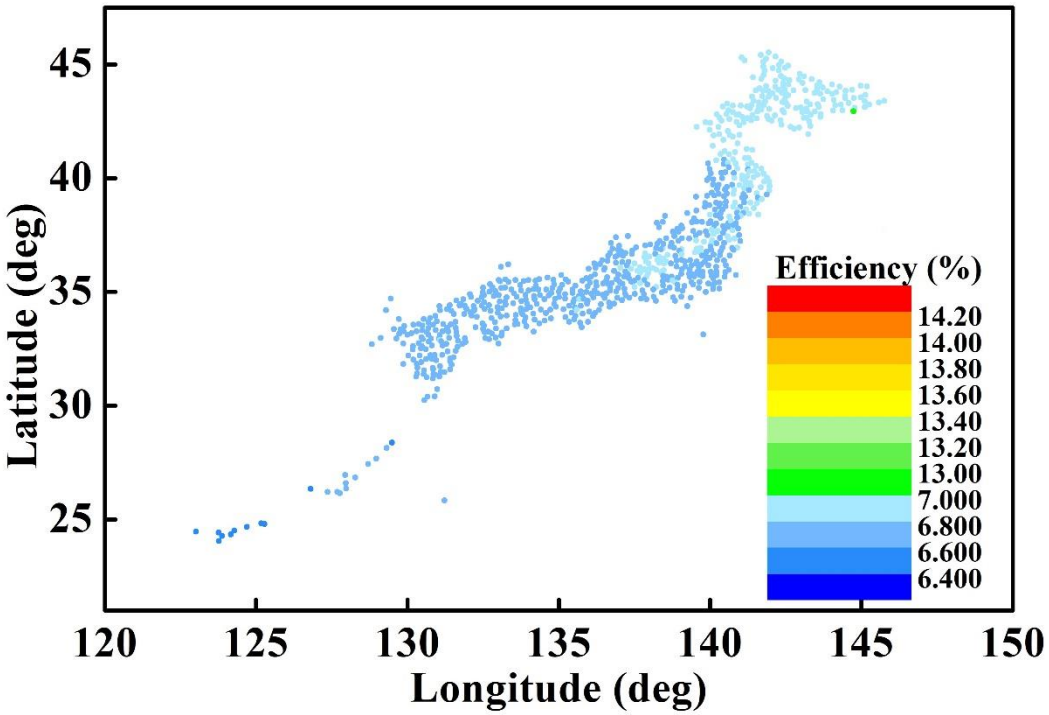

Fig. 4.7 (a) Forecasted graph of nationwide annual solar-to-methane conversion efficiency from the Si-PV module.

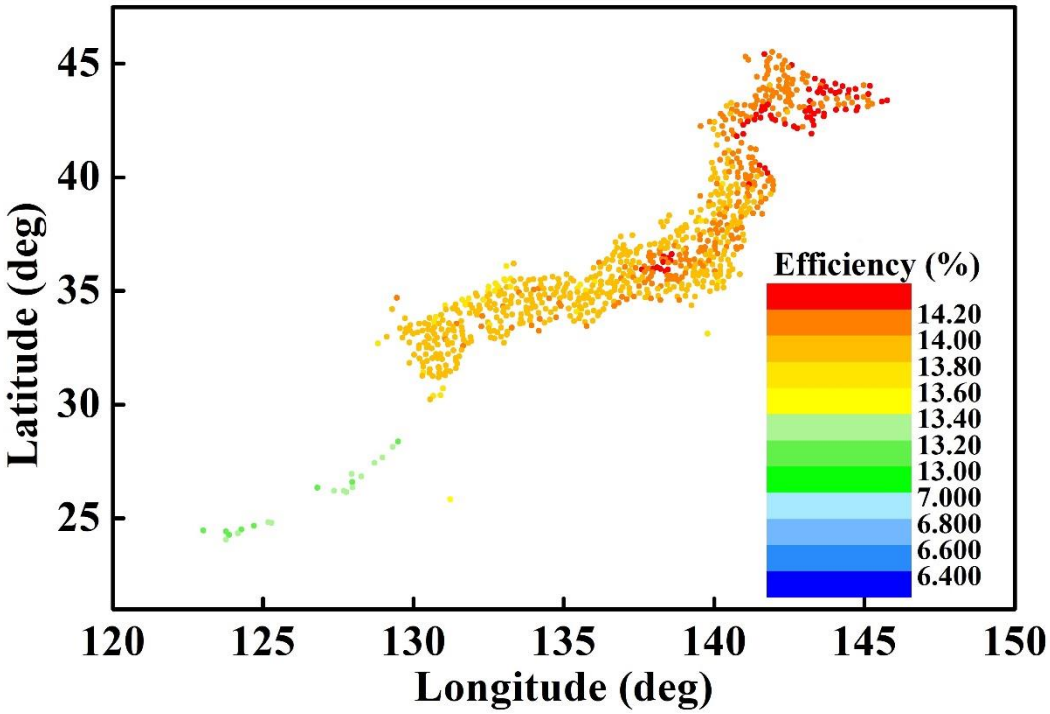

Fig. 4.7 (b) Forecasted graph of nationwide annual solar-to-methane conversion efficiency from the IMM-PV module.

In this study, we provided the potential annual StG conversion efficiency of two types of PV systems based on the MS2E PV energy prediction method. Since the StG conversion was performed on a set of converters-EC cells, the conversion efficiency of DC/DC and EC cells was approximated on the outdoor results. However, the efficiency of DC/DC converters is influenced by the input value of the PV module, which provides a low conversion if the input power is low. Therefore, we discussed the potential types of PV for efficient StG conversion in Japan as follows. Fig. 4.8 provides the monthly conversion efficiencies of the Si and IMM PV modules. Note that the monthly conversion efficiency was estimated only for Miyazaki.

As shown in Fig. 4.8, the conversion from the IMM module decreased, especially in spring and summer. This is due to the spectrum mismatch loss behavior that mainly appears in the muti-junction cells. In the summer season, Japan has a warm air surface, which results in frequent precipitation of water. Accordingly, the IMM module was considerably affected by spectral changes in the atmospheric parameters and cloud conditions. The Si module provided a steady conversion throughout the year. The StG efficiency is influenced by the value of efficiency of each subsystem. Therefore, it is important to identify the highest conversion system for installing outdoor PtG systems. Accordingly, in the proposed simulation, the number of modules was increased until the output power reached the maximum value provided by the outdoor CPV module. Therefore, three modules were proposed for Si-based StG conversion, and 15 modules were considered for the IMM-based StG simulation. Table 4.1 and 4.2 show the comparison of the one-day predicted values of sub-system conversion efficiencies on Si and IMM modules.

Under the same output conditions, the proposed IMM modules provided a high one-day efficiency that was close to the value (Ref. 24) provided by the outdoor CPV system. However, the module number for IMM PV-based method would increase the capital cost for the StG conversion. On the other hand, Si modules offered relatively equivalent values for converters

and EC cells to the outdoor system. However, the one-day StH and StM conversion efficiencies decreased comparatively. Tracking technology brings an advanced utilization of PV modules under an outdoor system. Si modules with two-axis tracking can produce the highest energy yield [17]. However, the StG conversion in this type of PV system was not analyzed in this simulation. On the other hand, the multijunction type IMM module has the potential to provide a developing conversion with a cost reduction improvement. The IMM module is promising to for effective StG conversion if it can improve the efficiency of the cell within the module area. Therefore, this study could contribute to identifying a highly efficient PV module that could provide a large power output to the converters, as well as the potential for high StG conversion in Japan.

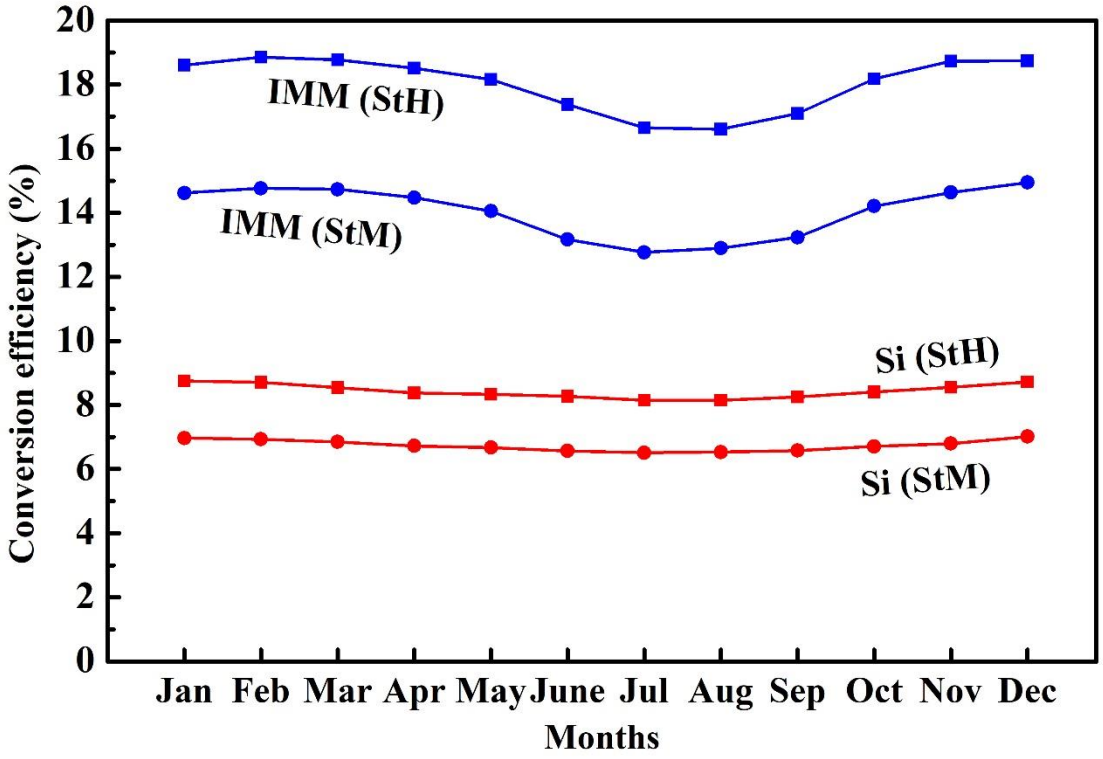

Fig. 4.8 Solar-to-hydrogne and solar-to-methane monthly conversion efficiency using the Si-PV and IMM-PV modules (a case-study for Miyazaki).

Table 4.1. Summary of the one-day predicted energy yield by each sub-system in the Si-PV and IMM-PV modules.

System configuration	$E_{TSI\ (PV)}$ (kWh/m^2)	$E_{out\ (PV)}$ (kWh/m^2)	$E_{out\ (DC/DC)}$ (kWh/m^2)	$E_{out\ (EC)}$ (kWh/m^2)
Si-PV module	5.652	0.792	0.711	0.492
IMM-PV module	6.628	2.006	1.803	1.236

Table 4.2. Summary of the one-day predicted sub-system efficiencies in the Si and IMM PV modules.

System configuration	$\eta_{(PV)}$ (%)	$\eta_{(DC/DC)}$ (%)	$\eta_{(EC)}$ (%)	$\eta_{(StH)}$ (%)	$\eta_{(StM)}$ (%)
Si-PV module	14.01	89.77	69.12	8.705	6.994
IMM-PV module	30.27	89.88	68.56	18.65	15.04

4.4 Conclusion

In this section, we approximated the potential solar-to-hydrogen and solar-to-methane conversion efficiencies in Japan form two types of flat PV modules. Since DC/DC-EC sets are main core in the solar-to-gas conversion, the estimation of their efficiency was approached from the outdoor performance. Based on the outdoor results, the conversion efficiency of DC/DC converters, EC cells and reactor's power consumption was approximated using the regression method. While irradiance energy input, power and energy output of proposed PV modules were estimated on Mathcad by using the METPV-11 database and MS2E method. Then, the energy output of each sub-system in solar to gas conversion was estimated.

In this study, we presented the potential solar-to-gas conversion from flat-type Si PV and IMM-PV modules. These types of modules have been installed and demonstrated their high outdoor performance at the University of Miyazaki. To fairly compare to our outdoor StG conversion system, the number of proposed modules was increased till their output match the value provided by our outdoor system. After that, we forecasted monthly and a one-day StG conversion for Miyazaki from Si-PV and IMM-PV modules and compared the estimated results. Then, we approached nationwide annual StG conversion in Japan.

According to the simulation results, IMM modules provided a high conversion with 17–18% for StH and 13–14% for StM nationwide, which is close to the world's highest value for the outdoor StG system performed at the University of Miyazaki (our previous studies). However, the number of IMM modules used for the conversion could be a matter from the economical viewpoint. While fixed Si-PV provided a low conversion efficiency of 8–9% and 6–7% for StH and StM, respectively. Nonetheless, IMM modules are promising to improve their efficiency and output. Compared to our outdoor performance, an IMM module or a tracking CPV system would be a promising technology for solar to gas conversion if the system could provide a high value of conversion.

References

[1] Beuls A, Swalus C, Jacquemin M, Heyen G, Karelovic A, Ruiz P. Methanation of CO_2: further insight into the mechanism over Rh/Al_2O_3 catalyst. Appl Catal B Environ. 2012; 113–114: 2–10.

[2] Aakko-Saksa PT, Cook C, Kiviaho J, Repo T. Liquid organic hydrogen carriers for transportation and storing of renewable energy- review and discussion. J Power Sources. 2018; 396: 803–823.

[3] IEA. The future of hydrogen. June 2019. IEA, Paris. Available online: https://www.iea.org/reports/the-future-of-hydrogen (Accessed on 03 March 2022).

[4] Nagashima M. Japan's hydrogen strategy and its economic and geopolitical implications. October 2018. Etudes de l'ifri, IFRI. Available online: https://www.ifri.org/sites/default/files/atoms/files/nagashima_japan_hydrogen_2018_.pdf. (Accessed on 03 March 2022).

[5] Shibata Y. Is power to gas feasible in Japan? IEEJ. 2016. 123.

[6] Zhang X, Chan SH, Ho HK, Tan SC, Li M, Li G, et al. Towards a smart energy network: the roles of fuel/electrolysis cells and technological perspectives. Int J Hydrogen Energ. 2015; 40: 6866–6919.

[7] Li Y, Gao W, Ruan Y. Potential and sensitivity analysis of long-term hydrogen production in resolving surplus RES generation–a case study in Japan. J Energ. 2019; 171: 1164–1172.

[8] Touili S, Merrouni AA, Hassouani YE, Amrani A, Rachidi S. Analysis of the yield and production cost of large-scale electrolytic hydrogen from different solar technologies and under several Moroccan climate zones. Int J Hydrogen Energ. 2020; 45: 26785–26799.

[9] Boudries R. Techno-economic study of hydrogen production using CSP technology. Int J Hydrogen Energ. 2018; 43: 3406–3417.

[10] Boudries R. Techno-economic assessment of solar hydrogen production using CPV-electrolysis systems. Energ Procedia. 2016; 93: 96–101.

[11] Paoli C, Voyant C, Muselli M, Nivet ML. Forecasting of preprocessed daily solar radiation time series using neural networks. Sol Energ. 2010: 84: 2146–2160.

[12] Sfetsos A, Coonick H, Univariate and multivariate forecasting of hourly solar radiation with artificial intelligence techniques. Sol Energ. 2000; 68: 169–178.

[13] Zhang X. A statistical approach for sub-hourly solar radiation reconstruction. Renew Energ. 2014; 71: 307–314.

[14] Diagne M, David M, Lauret P, Boland J, Schmutz N. Review of solar irradiance forecasting methods and a proposition for small-scale insular grids. Renew Sus Energ. 2013; 27: 65–76.

[15] Bahgat ABG, Helwa NH, Ahamd GE, El Shenawy ET. Esitmation of the maximum power and normal operating power of a photovoltaic module by neural networks. Renew Energ. 2004; 29: 443–457.

[16] Almonacid F, Rus C, Perez PJ, Hontoria L. Estimation of the energy of a pv generator using artificial neural network. Renew Energ. 2009; 34: 2743–2750.

[17] Tawa H, Saiki H, Ota Y, Araki K, Takamoto T, Nishioka K. Accurate output forecasting method for various photovoltaic modules considering incident angle and spectral change owing to atmospheric parameters and cloud conditions. Appl Sci. 2020; 10: 703.

[18] Ahshan R. Potential and economic analysis of solar-to-hydrogen production in the sultanate of Oman. Sust. 2021; 13: 9516.

[19] Gallardo FI, Ferrario AM, Lamagna M, Bocci E, Garcia A, Baeza-Jeria TE. A techno-economic analysis of solar hydrogen production by electrolysis in the north of Chile and the case of exportation from Atacama desert to Japan. Int J Hydrogen Energ. 2021; 41: 13709–13728.

[20] Nakamura A, Ota Y, Koike K, Hidaka Y, Nishioka K, Sugiyama M, Fuji K. A 24.4% solar to hydrogen energy conversion efficiency by combining concentrator photovoltaic modules and electrochemical cells. Appl Phys Express. 2015; 8: 107101.

[21] Ota Y, Yamashita D, Nakao H, Yonezawa Y, Nakashima Y, Ebe H, et al. Highly efficient 470W solar-to-hydrogen conversion system based on concentrator photovoltaic modules with dynamic control of operating point. Appl Phys Express. 2018; 11: 077101.

[22] Wai SH, Ota Y, Yamashita D, Sugiyama M, Nishioka K. High efficiency solar to gas conversion system using concentrator photovoltaic and electrochemical cell. Proceedings of Grand Renewable Energy Conference, 2018 June 17-22; Pacifico Yokohama, Yokohama. Japan: JCRE; 2018.

[23] Yamashita D, Nakao H, Yonezawa Y, Nakashima Y, Ota Y, Nishioka K. A new solar to hydrogen conversion system with high efficiency and flexibility. Proceedings of IEEE 6th International Conference on Renewable Energy Research and Applications ICRERA; 2017 Nov 5-8; San Diego, CA. USA: IEEE; 2017. p. 441–446.

[24] Wai SH, Ota, Y, Sugiyama M, Nishioka K. Evaluation of a Sabatier reaction utilizing hydrogen produced by concentrator photovoltaic modules under outdoor conditions. Appl Sci. 2020; 10: 3144.

[25] Yamaguchi M, Takamoto T, Araki K, Kojima N. Recent results for concentrator photovoltaics in Japan. Jpn J Appl Phy. 2016; 55: 04EA05.

[26] Wiesenfarth M, Philipps SP, Bett AW, ISE F, Kurtz S. Current status of concentrator photovoltaic (CPV) technology. NREL Version 1.3, April 2017. USA.

[27] Yamaguchi M, Takamoto T, Araki K, Ekins-Daukes N. Mulit-junction III-V solar cells: current status and future potential. J Solar Energ. 2005; 79: 78–85.

[28] Xing Y, Han P, Wang S, Liang P, Lou S, Zhang Y, et al. A review of concentrator silicon solar cells. Renew Sus Energ Rev. 2015; 51: 1697–1708.

[29] Geisz JF, Steiner MA, Jain N, Schulte KL, France RM, McMahon WE, et al. Pathway to 50% efficient inverted metamorphic concentrator solar cells. Proceedings of AIP conference. 2017; 1881, 040003.

[30] Geisz JF, France RM, Schulte KL, Steiner MA, Norman AG, Guthrey HL, et al. Six-junction III-V solar cells with 47.1% conversion efficiency under 143 suns concentration. Nat Enrg. 2020; 5: 326–335.

[31] Green MA, Dunlop ED, Hohl-Ebinger J, Yoshita M, Kopidakis N, Hao X. Solar cell efficiency tables (version 59). Prog Photovolt Res Appl. 2022; 30: 3–12.

[32] Sasaki K, Agui T, Nakaido K, Takahashi N, Onituska R, Takamoto T. Development of InGaP/GaAs/InGaAs inverted triple junction concentrator solar cells. Proceedings of AIP conference. 2013, 1556: 22.

[33] Takamoto T, Washio H, Juso H, Imaizumi M. Application of InGaP/GaAs/InGaAs triple junction solar cells to space use and concentrator photovoltaic. Proceedings of 2014 IEEE 40th Photovoltaic Specialist Conference (PVSC); 2014 June 8–13; Denver, CO, USA: IEEE; 2014. pp 0001–0005.

[34] Yamaguchi M, Dimroth F, Geisz JF, Ekins-Daukes N. Multi-junction solar cells paving the way for super high-efficiency. J Appl Phys. 2021; 129: 240901.

[35] Horowitz KAW, Remo T, Smith B, Ptak A. A techno-economic analysis and cost reduction roadmap for III-V solar cells. NREL technical report. November 2018. Golden CO: USA. Available online: https://doi.org/10.2172/1484349. (Accessed on 03 May 2022).

[36] Takamoto T, Juso H, Ueda K, Washio H, Yamaguchi H, Imaizumi M, et al. IMM triple-junction solar cells and modules optimized for space and terrestrial conditions. Proceedings of 2017 IEEE 44th Photovoltaic Specialist Conference (PVSC); 2017 June 25–30; Washington DC, USA: IEEE; 2017. pp 3506–3510.

[37] Itagaki A, Okamura H, Yamada M. Preparation of meteorological data set throughout Japan for suitable design of pv systems. Proceedings of 3rd World conference on Photovoltaic Energ Conversion; 2003 May 11–18; Osaka, Japan: IEEE; 2003. pp 2074–2077.

[38] New Energy and Industrial Technology Development Organization, Spectrum database. Available online: http://app0_2.infoc.nedo.go.jp/ (Accessed on 17 February 2022).

[39] Ota Y, Ueda K, Takamoto T, Nishioka K. Output evaluation of a world's highest efficiency flat sub module with InGaP/GaAs/InGaAs inverted triple-junction solar cell under outdoor operation. Jpn J Appl Phys. 2018; 57. 08RD08.

[40] Araki K, Ota Y, Saiki H, Tawa H, Nishioka K, Yamaguchi M. Super-multi-junction solar cells—device configuration with the potential for more than 50% annual energy conversion efficiency (non-concentration). Appl Sci. 2019; 21: 4598.

[41] Wai SH, Ota, Y, Nishioka K. Performance analysis of sabatier reaction on direct hydrogen inlet rates based on solar-to-gas conversion system. Int J Hydrogen Energ. 2021, 46: 26801–26808.

Chapter 5

Summary and conclusion

5.1 Conclusion

In this thesis, we presented outdoor solar-derived methanation performance on concentrator photovoltaic (CPV) modules and a relationship of its operating parameters with the hydrogen generation rate to the reaction. We also presented potential solar-to-hydrogen and solar-to-methane conversion efficiencies in Japan by proposing two types of PV modules. The first approach was to analyze the performance of methanation reaction from solar-derived hydrogen and estimate the efficiencies of CO_2 to CH_4 conversion and solar-to-gas conversion while the operating parameters of the methanation system were analyzed. This outdoor methanation study was performed on the direct hydrogen gas produced from the water electrolysis process by InGaP/InGaAs/Ge triple-junction CPV modules. We studied the performance of the methanation system on a sunny day and an overcast day, respectively.

The second approach was to focus on the methanation energy consumption on the inlet hydrogen flow rate provided by the electrolysis process. It plays a vital role in estimating solar-to-methane conversion efficiency. Therefore, it is required to identify the amount of hydrogen generation rate that could result in low energy consumption and maintain a constant reaction temperature. Solar-derived hydrogen production is intermittent on climate conditions, and it would be inappropriate to moderate the hydrogen generation rate under sunlight. Therefore, the methanation reaction in this study was conducted on various hydrogen flow rates in which hydrogen generation was regulated by using a DC supply. The relationship of hydrogen flow rate to the methanation total power consumption was analyzed.

After that, we predicted potential StG conversion efficiency in Japan based on our outdoor results. In this study, we proposed two types of PV system and predicted their output energy

using the METPV-11 database and the MS2E method. Besides, we approached potential conversion efficiencies of DC/DC converters and EC cells from the outdoor results.

Chapter 2

An outdoor solar to gas conversion was attempted on a sunny day and an overcast day from CPV modules with a tracking system. In our system, CPV modules utilized the MPPT technique, and EC cells were linked to the DC/DC converters proposed with “the perturb and optimizing (P&O) with converter scoring” method. It adaptably performed on both sunny and cloudy days and was designed to turn off some converters' operation at low output resulting in a high StH conversion under outdoor conditions. Hydrogen generated by the solar-based electrolysis process was directly supplied to the methanation reaction. Methanation reaction was carried out on two reactors provided with Ni-based catalyst. With the support of a catalyst, hydrogen gas from solar-derived electrolysis was reacted inside the reactors to CO_2 gas introduced via a tank.

In this chapter, we introduced each system utilized in conducting StG conversion. Then, the performance of the methanation system was fully described. CO_2 to CH_4 conversion efficiency was estimated at various operating temperatures. Based on the results, an optimum operating temperature was determined. After that, we verified the best stoichiometric ratio that yielded a high CO_2 conversion efficiency. The system provided a high CO_2 to the CH_4 conversion efficiency of 97.6% at the operating temperature of 260 °C. We also analyzed the reactors’ temperature during the reaction on these two weather conditions. On a sunny day operation, the first reactor increased over the operating setting temperature (260 °C) while its power consumption was stable after an initial increase.

Conversely, the second reactor was maintained and stable at the operating temperature, whereas its power consumption was high during the reaction. On the other hand, the power consumption of both reactors increased consecutively under the overcast operation. Subsequent

to this, we estimated one-day elementary efficiencies of each system and solar-to-methane conversion efficiency on a sunny day condition. Methane generation rate was evaluated on the generation rate of input H_2 into the reaction and calculated in moles. In that calculation, we assumed that the CH_4 generation rate corresponds to ¼ times input H_2. It was multiplied with CO_2 to CH_4 conversion (97.6%). The conversion of CO_2 to CH_4 was quantified by QMS. We achieved solar to the methane conversion efficiency of 13.8% on sunny day conditions.

From the previous results, we can conclude that high conversion efficiency of solar to methane (13.8%) was obtained during the outdoor operation on a sunny day. Additionally, we observed that the reaction (a heat release process) increased the temperature of first reactor whereas it maintained a constant power consumption after an initial increase. On the other hand, a low reaction rate resulted the power consumption of the second reactor to increase. Therefore, the next step was to emphasize the power consumption of the reactors on the inlet hydrogen flow rate (which is also the generation rate of the electrolysis process) to the methanation system.

Chapter 3

Since the reaction is a heat-released process, it is necessary to reduce the reactor's temperature as well as the energy consumed by the reactors. The reaction is influenced by the inlet flow rate of feed gases (CO_2 and H_2). In our system, we directly applied hydrogen from the electrolysis process to the methanation reactors while pure CO_2 was provided through the pipeline from the tank. Therefore, we focused on the methanation energy consumption on the inlet hydrogen flow rate in this chapter.

In this study, we performed the electrolysis process using DC supply to steady its generation rate and to better understand its influence on the methanation power consumption. Firstly, the generation rate was regulated and performed at the previous operating temperature (260 °C). The highest methane concentration was figured out based on two optimum hydrogen

generation rates (0.337 and 0.449 NL/min). Then, we analyzed the optimum operating temperature on these hydrogen generation amounts. The results provided that the highest methane concentration was achieved at the operating temperature of 220 ℃ on controlled hydrogen.

Subsequently, we verified the stability of methane composition for a 4 h operation period and performed two different days for each GR_{H2} (0.337 and 0.449 NL/min). Then, we analyzed and measured the temperatures of the reactors in which the operating temperature was set to 220 ℃. After that, we evaluated the total power consumption of the reactors on these corresponding GR_{H2}. Based on the results, we determined the optimum GR_{H2} that provided the highest methane concentration and resulted in low power consumption. We also discussed a hypothesis on the energy loss on fully-operated GR_{H2} (1.19 NL/min: previous outdoor results) from the CPV module and a controlled GR_{H2} (0.449 NL/min) by a battery storing hydrogen from the solar energy.

This chapter provided that the reactor's temperature was constant at a set operating temperature if moderate and constant hydrogen flow was provided. Additionally, we also observed that high GR_{H2} resulted in low total power consumption. Methane concentration improved at a moderate and controlled hydrogen generation. The required energy for the reactors was reduced on a fully-operated GR_{H2} under sunny day conditions; additionally, there would be energy loss (36.5%) due to impractical hydrogen generation and flow to the reactors on cloudy days. Therefore, we concluded that a flexible solar to methane conversion system under any climate conditions can be obtained if the hydrogen inlet flow is controlled or moderate and stable hydrogen generation is provided using a battery.

Chapter 4

In this chapter, an approach to realizing solar to gas conversion in Japan was introduced using the simulation method. This approach utilized the METPV-11 database and MS2E

method to predict the energy output of proposed PV modules. MS2E energy prediction method is well-developed with an estimation of the solar spectrum on all climate conditions and accurate output forecasting results. The conversion efficiencies of DC/DC converter and EC cells were approximated based on the previous outdoor results. In this approach, we used the outdoor results performed at the operating temperature of 260 °C.

In this simulation, we proposed solar to gas conversion from the flat PVs. Silicon PV modules are well-established and commercially available in solar cell production. On the contrary, multi-junction cells are improving their efficiency and are being developed with a low cost. Therefore, we forecasted output energy and estimated solar to gas conversion efficiency from these modules. Since DC/DC converters were linked to the electrolyzers in our outdoor system, the efficiency of converter increased with an increasing number of PV modules. To match the output of each sub-system and make a fair comparison to our outdoor performance, we proposed 15 modules and 3 modules for the IMM-PV and Si-PV in this approach.

Approximation curves for the converter and EC cells efficiencies were identified based on our outdoor results. Then, they were approximated on the output of PV modules and converters, respectively. After that, the energy output of EC cells was predicted. We also forecasted the annual amount of hydrogen production in 837 locations in Japan. Subsequently, we approached the efficiency of solar to hydrogen conversion.

In the latter part of solar to gas conversion, we considered the reactors' energy consumption as an input value to estimate the solar to methane conversion efficiency. Accordingly, we initially identified the energy consumption profile of the reactors on the outdoor hydrogen generation results. Then, we forecasted these values on the predicted amount of hydrogen and methane generation. The amount of methane was estimated ¼ times that of hydrogen and the concentration of methane in percentage. After that, we approximated nationwide solar to

methane conversion efficiency at 837 places. We also discussed the values of the monthly solar to the gas conversion efficiency of these two proposed systems. After that, we summarized the predicted values of one-day conversion efficiency and energy yield by each sub-system.

The results in this chapter provided that a low StH and StM conversion resulted in the southwest regions of Japan. On the contrary, it showed high values in the northwest parts for both PV modules. However, the amount of the proposed IMM modules system was double (17–18% for StH and 13–14% for StM) compared to that of the conversion from the Si system. The southern part of Japan has a hot climate condition than the northern region. Additionally, the PV efficiency is influenced by the ambient temperature. Therefore, we concluded that solar cells' conversion efficiency is one of the dominant factors in the estimation of StG conversion to provide a high value in efficiency. This simulation method can be applied to predict worldwide potential StG conversion efficiency anywhere if the global solar irradiance data are available. Therefore, this StG efficiency prediction method would be a promising approach to broaden green hydrogen and CO_2 reduction, resolving global warming.

5.2 Future work

The reactors' energy consumption is one of the critical factors in estimating the StM conversion efficiency and is dependent on the reaction rates, which are influenced by the hydrogen flow rate to the reactors. The previous results in Chapters 2 and 3 provided the power consumption of the reactors under two different climate conditions: a sunny day and an overcast day. Additionally, these chapters highlighted the relationship between its energy consumption on the amount of hydrogen generated by the electrolysis process. Chapter 3 provided an improved system with a controlled hydrogen generation; however, regulating its production under sunlight could be impractical due to intermittent energy production. For future work, we suggest an idea to use a battery storing solar energy in the daytime and perform the electrolysis and methanation system, especially on night-time and overcast days.

Another possible suggestion is to reduce the consumption and control the set operating temperatures by providing two different temperatures to the reactors. However, manipulating the released heat during the reaction could be difficult because of the exothermic process. Although the energy consumption of the reactors can reduce at low operating temperatures, the temperature of the reactors will increase with the reaction unless the inlet of hydrogen rates is not controlled. This kind of behaviour would accelerate catalyst deactivation over a long operation period. Additionally, intermittent hydrogen generation cannot be negligible under sunlight operation. However, the conversion efficiency could be improved by reducing the energy consumption of the reactors.

Appendix A

Nomenclature and Abbreviations

GHG	Greenhouse gas
IEA	International energy agency
PV	Photovoltaic
PtG	Power-to-gas
SNG	Synthetic natural gas
SDGs	Sustainable development goals
AEL	Alkaline electrolysis
PEM	Proton exchange membrane
StG	Solar-to-gas
CPV	Concentrator photovoltaic
EC	Electrochemical
MPPT	Maximum power point tracking
StH	Solar-to-hydrogen
DNI	Direct normal irradiance
MEA	Membrane electrode assembly
GR_{H2}	Hydrogen generation rate
MFM	Mass flow meter
PID	Proportional, integral, derivative
MFC	Mass flow controller
QMS	Quadrupole mass spectrometer
ηStM	Solar to methane efficiency
ΔH	Combustion energy of methane

E_{DNI}	Integrated irradiance
$E_{reactors}$	Energy consumed by the reactors
η_{CPV}	Conversion efficiency of CPV module
η_{DCDC}	Conversion efficiency of the DC/DC converters
η_{EC}	Energy conversion efficiency from DC electricity into the free energy of hydrogen at the electrolyzer
GC	Gas chromatography
Ar	Argon
$E_{r\ con}$	Total power consumptions on two days under the conventional system
$E_{r\ app}$	Total power consumptions on two days under the assumed system
StM	Solar-to-methane
MS2E	Miyazaki spectrum to energy
METPV-11	Meteorological test data for photovoltaic systems
Si	Silicon
IMM	Inverted metamorphic
NEDO	New energy and industrial technology development organization
DHI	Direct horizontal irradiance
SI	Scatter irradiance
T_{amb}	Ambient temperature
I_{sc}	Short circuit current
V_{oc}	Open-circuit voltage
FF	Fill factor
P_{PV}	Power output of PV module
J_{sc}	Short-circuit current density
A_{mod}	Area of module

η_{sys}	System efficiency
t	Duration in hour
$f_{DC/DC}$	Approximated conversion efficiency from the curve as a function of DC/DC input energy
$E_{out\text{-}PV}$	Output energy of PV module
$E_{in\text{-}DC/DC}$	Input energy of DC/DC
$E_{out\text{-}DC/DC}$	Integrated output power of DC/DC
$E_{out\text{-}EC}$	Energy produced by the electrolyzer
f_{EC}	Approximated conversion efficiency from the curve as a function of DC/DC output energy
E_{TSI}	Integrated annual solar irradiance on the proposed module
E_{H2}	Total energy stored by the generated hydrogen
n_{H2}	Amount of hydrogen in moles produced by the electrolysis process
F	Faraday's constant
E_{CH4}	Energy stored by the generated synthetic methane
$\eta_{CO2\rightarrow CH4}$	Percentage of CO_2 to CH_4 conversion
E_{r1}	Consumption energy of first reactor
E_{r2}	Consumption energy of second reactor
η_{PV}	Conversion efficiency of PV module
η_{StH}	Conversion efficiency of solar-to-hydrogen
η_{StM}	Conversion efficiency of solar-to-methane

List of publications

I. Academic journals

1. Evaluation of a Sabatier Reaction Utilizing Hydrogen Produced by Concentrator Photovoltaic Modules under Outdoor Conditions

   SoeHtet Wai, Yasuyuki Ota, Masakazu Sugiyama and Kensuke Nishioka

   Applied Sciences, Vol. 10, 3144-1- 3144-12 (2020).

2. Performance analysis of sabatier reaction on direct hydrogen inlet rates based on solar-to-gas conversion system

   SoeHtet Wai, Yasuyuki Ota, Kensuke Nishioka

   International Journal of Hydrogen Energy, Vol. 46, pp. 26801-26808 (2021).

3. Forecasting solar-to-hydrogen and solar-to-methane energy conversion efficiency using Si and IMM PV-modules: A case-study in Japan

   SoeHtet Wai, Yasuyuki Ota, Kensuke Nishioka

   Journal of Power Sources, Vol. 546, 231991 (2022).

II. International conference proceedings

1. High efficiency solar to gas conversion system using concentrator photovoltaic and electrochemical cell.

   Soe Htet Wai, Yasuyuki Ota, Daiji Yamashita, Masaka Sugiyama, Kensuke Nishioka.

   Grand Renewable Energy Conference, Vol. 1, (2018). DOI: 10.24752/gre.1.0_44

2. Performance analysis of power-to-gas system based on concentrator photovoltaic modules in outdoor operation

   Soe Htet Wai, Thet Htar Swe, Yasuyuki Ota, Masakazu Sugiyama, Kensuke Nishioka

   AIP Conference Proceedings, Accepted (2021).